공학박사 학위논문

Robust and Energy Efficient MAC/PHY Layer Strategies of Wi-Fi

Wi-Fi의 신뢰성 및 에너지 효율성 향상을 위한 MAC/PHY 기법

2015년 8월

서울대학교 대학원

전기컴퓨터공학부

이 옥 환

공학박사 학위논문

Robust and Energy Efficient MAC/PHY Layer Strategies of Wi-Fi

Wi-Fi의 신뢰성 및 에너지 효율성 향상을 위한 MAC/PHY 기법

2015년 8월

서울대학교 대학원

전기컴퓨터공학부

이 옥 환

Robust and Energy Efficient MAC/PHY Layer Strategies of Wi-Fi

지도교수 최 성 현

이 논문을 공학박사 학위논문으로 제출함

2015년 7월

서울대학교 대학원

전기컴퓨터공학부

이 옥 환

이옥환의 공학박사 학위 논문을 인준함

2015년 6월

위 원 장: 이 병 기 (인)

부위원장: 최 성 현 (인)

위 원: 박 세 웅 (인)

위 원: 임 종 태 (인)

위 원: 진 성 근 (인)

Abstract

Robust and Energy Efficient MAC/PHY Layer Strategies of Wi-Fi

Over the last quarter century, wireless local area network (WLAN) technology has become an essential and indispensable part of our daily lives. Recently, a tremendously growing number of portable devices, such as smartphones, tablets and laptops, are being equipped with Wi-Fi, the hallmark of the IEEE 802.11 WLAN, in order to meet ever-increasing traffic demands at extremely low cost.

Encouraged by this remarkable success, Wi-Fi is facing two trends. First, the state-of-the-art IEEE 802.11 specifications, e.g., IEEE 802.11n and 802.11ac, have focused on improving physical layer (PHY) rate by enabling multiple antennas, called multiple-input multiple-output (MIMO), and bandwidth widening, known as channel bonding [1, 2]. Second, to achieve high throughput and transmission efficiency at medium access control (MAC) layer, IEEE 802.11n/ac standards have defined two types of frame aggregation techniques: MAC service data unit (MSDU) aggregation and MAC protocol data unit (MPDU) aggregation which amortize PHY/MAC protocol overhead e.g., binary random backoff, physical layer convergence protocol (PLCP) preamble, and acknowledgement (ACK), over multiple frames by packing several MSDUs and MPDUs into a single aggregate MSDU (A-MSDU) and aggregate MPDU (A-MPDU), respectively.

Apparently, there is no doubt that these state-of-the-art features meet and fulfill

the requirements of Wi-Fi equipped device users by offering several hundred-fold increases in PHY rate and ubiquitous access. However, with respect to the demands of the *battery-powered portable* device users, the belief is easily broken from two perspectives. First, since using higher PHY rate and longer A-MPDU are more vulnerable to channel errors especially for mobile users, the significant throughput performance degradation can be observed. Second, the emerging Wi-Fi chipsets, based on IEEE 802.11n/ac, consume much more energy than its legacy IEEE 802.11a/b/g counterparts due to the usage of MIMO and channel bonding. Nowadays, as the battery-powered portable device users place increasingly complex demands on the functionality of their devices which have strict power limitation, satisfaction with robust communication and battery life time is becoming increasingly important. In this dissertation, to address these challenges, we propose robust and energy efficient MAC/PHY layer strategies of Wi-Fi.

First of all, to confirm those changes, we have conducted extensive experiments using state-of-the-art commercial IEEE 802.11n/ac-equipped devices and Microsoft's Software Radio (Sora) platform. Our experiment results have revealed strong evidence that the use of long A-MPDU frames seriously deteriorates the Wi-Fi performance, i.e., throughput, especially for the pedestrian mobile users. Besides, we have found that the use of channel bonding remarkably consumes more energy, thus making Wi-Fi a primary energy consumer in the battery-powered portable devices. Especially, the energy cost is dominated by excessive and unnecessary listening and receiving operations.

We begin an intra-frame rate control algorithm (Intra-RCA) design, called *SNR-aware Intra-frame Rate Adaption* (SIRA), which enhances the system performance of Wi-Fi in fast time-varying environments [3]. Widely used inter-frame rate control algorithms (Inter-RCAs), which select the PHY rate of each frame based on the time-

averaged frame loss rate and the signal strength statistics, perform poorly for a long A-MPDU due to the channel variation in mobile environments. Unlike the previous approaches, SIRA adapts the PHY rate on intra-frame basis, i.e., the PHY rate is updated in the middle of a frame according to user mobility. The performance of the proposed scheme is also evaluated by a trace-driven link level simulator employing the collected channel traces from real measurements. The simulation results show that SIRA outperforms a standalone Inter-RCA in all tested traces. Despite its enhanced performance and considerable frame error reduction, the performance degradation caused by the impact of user mobility still remains due to the inherent limitation of IEEE 802.11 PHY design.

Therefore, we conclude that this challenge should be solved with the assistance of PHY modification, and propose *Channel-Aware Symbol Error Reduction* (ChASER), a new practical channel estimation and tracking scheme for Wi-Fi receivers [4]. ChASER utilizes re-encoding and re-modulation of the received data symbol to keep up with the wireless channel dynamics at the granularity of orthogonal frequency division multiplexing (OFDM) symbols. In addition, its low-complexity and feasibility of standard compliance is demonstrated by Microsoft's Sora prototype implementation and experimentation. To our knowledge, ChASER is the first IEEE 802.11n-compatible channel tracking algorithm since other approaches addressing the time-varying channel conditions over a single (aggregated) frame duration require costly modifications of the IEEE 802.11 standard. Even though the above proposed approaches enhance the Wi-Fi's throughput performance and robustness over conventional technique, the rest requirement of the portable device user, i.e., energy efficient Wi-Fi system design, should be addressed as ever.

Accordingly, we propose a new power save operation as well as the corresponding protocol, called WiFi in Zizz (WiZizz), which judiciously exploits the characteristic

of the channel bonding defined in IEEE 802.11ac and efficiently handles the channel bandwidth in an on-demand manner to minimize the traumatic energy spent by IEEE 802.11ac devices [5]. Our extensive measurement and simulation show significant performance improvement (as high as 73% energy saving) over a wide range of communication scenarios. In addition, the feasibility of easy implementation is demonstrated by a prototype with a commercial 802.11ac device. To the best of our knowledge, WiZizz is the first IEEE 802.11ac-congenial energy efficient bandwidth management while other existing approaches require costly modifications of the IEEE 802.11ac specification.

In summary, we propose a number of compelling algorithms and protocols to improve the robustness and energy efficiency in accordance with the paradigm shift of Wi-Fi. Moreover, our evaluation results show that the proposed schemes in this dissertation are effective and yield considerable performance gain based on both the trace-driven link level simulation and the network level simulation which well reflects the wireless channel characteristics of the real world and the operation of IEEE 802.11 WLAN, respectively. We demonstrate the feasibility of our approaches by implementing prototypes in off-the-self IEEE 802.11n/ac devices and software-defined radio.

Keywords: Wireless communication, Wireless LAN (Wi-Fi), Robustness, Energy saving, Power consumption modeling, Prototype design.
Student Number: 2007-21046

Contents

List of Tables

List of Figures

Chapter 1

Introduction

1.1 Paradigm Shift of Wi-Fi

Over the last few years, the high-speed wireless local area network (WLAN) technology has undergone tremendous growth since its inception, offering several hundred-fold increases in data rate and ubiquitous access at extremely low cost. Much of this technological and commercial success is attributed to Wi-Fi, the hallmark of the IEEE 802.11 WLAN working group (WG), as it is now an indispensable part of our daily lives with the ever-increasing demands for higher data rates. Furthermore, technological evolution and diversified frequency spectra have made Wi-Fi powerful and agile enough to be suitable for various environments, not solely restricted to indoor uses as shown in Fig. 1.1.

However, since it was first introduced, medium access control layer (MAC) and physical layer (PHY) strategies of Wi-Fi have been primarily designed for indoor and nomadic (but stationary during communication) users where the assumption of quasi-stationary channel over the duration of a single frame transmission has matched the reality extremely well.

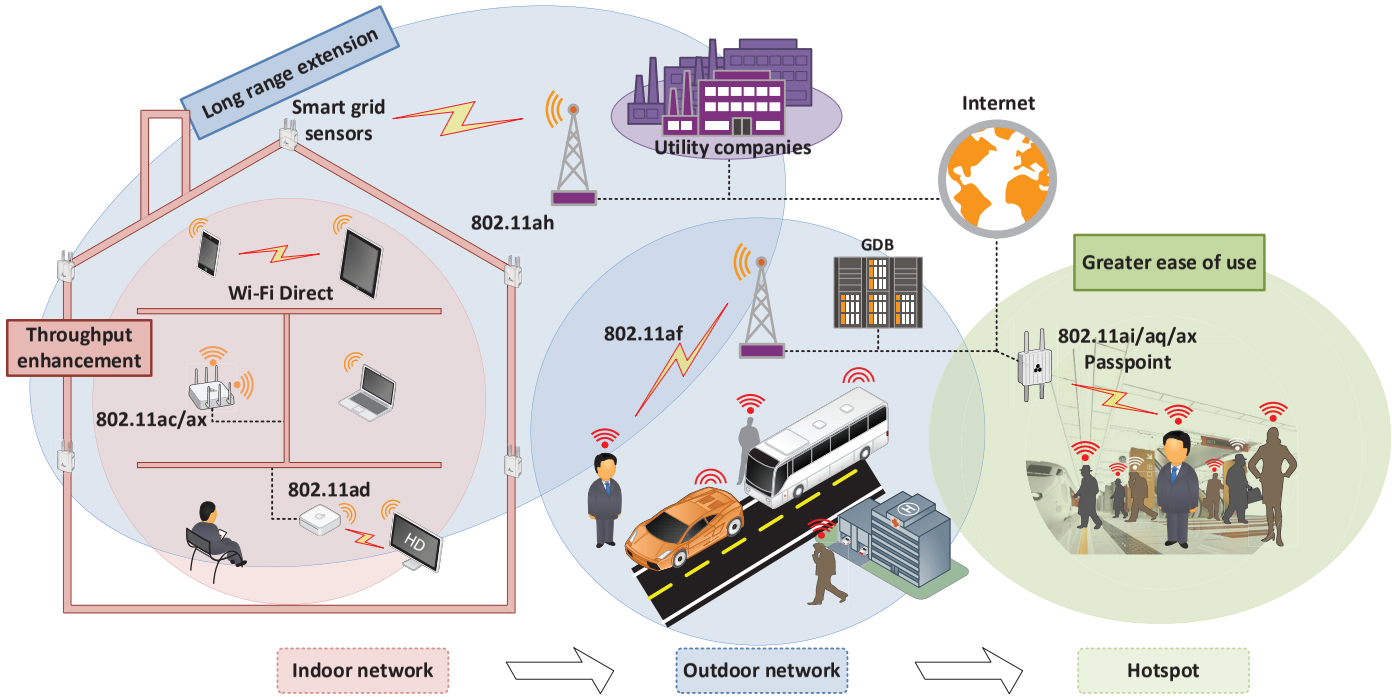

Figure 1.1: Paradigm shift of Wi-Fi.

Three recent trends, however, are challenging this fundamental assumption of the quasi-stationary channel condition. First, the usage pattern of Wi-Fi users is increasingly becoming "mobile during communication," thanks to the explosive growth of various portable devices such as smartphones, tablets, and emerging wearable gadgets. Second, much longer frames are frequently used by recent Wi-Fi standards such as IEEE 802.11n and IEEE 802.11ac in order to enhance the throughput performance by minimizing inter-frame protocol overhead [1, 2]. Third, the specifications have adopted higher order modulation and coding schemes (MCS), multiple input multiple output (MIMO), and channel bonding technologies which are more sensitive to the variation of channel condition.

These trends aggravate the performance of the emerging Wi-Fi equipped mobile devices significantly due to the fundamental limitation of IEEE 802.11. When the wireless channel does not change significantly during the period of a single frame transmission (i.e., frame duration is within the scale of channel coherence time), the channel state information (CSI) needs to be estimated only once at the preamble at the beginning of the frame, and can be exploited throughout the entire frame reception process. The existing IEEE 802.11 standards abide by this practice of "estimate once, apply throughout" during the receiver process of demodulation/decoding. Furthermore, the traditional rate control algorithms (RCAs) that assume wireless channel to be quasi-stationary throughout one frame duration, thus the same MCS is used within a specific frame.

Meanwhile, despite its high performance and inexpensive availability, the energy efficiency of Wi-Fi has remained a challenging problem. Wi-Fi's energy inefficiency basically comes from its intrinsic carrier sense multiple access (CSMA) mechanism, the radio should perform listening continuously in order to detect unpredictably arriving packets or assess a clear channel. Rather, as the paradigm shift of Wi-fi, the

energy efficiency has become an ever-growing issue, because the newly adopted techniques, which provide ever-increasing physical layer data rates, inherently cause the high power consumption It is undesirable for the portable Wi-Fi devices which have the strict power limitation.

Nevertheless, the considering both robust wireless communication and energy efficient protocol design have been pushed aside. We believe that more robust and energy efficient MAC/PHY strategies is required to meet the ever-increasing demand and satisfaction for the high-throughput WLANs by considering the newly adopted Wi-Fi techniques and the fast-paced communication environment.

1.2 Development Trend of IEEE 802.11

We now introduce the prerequisites of the dissertation. As stated in Section 1.1, the recent IEEE 802.11 specifications have developed innovative MAC/PHY features, such as frame aggregation, MIMO, channel bonding, and higher order MCSs, to increase PHY data rate significantly. We describes the details of the features in this section.

1.2.1 MAC Features

Frame aggregation

Frame aggregation is a core feature of IEEE 802.11n to send multiple frames in a single transmission. Every data frame has a significant amount of overhead including PLCP preamble, MAC/PHY header, acknowledgement (ACK) transmission, and several Inter Frame Spaces (IFSs). These overheads often consume bandwidth comparable with the actual data payload, which results in much lower throughput compared with the underlying PHY data rate. To address this issue, the 802.11n defines two types of frame aggregation: MAC service data unit (MSDU) and MAC protocol data unit (MPDU)

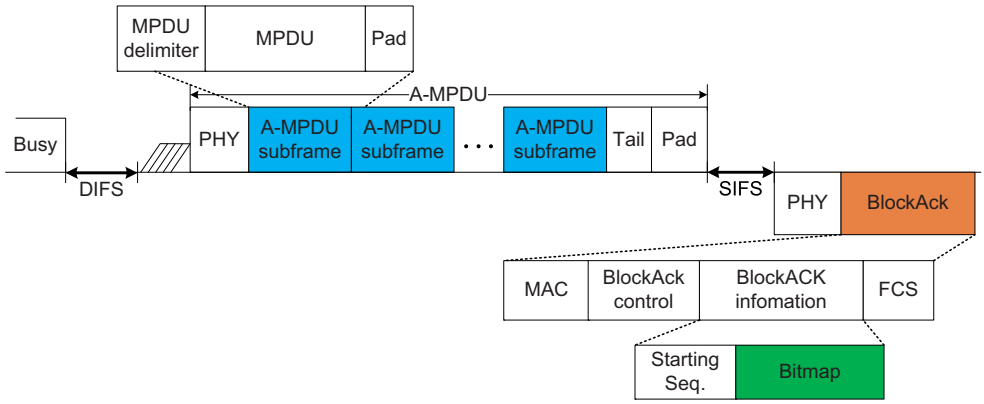

Figure 1.2: A-MPDU and BlockAck exchange.

aggregation [1].

Aggregate MSDU (A-MSDU) is literally the aggregation of MSDUs into a single frame at the upper MAC layer with the maximum size of 7,935 bytes. Since all aggregated MSDUs share a single MAC header and a single cyclic redundancy check (CRC) code, used for error detection by the receiver, the transmission of an A-MSDU fails as a whole even when just one of the aggregated MSDUs is corrupted.

On the other hand, aggregate MPDU (A-MPDU), which is more commonly used in practice due to the merit explained below, combines multiple MPDUs into a single PPDU as shown in Fig. 1.2. The maximum A-MPDU length is $65,535$ bytes, and the A-MPDU transmission time should be smaller than the maximum PPDU duration, *aPPDUMaxTime*, defined as 10 ms [1]. Unlike A-MSDU, A-MPDU is more efficient in high error rate environment, because all individual subframes (or MPDUs conveyed in subframes) are positively/negatively acknowledged using BlockAcks as shown in Fig. 1.2, and hence, can be individually retransmitted.

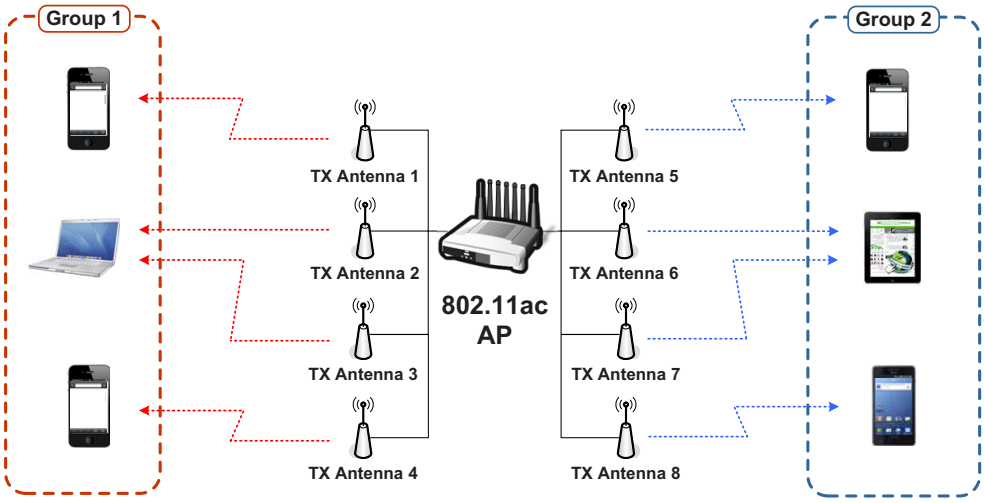

Figure 1.3: Example of IEEE 802.11ac MU-MIMO.

1.2.2 PHY Features

Multiple Input Multiple Output

IEEE 802.11n and IEEE 802.11ac have supported MIMO operation which utilizes multiple antennas at both transmitter and receiver. MIMO can achieve much higher data rates. IEEE 802.11n and IEEE 802.11ac support up to four spatial streams and eight spatial streams, respectively. There are two transmission techniques which use multiple antennas, namely spatial multiplexing (SM) and space-time block coding (STBC). SM transmits multiple data streams through multiple antennas to enhance the data rate. On the other hand, STBC transmits multiple coded copies of a data stream through multiple antennas to improve the reliability. However, MIMO techniques require a more accurate channel state information (CSI) estimation and compensation procedure to eliminate the spatial interference, and consumes more energy resource because each antenna has a radio frequency (RF) chain.

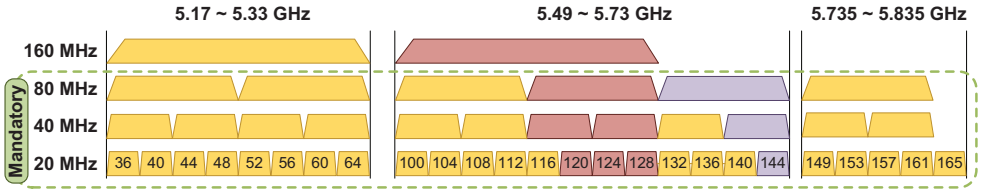

Figure 1.4: Channel bandwidth allocation map in 5 GHz unlicensed band.

Multi-user MIMO

IEEE 802.11ac standard has defined the advanced MIMO feature, multi-user MIMO (MU-MIMO). MU-MIMO advances SU-MIMO (Section 1.2.2) by enabling an Access Point (AP) to transmit multiple spatial streams via multiple antennas, to multiple receivers simultaneously.

As shown in Fig. 1.3, MU-MIMO improves the performance by serving multiple Wi-Fi clients in parallel rather than serially, as was the case in 802.11n, where the highest rate, 600 Mb/s, is available only when both AP and client are equipped with four antennas such that there are four spatial streams available to MIMO transmission. The number of antennas embedded in the client (e.g., smartphone, and tablet PC), however, is usually limited to one or two due to the space limit of the device, although the AP with three to four antennas has become a commonplace, that resulted in the bottleneck of maximum data rate available in practice.

MU-MIMO alleviates such inefficiency by enabling simultaneous reception at multiple clients so that the number of spatial streams is governed by the total number of antennas embedded in the clients, not per-client. IEEE 802.11ac supports downlink MU-MIMO only, with up to four receivers and up to eight spatial streams, thus doubling the number of supported spatial streams in 802.11n.

Wider Bandwidth Channels

The widening of channel bandwidth, namely channel bonding, was first adopted in 802.11n, where the maximum channel bandwidth of 40 MHz is yielded by bonding two adjacent 20 MHz channels. When combining two channels, the theoretical data rate more than doubles since the guard band between the two bonded channels is removed. IEEE 802.11ac takes further steps to support 80 MHz and optionally 160 MHz channels by bonding adjacent channels. Moreover, to increase the probability of composing a 160 MHz channel, 802.11ac also allows to generate a 160 MHz channel by combining two physically non-adjacent 80 MHz channels, called 80+80 MHz.

However, the channel bonding has its drawbacks. IEEE 802.11 specification mandates that WLAN devices use below a maximum transmit power regardless of the usage of channel bonding. Therefore, by doubling channel bandwidth, the received SNR is effectively decreased by 3 dB. For example, the received SNRs of 40 MHz, 80 MHz, and 160 MHz is 3, 6, and 9 dB lower than that of 20 MHz. Moreover, to decode the wider bandwidth signal correctly, the sampling rate of analog-to-digital converter (ADC) should be increased according to the Nyquist's theorem [6]. Accordingly, the power consumption of ADC increases proportionally to the channel bandwidth.

Fig. 1.4 shows channel allocation map of 5 GHz unlicensed band in United States. There are some missing channel from 68 to 96 and from 120 to 128.[1] 40 MHz channel consists of two adjacent 20 MHz channels, and two adjacent 40 MHz channels form 80 MHz channel. Additionally, 160 MHz channel can be merged by two adjacent or separated 80 MHz channels. All 802.11ac devices are required to support 80 MHz

[1] Within the 5.47–5.73 GHz band, WLANs are considered secondary users, meaning they must avoid interfering with the primary band users. One of the primary band users is terminal-area Doppler weather radar (TDWR) at 5.59–5.65 GHz, a technology that monitors airport approaches for hazardous wind shear conditions [7].

channel bandwidth. It further adds a 160 MHz channel bandwidth option for even higher PHY rate.

For backward compatibility, IEEE 802.11ac has defined a transmission format of the PHY that replicates 20 MHz legacy PLCP protocol data unit (PPDU) transmission over multiple adjacent 20 MHz channels, refers to non-VHT duplicate PPDU. Moreover, the preamble of data frame in the bonded channel (e.g., 80 MHz or 160 MHz) takes the form of the replicated 20 MHz preamble structure. By means of this, the station which operates on 20 MHz channel bandwidth can detect and receive the preamble of the data in the bonded channel and the crucial control frames in the form of the duplicate PPDU, such as ready-to-send (RTS), clear-to-send (CTS), and acknowledgement (ACK), from the 802.11ac-enabled AP.[2]

Higher Order MCSs

MCSs are used to denote the combination of the number of modulation type and code rate. The highest order modulation in 802.11 WLAN has been 64-QAM ever since the adoption of the 802.11a. IEEE 802.11ac newly adopts 256-QAM, thus enabling encoding four times as dense as 64-QAM used by 802.11n. In the 160 MHz channel bandwidth (with 468 data subcarriers per OFDM symbol), a data rate of 866.7 Mb/s can be achieved with a single spatial stream using 256-QAM (i.e., 8 bits per sub-carrier per OFDM symbol), 5/6-rate coding, and a short guard interval, i.e., $8\,\text{(bits)} \times 468\,\text{(data sub-carriers)} \times \frac{5}{6}\,\text{(code rate)} \times 277.8\,\text{(ksym/s)}$. With the maximum number of spatial streams, i.e., eight, data rates up to 6.9 Gb/s are possible. Table 1.1 shows the detailed information of MCSs when 1 spatial stream and 20 MHz channel bandwidth are used.

[2]Due to the low data rate of the non-VHT duplicate PPDU, it is not used for data frames.

Table 1.1: MCS information with 1 spatial stream and 20 MHz channel bandwidth.

	Modulation	Code rate	Data rate (Mb/s)
MCS 0	BPSK	1/2	6.5
MCS 1	QPSK	1/2	13
MCS 2	QPSK	3/4	19.5
MCS 3	16 QAM	1/2	26
MCS 4	16 QAM	3/4	39
MCS 5	64 QAM	2/3	52
MCS 6	64 QAM	3/4	58.5
MCS 7	64 QAM	5/6	65
MCS 8	256 QAM	3/4	78
MCS 9	256 QAM	5/6	86.7

1.3 Overview of Existing Approaches

There exists a considerable body of research available in the literature that attempt to adapt to wireless channel fluctuations and to reduce the power consumption of Wi-Fi. Existing approaches can be classified into three categories: (1) rate adaptation, (2) MPDU length optimization, (3) channel estimation, (4) demystifying Wi-Fi power consumption, and (5) Minimizing Energy Consumption.

1.3.1 Rate Adaptation

Accurate rate selection in time-varying wireless channel for Wi-Fi systems has remained a challenging problem. CARA [8] and RRAA [9] continuously track the success/failure of packet transmissions to select the most appropriate PHY rate that maximizes the throughput.

SoftRate [10] and AccuRate [11] employ new methodologies which exploit the output information of DSP blocks during the receiver processing in order to enhance the accuracy and responsiveness against the channel variation.

However, these approaches rely on channel characterization at the granularity of frames (i.e., at the end of each frame reception), and hence, do not address the channel dynamics present within a frame.

1.3.2 MPDU Length Optimization

In [12, 13], the authors attempt to optimize the A-MPDU subframe length according to the signal-to-noise ratio (SNR) observed under the corresponding wireless channel condition. Their MPDU length selection mechanisms are, however, based on the subframe error rate corresponding to the measured SNR over the entire A-MPDU, effectively assuming that the error rate is uniform during the entire duration of the A-MPDU frame. As a result, even a modest variation in channel dynamics from the effective SNR may lead to poor choice of the length.

Our work in [14] develop mobility-aware frame aggregation, namely MoFA, which adaptively optimize the A-MPDU length. MoFA detects and estimates the degree of user mobility based on the success/failure statistics of each subframe, updated after receiving a BlockAck. Then, It decides an appropriate length with respect to the degree of user mobility.

1.3.3 Channel Estimation

Numerous channel estimation algorithms have been proposed to enhance the accuracy of the estimation in a rapid dispersive fading channel environment. The work done in [15, 16] can be used to estimate the wireless channel based on the linear interpolation of partial channel information, i.e., pilot signal. However, the technique is

inappropriate for 802.11n where the pilot subcarriers are not spaced closely to estimate the channel fluctuation of data subcarriers in frequency domain.

It is worth noting that the authors in [17] have proposed midamble-based channel estimation techniques for high mobility vehicular channel (e.g., 802.11p vehicle-to-vehicle communication specification [18]), and found to improve the performance but suffer from two major disadvantages: (1) protocol overhead incurred by addition of the midamble; and (2) deviation from the 802.11n standard. In particular, the latter makes it extremely costly and impractical for large-scale adoption by commercial 802.11n vendors.

Other notable techniques include spectral temporal averaging (STA) and constructed data pilot (CDP) estimation methods proposed in [19, 20], both of which also use the estimated transmit data symbols which can be obtained based on the information from the receiver's demapper to track the channel variation.

However, according to the results provided in [19, 20], the error rate performance appears too high to be acceptable in practical communication environment, because the information is obtained in the absence of error correcting. The authors in [21] have proposed the iterative channel estimation with postamble, the concept of which is similar to that of the turbo channel estimation [22]. Unfortunately, the requirement of the iterative operation brings high computational complexity which is undesirable for Wi-Fi. Moreover, the postamble causes incompatibility with the 802.11n standard.

1.3.4 Demystifying Wi-Fi Power Consumption

In [23], the authors measure the power consumption of off-the-shelf IEEE 802.11n NIC with various operating states. The most recent work in [24] provides the synthetic view of 802.11ac devices' performance including the energy efficiency. These however do not present an in-depth study of Wi-Fi power consumption and make some

inadequate conclusions as discussed in Chapter 5.

1.3.5 Minimizing Energy Consumption of Wi-Fi

In IEEE 802.11 standard [1], several power saving schemes have been defined to reduce the power consumption. Power save mode (PSM) is a basic power saving protocol that allows Wi-Fi station to suspend all activity in sleep mode, then wake up periodically to receive beacons which indicate the existence of pending frames at the access point (AP). Automatic power save delivery (APSD) is also defined to allow stations to save power without performance degradation of delay-sensitive traffic. IEEE 802.11n defines power save multi-poll (PSMP), which enables AP to schedule and announce reception and transmission instants of multiple stations such that stations can avoid receiving others' exchanges. It is known that APSD and PSMP are not commonly used in practice.

After adopting MIMO in Wi-Fi, energy saving techniques for MIMO have been introduced. In IEEE 802.11n, spatial multiplexing power save (SMPS) is defined to make stations save energy by allowing stations to activate only a single RF-chain in idle period [1]. CMES [25] finds most energy efficient transmit and receive RF-chain setting, and furthermore, EERA [26] searches the most energy efficient PHY rate considering MIMO.

Downclocking Wi-Fi radio also enables energy saving. Samplewidth adaptively determines optimal bandwidth according to the distance between a sender and a receiver [27]. SloMo and Enfold propose downclocked reception to reduce Wi-Fi power consumption [28, 29], while E-MiLi downclocks the radio of Wi-Fi in idle period to minimize energy spent while enabling normal clock to receive/transmit frames [30]. The radio downclocking in wider bandwidth is standard-incompliant and requires costly modifications.

1.4 Main Contributions

In this dissertation, we propose some compelling algorithms, intra-frame rate adaptation and enhanced channel estimation and tracking, to improve the performance and robustness of the emerging Wi-Fi, i.e., IEEE 802.11n and IEEE 802.11ac based WLAN, for the pedestrian mobile users. Furthermore, we present a new power save mode and protocol to minimize the traumatic energy cost of IEEE 802.11n/802.11ac-enabled devices. More into detail, the research contributions of the dissertation are summarized as follows.

1.4.1 Impact of Mobility Analysis

we thoroughly study the impact of the pedestrian user mobility by conducting experiments using off-the-shelf IEEE 802.11n device to analysis the wireless channel dynamics. Based on our measurement results, the wireless channel is abruptly fluctuated when A-MPDU is used. Then, we investigate the impact of the wireless channel dynamics on the performance of A-MPDU in terms of throughput and robustness. The results reveal that the subframe error of A-MPDU dramatically increases along with the increase in the gap between the preamble and the corresponding subframe. Moreover, in order to better understand the root causes of the unreliability of A-MPDU in fast time-varying environments, we analyze how badly the OFDM symbols are distorted by the use of the baseline 802.11 channel estimation and compensation techniques which exploit the CSI from the preamble. The dispersion of the received OFDM symbol at the latter part of A-MPDU is much larger than that at the front part of A-MPDU. Therefore, we conclude that the performance degradation are induced by inaccurate CSI which is only estimated at the beginning of A-MPDU frame and used throughout the entire frame.

1.4.2 Intra-frame Rate Adaptation

Motivated by the strong evidence that the changes in channel conditions during a frame reception leads to poor Wi-Fi performance with user mobility and increased frame length. we propose SNR-aware Intra-frame Rate Adaptation Algorithm (SIRA) which allows the transceivers to effectively adapt the PHY rates within an individual frame. SIRA defines and uses the primary-secondary MCS pairs adaptively for a specific frame when user mobility is detected based on the PHY information. We further minimize the feedback overhead via zero-overhead feedback to notify the presence of user mobility from the receiver to the sender.

1.4.3 Enhanced Channel Estimation and Tracking

In addition, we propose Channel-Aware Symbol Error Reduction (ChASER), a novel standard-compliant channel tracking scheme that constantly updates the CSI during the entire course of the frame reception process. This is done by reconstructing the transmitted data symbols (in parallel with the normal receiver processing) and comparing it to the received data symbols so that the channel response can be estimated at any part of the frame at the granularity of a data symbol. Since reconstructing transmitted data symbols reliably (with minimum errors) and quickly (within the frame processing time) is the key enabler for symbol-level channel estimation and tracking, ChASER wittingly reuses the exactly same modulation and coding operations available in the transmitter's signal processing blocks (DSP) with the addition of a low-complexity adaptive filter. The adaptive filter is required to alleviate the error propagation incurred by falsely reconstructed data symbols. Furthermore, no extra protocol overhead is needed, and the estimation process can be done in parallel with the decoding process. With a ChASER-enabled Wi-Fi receiver, the CSI obtained from the preamble is replaced whenever a new CSI is estimated until the frame reception processing ends.

1.4.4 802.11ac Power Consumption Analysis

We model the power consumption characteristics of the 802.11ac NIC and present synthetic analysis on the power consumption of the commercial state-of-the-art IEEE 802.11ac hardware. It is shown that the proposed model accurately captures the power consumption characteristics with high fidelity, at most 2.3% estimation error for all of 1719 possible parameter combinations. From this, we reveal that it consumes the energy unnecessarily due to its inherent nature. So, considering wider channel bandwidth originated by channel bonding becomes increasingly important to save idle and receive state energy for the 802.11ac-enabled Wi-Fi which mandates the channel bonding up to 80 MHz.

1.4.5 Energy Efficient Bandwidth Management

Finally, we propose a new power save operation as well as the corresponding protocol, called Wi-Fi in Zizz (WiZizz), which judiciously exploits the characteristic of the channel bonding defined in IEEE 802.11ac and efficiently handles the channel bandwidth in an on-demand manner to minimize the traumatic energy spent by IEEE 802.11ac devices. Our extensive measurement and simulation show significant performance improvement (up to 73% energy saving) over a wide range of communication scenarios. In addition, the feasibility of easy implementation is demonstrated by a prototype with a commercial 802.11ac device. To the best of our knowledge, WiZizz is the first IEEE 802.11ac-congenial energy efficient bandwidth management while other existing approaches require costly modifications of the IEEE 802.11ac specification.

1.5 Organization of the Dissertation

The rest of the dissertation is organized as follows. Chapter 2 introduce the background of our work and the experiment study on the performance degradation of IEEE 802.11n-enabled device in mobile environments.

In Chapter 3, we present the proposed intra-frame rate adaptation algorithm for selecting the appropriate PHY rates on intra-frame basis by using PHY information without any protocol overhead.

Chapter 4 presents a novel, low-complexity, standard-compliant channel estimation and tracking design that achieves remarkably high performance even in the presence of pedestrian user mobility and frame aggregation.

Chapter 5 introduce the measured power consumption of an off-the-shelf IEEE 802.11ac chipset by considering the various IEEE 802.11 ac features described above. We also presents the proposed power model of the commercial IEEE 802.11ac-enabled NIC which accurately captures the power consumption characteristics of the NIC.

In Chapter 6n we propose a practical and energy efficient bandwidth management method which handles the active bandwidth of IEEE 802.11ac receiver to save the energy cost in idle and receive state with the simple modification of IEEE 802.11ac standard.

Finally, Chapter 7 concludes the dissertation with the summary of contributions and discussion on the future work.

Chapter 2

Impact of Mobility

2.1 Introduction

In this chapter, we present a brief description of the channel estimation and tracking method defined in the IEEE 802.11 standard. It is then followed by our extensive experiment study to demonstrate the impact of user mobility on performance of IEEE 802.11n-enabled device.

2.2 Background

In this section, we first describe briefly the IEEE 802.11 MAC/PHY features and operations considered in this dissertation briefly.

2.2.1 Channel Estimation and Compensation

Due to fading, shadowing, and other interference sources, the transmitted signal through wireless channel experiences multiplicative distortions. To cope with them, many of the IEEE 802.11 standards (e.g., 802.11n and 802.11ac) require the receiver function

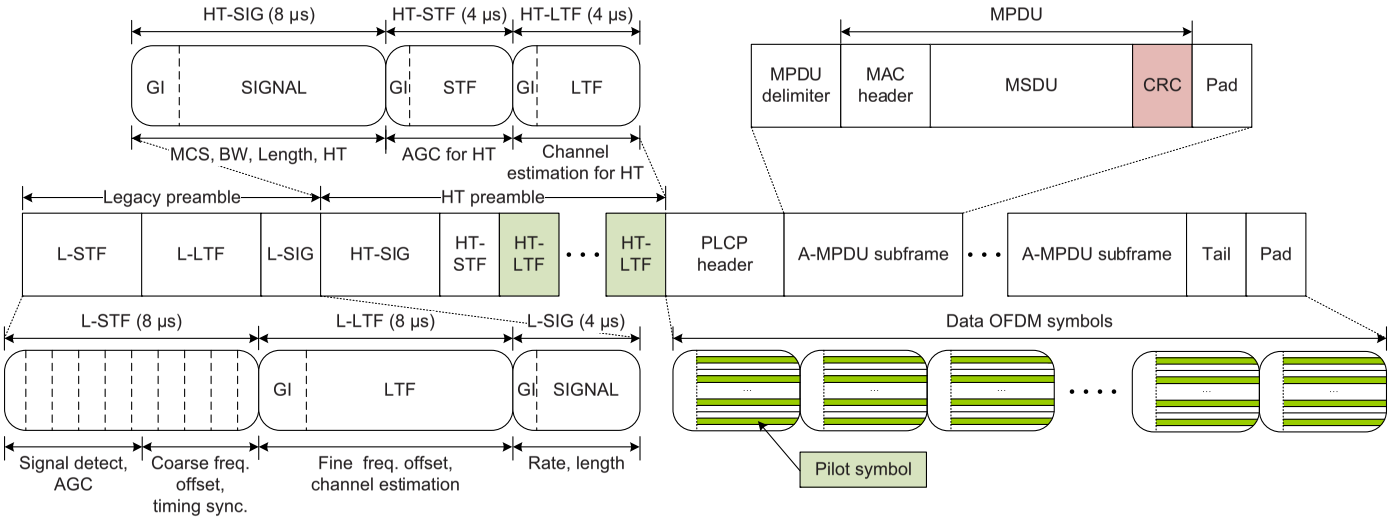

Figure 2.1: IEEE 802.11n MAC/PHY mixed-mode PPDU frame format of A-MPDU.

to measure the CSI at the beginning of the reception using the PLCP preamble. As shown in Fig. 2.1, the 802.11n PLCP preamble includes legacy preamble (from IEEE 802.11a) and high-throughput (HT) preamble (a new field added in IEEE 802.11n).[1]

Each PLCP preamble carries short training field (STF), long training field (LTF), and signal (SIG) field. The legacy STF (L-STF) is used for signal detection, automatic gain control (AGC), time synchronization, and coarse frequency offset estimation. L-LTF is composed of two repetitions of known long training sequences used for CSI estimation and fine frequency acquisition. On the other hand, the purpose of HT-STF is to improve AGC for MIMO system. HT-LTF also aims to estimate CSI by considering the additional HT features, i.e., MIMO and the increased number of subcarriers. In general, 802.11 devices commonly use least-squares (LS) estimation to obtain CSI, $\widetilde{H}$, given by

$$\widetilde{H} = \frac{Y_{\mathrm{LTF}}}{X_{\mathrm{LTF}}}, \tag{2.1}$$

where Y_{LTF} is the received LTF symbol corresponding to the transmitted known LTF sequence, X_{LTF}.

The receiver compensates the distorted OFDM data symbols by using the CSI obtained from LTF. The extent that the compensated received symbols in I-Q plane are dispersed from their ideal positions depends on the accuracy of the estimated CSI. Therefore, if wireless channel varies swiftly and considerably during the reception of a single frame, the CSI obtained at the PLCP preamble is likely to be inadequate to compensate the channel for the symbols belonging to the latter part of the frame.

[1]The 802.11n defines two PPDU formats, called *mixed* and *greenfield*. The greenfield format is rarely used due to the incompatibility with legacy devices In this dissertation, we consider the mixed format only.

2.2.2 Role of Pilot Subcarriers

Signal distortion between transmitter and receiver is caused not only by wireless channel, but also by symbol timing offset (STO). The STO stems from clock mismatch between transmitter and receiver, and is linearly proportional to the subcarrier index [31]. In 802.11n 20 MHz OFDM symbol, as shown in Fig. 2.1, four evenly spread pilot subcarriers are inserted to transmit predefined information [1]. The phase difference caused by STO can be eliminated by interpolating the measured phase offset values from these pilot symbols.

However, pilots are insufficient to track the CSIs for all the subcarriers. Typically, the maximum root mean square (RMS) channel delay spread (σ_τ) considered in 802.11 WLAN is about 250 ns long, corresponding to the 90% coherence bandwidths,[2] $B_{c,90\%} = 1/50\sigma_\tau = 80$ kHz, which is much smaller than the spacing between two consecutive pilots in frequency domain, i.e., 4,375 kHz [32]. Thus, the receiver cannot estimate the CSI of all the subcarriers using pilot subcarriers alone.[3]

In summary, even though there are mechanisms designed to track the channel status for the entire frame, i.e., preamble and pilots, if the channel varies significantly during the duration of the frame, the CSI obtained from them might not be sufficiently accurate to decode a long frame, especially when the transmission duration is much longer than the channel coherence time.

[2] $B_{c,x\%}$ is the bandwidth where the autocorrelation of the channel in the frequency domain is equal to $x\%$ of the peak.

[3] In the case of LTE system, reference signal similar to the pilot symbols of Wi-Fi is used to estimate the CSI of data symbols. Unlike LTE, since the pilot subcarrier spacing of Wi-Fi is much larger than the coherence bandwidth, the pilots are inappropriate to estimate the CSI of the whole bandwidth [33].

2.2.3 Frame Aggregation

To improve the network efficiency, 802.11n and 802.11ac have defined frame aggregation scheme, e.g., A-MPDU [1, 2]. When applying A-MPDU, the transmission is conducted on the basis of a frame consisting of several aggregated MPDUs, by which the proportion of the protocol overheads, such as channel access delay, is reduced compared to the single MPDU-based legacy protocol. Each MPDU is called subframe of the A-MPDU. Moreover, A-MPDU allows each subframe to be individually acknowledged and selectively retransmitted thanks to the usage of cyclic redundancy check (CRC) at the end of each subframe.

However, the aggregation leads to longer frame duration and less correlation between CSI of the first and the last parts of the frame. Specifically, the default maximum PPDU duration, $T_{\max}$, of 802.11n (10 ms) is likely to be longer than the channel coherence time.

2.3 Measurement Study

In this section we first quantify the changes of wireless channel behaviors affected by pedestrian mobility based on the CSI measurement study. Then, based on the extensive experiments, we show the significant degradation of Wi-Fi performance when A-MPDU is enabled in the pedestrian mobile environment, and reveal its causes which led to the design of our proposed algorithms.

2.3.1 Experimental Settings

We have conducted our experiments in a controlled office environment, i.e., the basement of INMC building at Seoul National University, Korea. Figure 2.2 illustrates the floor plan used for our experiments, and points P1 to P9 represent different locations

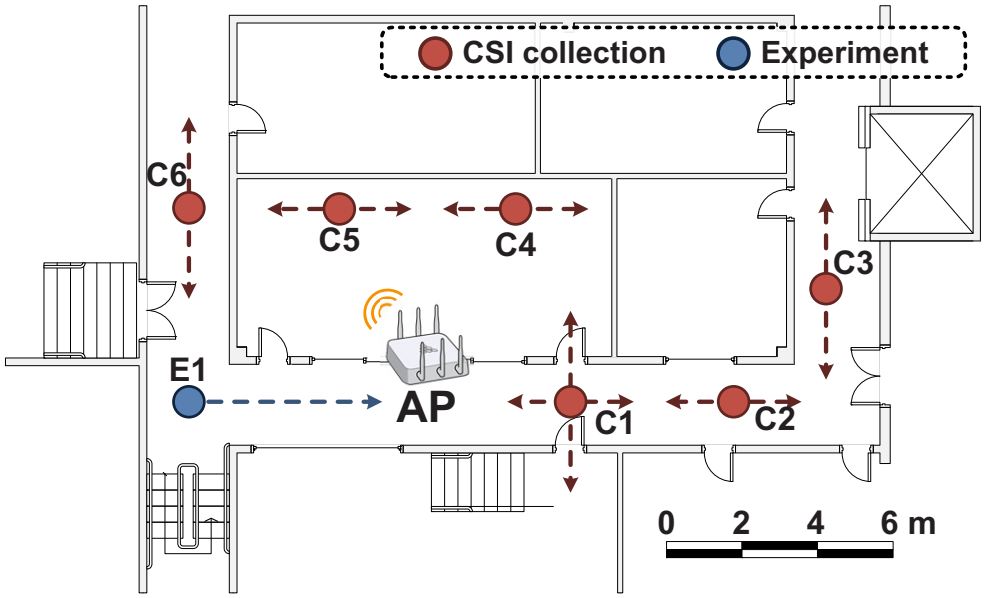

Figure 2.2: Topology.

where stations are located. IEEE 802.11n devices supporting A-MPDU, 3x3 MIMO (SM and STBC), and 40 MHz channel bonding are used. The operating channel number 44, i.e., 5,220 MHz center frequency, is used, where no external interference has been detected. We mainly use a programmable 802.11n device, Qualcomm Atheros AR9380 NIC, along with *hostAP* [34] to build an AP on a *Ubuntu* 10.04 machine [35]. Both AR9380 and IWL5300 (from Intel) NIC are utilized on the station side to consider various Wi-Fi devices [36]. We generate UDP downlink traffic from AP to stations using *Iperf* 2.0.5 to generate fixed length frames (of 1,534 bytes including MAC header), and control the frame aggregation time bound by modifying the device drivers *ath9k* and *iwlwifi* for AR9380 and IWL5300, respectively [37, 38].

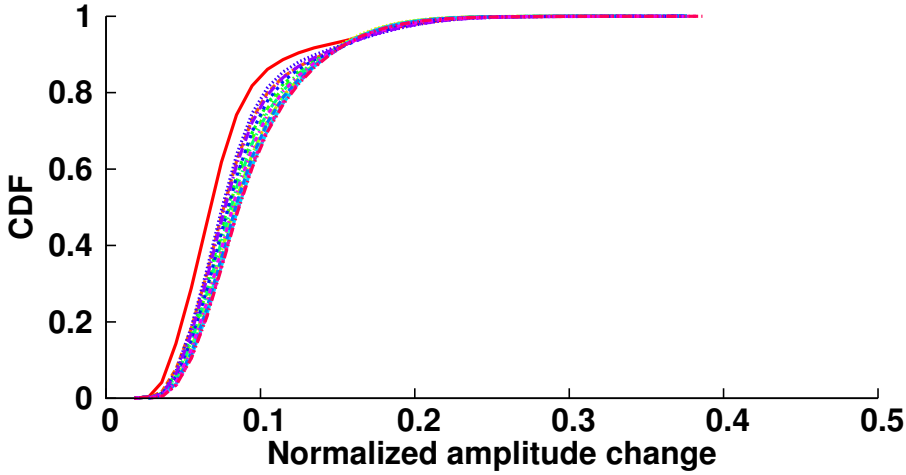

(a) Static trace

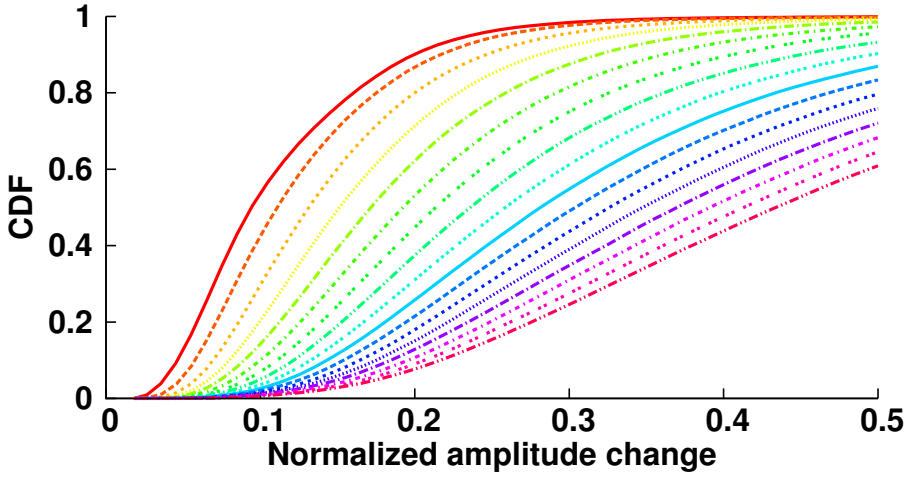

(b) Mobile trace

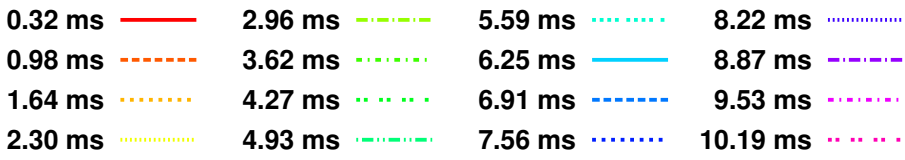

Figure 2.3: Normalized amplitude changes of the measured CSI with time gap, τ.

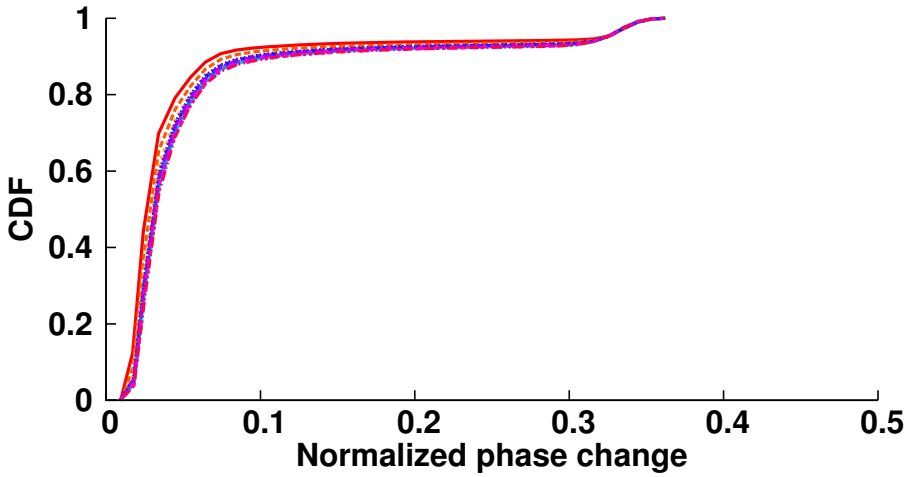

(a) Static trace

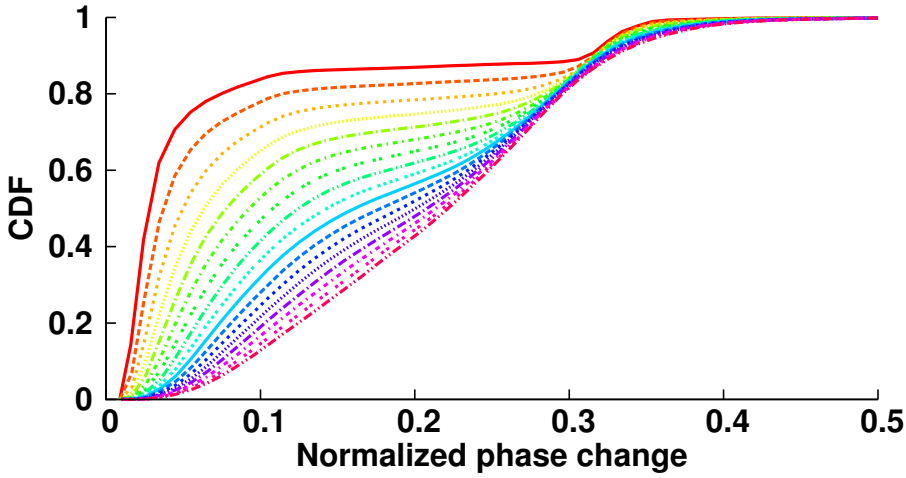

(b) Mobile trace

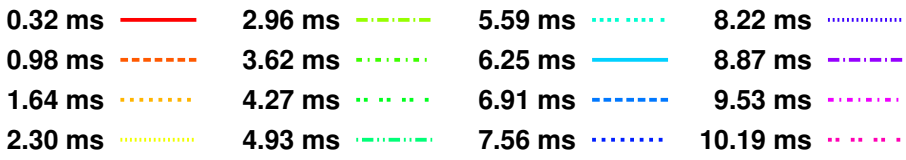

Figure 2.4: Normalized phase changes of the measured CSI with time gap, τ.

2.3.2 Temporal Selectivity

We now analyze the temporal selectivity of the real wireless channel to quantify the degree of variation of wireless channel during $T_{\max}$, i.e., 10 ms in static and mobile scenarios.

We first use Intel Wi-Fi Link (IWL5300) network interface card (NIC) and the modified device driver to collect CSI trace from HT-LTF of each successfully received frame [36, 39]. We collect 14 traces with various speeds of the receiver at different locations (red points in Fig. 2.2). Each CSI contains the complex channel frequency responses, which represent amplitude and phase differences between transmitter and receiver, of 30 OFDM subcarriers.[4] To build the actual channel response experienced by data OFDM symbols, we eliminate the phase offset induced by STO or sampling clock difference between transmitter and receiver, which is the same functionality of pilot subcarriers as described in the previous section. For the mobile scenario, we walked with the device at approximately 1 m/s speed.

We employ the following metrics which represent the normalized amplitude changes (∇_A) and phase changes (∇_θ) to evaluate the temporal selectivity [40]:

$$\begin{aligned} \nabla_A(\tau) &= \frac{\|A(t) - A(t+\tau)\|_2}{\|A(t+\tau)\|_2}, \\ \nabla_\theta(\tau) &= \frac{\|\theta(t) - \theta(t+\tau)\|_2}{\sqrt{\sum_{N_{sc}} \pi^2}}, \end{aligned} \tag{2.2}$$

where the vectors $A(t)$ and $\theta(t)$ represent all the subcarriers' amplitudes and phases of the frame received at t, respectively, and τ is the time gap. $\|\cdot\|_2$ is the l^2-norm, and τ varies from 250 μs to 10 ms. In this case, phase change is normalized by π, of which 10% change is equivalent to 0.314 radians or 18°.

[4]The device driver we used just reports the channel responses of a group of 30 subcarriers instead of all the 56 subcarriers.

Figs. 2.3 and 2.4 show the cumulative distribution functions (CDF) of $\nabla_A(\tau)$ and $\nabla_\theta(\tau)$ between the CSI of two frames with varying τ. As shown in Figs. 2.3(a) and 2.4(a), $\nabla_A(\tau)$ and $\nabla_\theta(\tau)$ remain relatively steady in the static scenario. More than 80% of samples show the changes within 10% even if τ is 10 ms.

However, the amplitude and phase variations increase with τ in the mobile scenario as shown in Figs. 2.3(b) and 2.4(b). When τ is set to 10 ms, $\nabla_A(\tau)$ and $\nabla_\theta(\tau)$ vary by more than 10% between two CSIs for over 99% and 95% of samples, respectively.

Consequently, both amplitude and phase response of the latter part frame are expected to considerably deviate from the values predicted by the CSI estimated at the PLCP preamble when using A-MPDU, and hence the symbols at the latter part is compensated by a false CSI. Thus, the preamble-based channel estimation is highly unreliable when employing A-MPDU and users are mobile.

2.3.3 Unreliability of A-MPDU in Mobile Environments

In order to verify the observation that the latter part of an A-MPDU is likely to suffer from more severe decoding error, we have conducted measurement using off-the-shelf 802.11n devices, which support A-MPDU. We use the AP described in Section 2.3.1 and use both Qualcomm Atheros AR9380 and IWL5300 NICs on the station side. Our experiments operate at 5.22 GHz unlicensed band in a controlled office environments; no interference is observed.

We place the station device approximately 5 m away from the AP (**E1** in Fig. 2.2), where the distance is relatively short such that frames can be transmitted with the highest rate (i.e., MCS 7 with 64QAM and 5/6 code rate) almost perfectly. Then, we carry the station and walk towards the AP at two pedestrian speeds of 0.5 and 1 m/s until we arrive at the AP. We let the AP transmit frames whose size is 1,538 bytes continuously with MCS 7. The results are averaged over 5 runs.

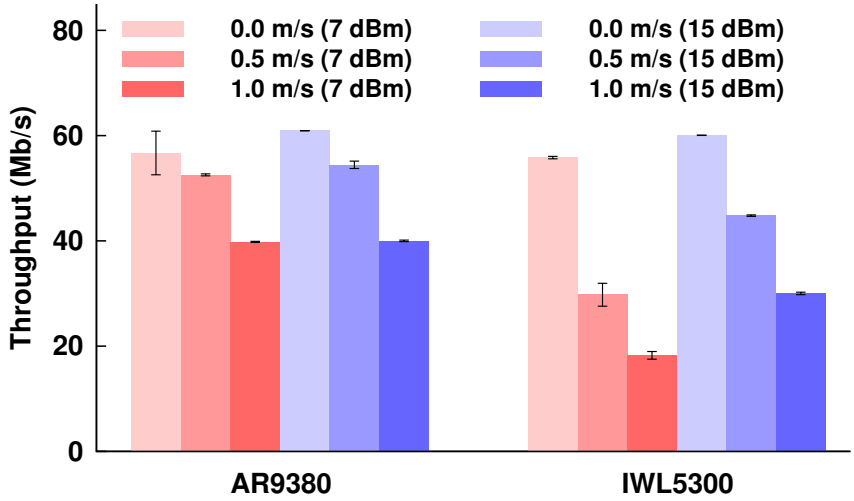

(a) Throughput perfromance.

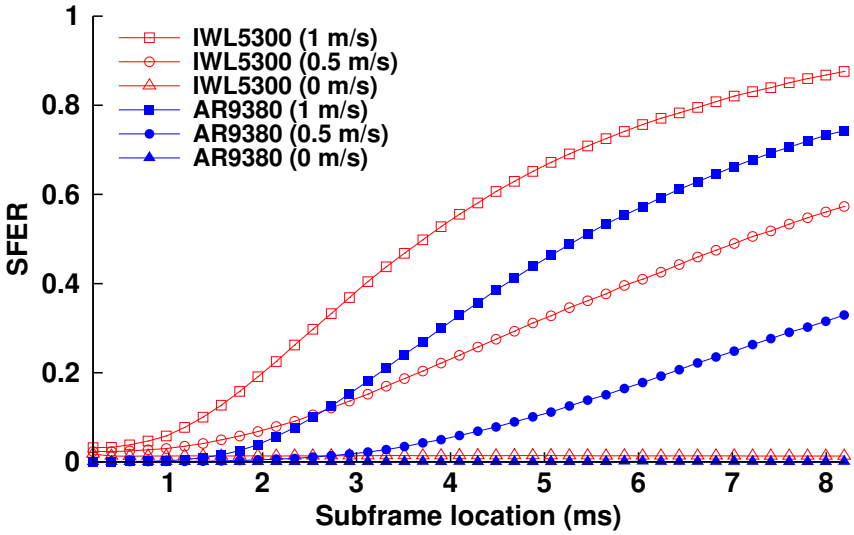

(b) SFER perfromance.

Figure 2.5: Measured robustness of A-MPDU. The subframe location indicates the beginning of the transmission of the corresponding subframe relative to the beginning of the entire frame in ms.

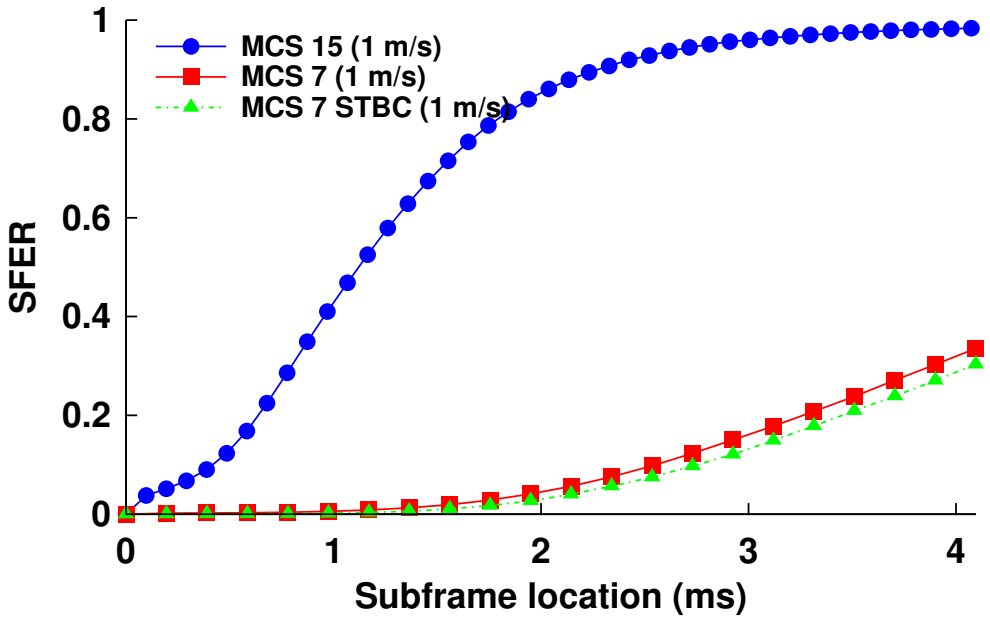

Figure 2.6: SFER performance with MIMO features.

We first investigate whether there exists significant performance degradation in mobile scenarios. Fig. 2.5(a) depicts that the throughput decreases regardless of the NIC type and transmit power, as the degree of the mobility increases. Note that the wireless channel between the AP and the station is pretty good in terms of signal-to-noise ratio (SNR). As an evidence, the results of the static case (0 m/s) achieve almost maximum throughput performance. However, in the case of the mobile scenario, the losses of throughput for both AR9380 and IWL5300 are as high as one third and two thirds, respectively

Fig. 2.5(b) shows the SFER performance for three different mobility scenarios (0, 0.5, and 1 m/s) for two different Wi-Fi devices. SFER represents the frame error rate of a certain subframe, through which we can examine the relationship between subframe error rate and the subframe location. In the static case (0 m/s), the SFER holds rela-

tively steady regardless of the subframe locations. However, when we walk towards the AP, even though the AP and station are getting closer, the SFER dramatically increases along with the increase in the gap between the preamble and the respective subframe. Moreover, the slope of SFER curves becomes higher as the speed of the station increases.

We then conduct experiments by enabling MIMO at the AP side. As shown in Fig. 2.6, the SFER is further deteriorated when spatial multiplexing (i.e., MCS 15) is enabled. Besides, the MCS 7 with STBC, which exploits diversity gain to increase the robustness of communication, shows similar performance to that without STBC, because MIMO techniques require a more accurate channel estimation and compensation procedure to eliminate the spatial interference. We call such losses *caudal losses* as they tend to appear more frequently towards the end of the frame.

2.3.4 Relation between Symbol Dispersion and Mobility

In order to better understand the root causes of caudal losses, we investigate how badly the OFDM symbols are distorted by the use of CSI from the preamble in mobile scenarios. This experiment have been conducted using the Sora platform which contains the open source implementation of 802.11a specification [41]. Our testbed operates at 5.22 GHz band and all the experiments have been done under a clean channel environment; no interference signal was detected throughout the test. We first install the programmable AP equipped with AR9380 NIC, $ath9k$, and $hostap$ [34, 37, 42]. We let Sora operate as the receiver of the AP, whose downlink buffer is always filled with A-MPDUs, each of which consists of several 1000-byte MPDUs. Since Sora testbed is too heavy to move swiftly, we moves the AP at an approximately, pedestrian speed, e.g., 0 m/s, 0.3 m/s, 0.6 m/s, and 1 m/s on average, and sets the transmission rate as

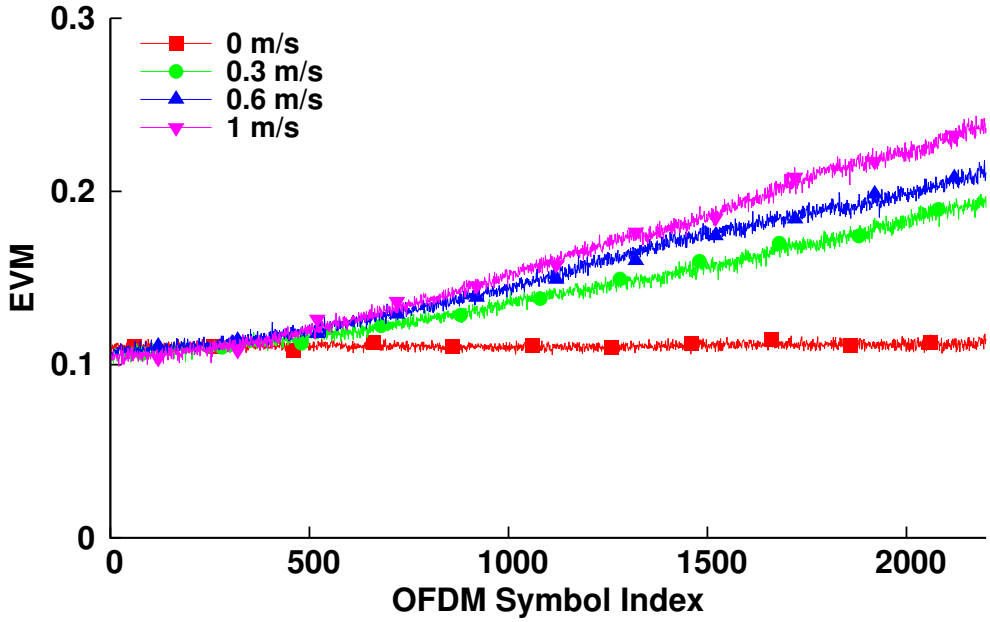

Figure 2.7: Pilot symbol dispersion.

MCS 3 (16QAM and 1/2 code rate).[5]

Let Y be the compensated received symbol position and X be its ideal position in I-Q plane. The amount of symbol dispersion is then defined as $\frac{|Y-X|}{|X|}$, so-called error vector magnitude (EVM) [43].

Fig. 2.7 shows the average pilot symbol dispersion for each OFDM symbol when the sender moves at an approximately constant speed of 0 m/s, 0.3 m/s, 0.6 m/s, and 1 m/s. Note that since we must know the symbol's ideal position, X, to calculate EVM, we use the known pilot symbols instead of unknown data symbols. In mobile environments, the dispersion increases as OFDM symbol index increases, which means the

[5]Since Sora is inherently lack of fine AGC operation, we tuned the receiver gain offline to an appropriate value. Thus, the AP should move over relatively short distances (e.g., 1 m) so that the tuned value can be valid for a while. Moreover, because the capabilities of RF front-end of Sora is far from being decent, it is difficult to use a higher order MCS, e.g., MCS 7.

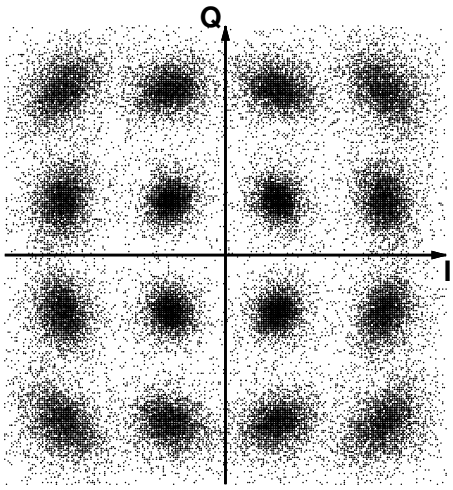

(a) Data symbol dispersion at the front part of A-MPDU.

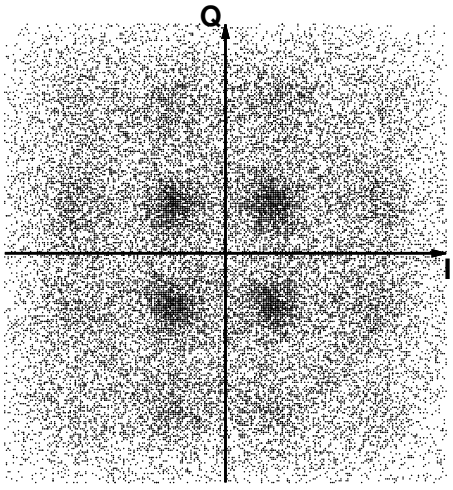

(b) Data symbol dispersion at the latter part of A-MPDU.

Figure 2.8: Symbol dispersion increases in the presence of user mobility. All symbols are corrected by CSI and pilots.

compensated symbol moves gradually farther away from its ideal position. Furthermore, the slope of EVM curves becomes higher as the average speed of the sender increases. However, when the sender holds its location, the dispersion is stable regardless of OFDM symbol index. In the case, since the dispersion is only affected by the random noise, the wireless channel variation between two transceivers is quite stable.

Figs. 2.8(a) and 2.8(b) show the received data symbol positions derotated by CSI from LTF when the sender moves at an average speed of 1 m/s. In the case of front part symbols, those are located in the vicinity of 16QAM signal constellations. On the other hands, the symbol dispersion at the latter part of A-MPDU is much larger than that at the front part of A-MPDU.

As we explain in Section 2.2.1, the dispersion mainly depends on the accuracy of the CSI used for compensating the distorted symbols. Therefore, we conclude that the caudal losses are induced by inaccurate CSI which is only estimated at the beginning of A-MPDU and pilots are insufficient to track the channel variation during a specific A-MPDU duration.

2.4 Summary

In summary, we thoroughly study the impact of the pedestrian user mobility. Based on our measurement results, the wireless channel is abruptly fluctuated in terms of amplitude and phase during a single A-MPDU frame duration in mobile environments.

Then, we investigate the impact of the wireless channel dynamics on the performance of A-MPDU in terms of throughput and robustness. The results reveal that the subframe error of A-MPDU dramatically increases along with the increase in the gap between the preamble and the corresponding subframe.

Moreover, in order to better understand the root causes of the unreliability of A-

MPDU in fast time-varying environments, we analyze how badly the OFDM symbols are distorted by the use of the baseline 802.11 channel estimation and compensation techniques which exploit the CSI from the preamble. The dispersion of the received OFDM symbol at the latter part of A-MPDU is much larger than that at the front part of A-MPDU.

Therefore, we conclude that the performance degradation are induced by inaccurate CSI which is only estimated at the beginning of A-MPDU frame and used throughout the entire frame.

Chapter 3

SIRA: SNR-aware Intra-frame Rate Adaptation

3.1 Introduction

Recently, Wi-Fi, wireless local area network (WLAN) technology based on IEEE 802.11, has been spotlighted as one of promising wireless network technologies. With the ever-increasing demand for high-throughput WLANs, IEEE-802.11 have allowed higher physical layer (PHY) rates and added MAC protocol/service data unit (MPDU/MSDU) aggregation mechanisms [1]. The improvement in throughput and efficiency leads to significant growth in the take-up of Wi-Fi equipped *mobile* devices, such as smartphone, tablet, and wearable devices. Accordingly, handling the mobility for the emerging Wi-Fi devices becomes increasingly important.

In this chapter, an intra-frame rate control algorithm (Intra-RCA), called SNR-aware Intra-frame Rate Adaption (SIRA), is proposed to enhance the system performance of Wi-Fi in fast time-varying environments. Widely used inter-frame rate control algorithms (Inter-RCA), which select the physical layer (PHY) rate of each frame based on the time averaged frame loss rate and the signal strength statistics, perform poorly for a long aggregate MAC protocol data unit (A-MPDU) due to the channel

variation in mobile environments. Unlike the previous approaches, SIRA adapts the PHY rate on intra-frame basis, i.e., the PHY rate is updated in the middle of a frame according to user mobility. The performance of the proposed scheme is also evaluated by a trace-driven link level simulator employing the collected channel traces from real measurements. The simulation results show that SIRA outperforms the standalone Inter-RCA in all tested traces.

3.1.1 Revisit of Rate Adaptation Algorithms

Rate adaptation is one of the key technologies to reflect the impact of user mobility. The well-known rate adaptation schemes, automatic rate fallback (ARF) and collision-aware rate adaptation (CARA), make rate decision based on frame loss statistics, but their adaptation speed is slow [44, 45]. Other algorithms such as receiver-based auto rate (RBAR) and SNR-guided rate adaptation (SGRA) [46, 47] utilize PHY information, specifically, SNR to improve the responsiveness and accuracy. These SNR-based rate adaptation algorithms, however, have a limitation in the use for fast time-varying channel because the relationship between bit error rate (BER) and SNR changes in different propagation environments [48]. Also, a constellation-based rate estimation algorithm has been proposed to overcome the limitation of the SNR-based rate adaptation algorithms, but it has extremely high computational complexity [10, 11]. All these algorithms are inter-frame rate control algorithms (Inter-RCAs) that assume wireless channel to be invariant throughout one frame duration, thus the same modulation and coding scheme (MCS) is used within a specific frame.

However, as stated in Section 2.3.2 the assumption of quasi-stationary channel over one frame duration is proved to be invalid, since the state-of-the-art Wi-Fi devices commonly employ long aggregate MPDU (A-MPDU) frames. A-MPDU unfetters the repressed PHY rate originated from MAC/PHY overhead by amortizing the overhead

over multiple MPDUs aggregated in a single frame. Nevertheless, A-MPDU requires long frame duration, e.g., the maximum 10 ms, which exceeds the coherence time frequently in mobile environments. Our experimental results confirm that the use of A-MPDU aggravates frame reception capability for mobile users, even if an appropriate PHY rate is chosen by Inter-RCA due to the *caudal losses* as presented in Section 2.3.3.

3.1.2 Channel and Mobility Condition

The caudal losses are not originated by fading, shadowing, and the noise of the RF hardware (channel condition), but by the gap between the CSI from the preamble and time-variant channel (mobility condition). We believe that it is important to differentiate channel condition from mobility condition. If the transmitter does not differentiate both conditions to choose the transmit PHY rate, most Inter-RCA may select more robust MCS even when the received signal strength (RSS) is strong enough due to the caudal losses. The use of the selected MCS is undesirable for the subframes located at the front part of A-MPDU, and decreases the overall throughput performance.

Since the existing algorithms have considered only the channel condition, more sophisticated rate adaptation algorithms utilizing the mobility condition need to be developed for Wi-Fi mobile devices.

3.2 Proposed Algorithm

The proposed rate adaptation algorithm, SIRA consists of four procedures: (1) pilot-based SNR estimation, (2) unequal MCS, (3) mobility detection, and (4) zero-overhead feedback.

3.2.1 Pilot-based SNR Estimation

In developing an algorithm which quickly adapts the PHY rate by considering mobility condition, two issues must be addressed: the differentiation of the loss caused by the mobility condition from the loss caused by the channel condition, and the determination of the starting point, I_U, where the OFDM symbols begin to suffer severe BER due to the inaccurate CSI.

To solve these issues, we use the estimated SNR obtained by PHY information, i.e., EVM, as the root mean squared value of the difference between the received symbol (S_r) and the corresponding transmitted symbol (S_t). Using the relationship between SNR and $\mathrm{EVM}_{\mathrm{rms}}$, if the number of the received symbols (N) is large, SNR can be obtained as follows [49]:

$$\mathrm{SNR} = \frac{E_s}{N_0} \approx \frac{1}{\mathrm{EVM}_{\mathrm{rms}}^2} = \frac{\frac{1}{N}\sum_{n=1}^{N} |S_t(n)|^2}{\frac{1}{N}\sum_{n=1}^{N} |S_r(n) - S_t(n)|^2}, \tag{3.1}$$

where $N_0/2$ is the noise power spectral density and E_s is the average symbol energy.

Since it is difficult to obtain $\mathrm{EVM}_{\mathrm{rms}}$ from unknown data symbols, we exploit the known pilot symbol sequence. However, each OFDM symbol has very small number of pilots, i.e., the number of pilots per an OFDM symbol, N_p is 4 or 6 for 20 or 40 MHz channel bandwidth, respectively. Thus, we group N_i pilots corresponding to N_S OFDM symbols into a received pilot group, $\mathbf{P}_i^{\mathrm{rx}} = \left[p_{i,1}^{\mathrm{rx}}, p_{i,2}^{\mathrm{rx}}, \cdots, p_{i,N_i}^{\mathrm{rx}}\right]$, $N_i = N_S \times N_p$. Let $p_{i,j}^{\mathrm{rx}}$ be the j^{th} pilot sample in the i^{th} received pilot group ($\mathbf{P}_i^{\mathrm{rx}}$) corresponding to the i^{th} transmitted pilot group, $\mathbf{P}_i^{\mathrm{tx}}$. The receiver then estimates SNR_i based on Eq. (3.1), for each group i of symbols:

$$\mathrm{SNR}_i = \frac{E_s}{\frac{1}{N_i}\sum_{j=1}^{N_i} \left| p_{i,j}^{\mathrm{rx}} - p_{i,j}^{\mathrm{tx}} \right|^2}, \qquad 1 \le i \le K, \tag{3.2}$$

where K is the number of pilot groups in an A-MPDU.

SNR_i is proportional to the accuracy of CSI which is defined as the similarity between the CSI from LTF and the channel response experienced by the group i. For example, SNR_i is very high for perfect CSI. Based on the SNR distribution, $\underline{\mathbf{SNR}} = [\mathrm{SNR}_1, \mathrm{SNR}_2, \cdots, \mathrm{SNR}_K]$, the mobility detection and the determination of I_U are performed.

3.2.2 Mobility Detection

Using the SNR distribution, SIRA decides the presence of the mobility at the receiver side. In mobile environments, the accuracy of CSI and SNR monotonically decrease during a frame reception due to the fact that the human mobility pattern does not change significantly within a single A-MPDU duration (e.g., 10 ms, the maximum frame duration [1]). Otherwise, the accuracy and SNR slightly fluctuate in static environments and abruptly change under the interference.

To demonstrate this phenomenon, we have developed a trace-driven link level simulator described in Section 3.3.1. Fig. 3.1 shows that the average EVM monotonically increases as the OFDM symbol index increases in mobile traces, whereas it remains steady in static trace. In addition, if there is hidden interferer, the measured EVM at the receiver side sharply increases. Therefore, SIRA can differentiate the impact of mobility from the impact of the hidden interference. Based on this observation, we suggest that the detection of mobility can be determined by testing the monotonicity of $\underline{\mathbf{SNR}}$. SIRA calculates the coefficients of the first-degree polynomial from the measured SNR distribution as follows:

$$\widehat{\mathrm{SNR}}_i = \alpha \times i + \beta \tag{3.3}$$

If the slope, α, is smaller than α_{th}, SIRA conclude that the received frame is affected

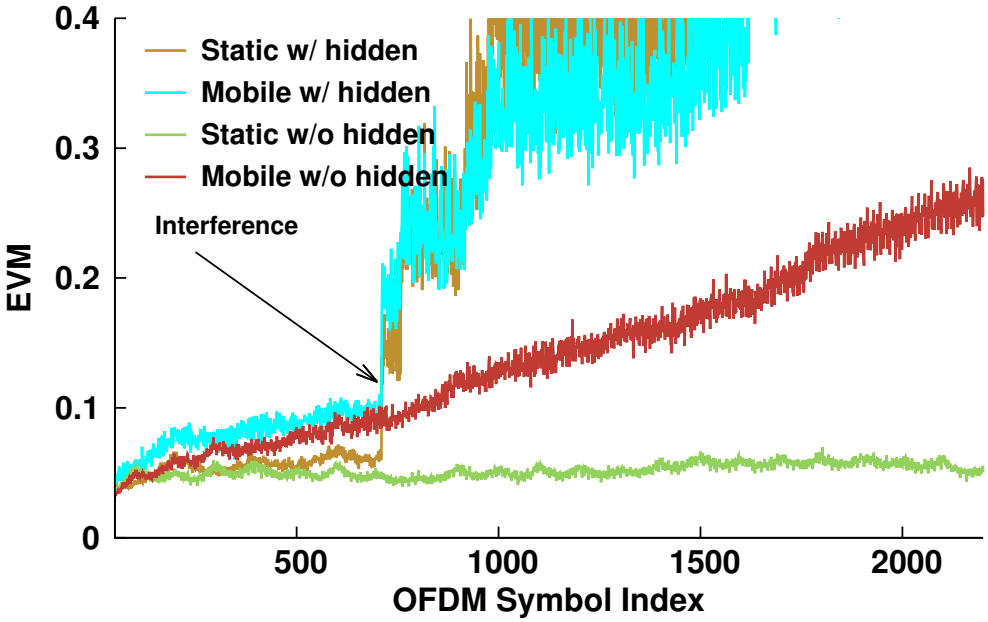

Figure 3.1: EVM performance under the hidden interference.

by mobility or interference signal. To differentiate the mobility condition from the hidden interference condition, SIRA then obtains the standard deviation of the difference between SNR_i and $\widehat{\mathrm{SNR}}_i$. If the standard deviation is larger than STD_{th}, SIRA detects the hidden interference. Otherwise, the estimated SNR monotonically decreases with the increase of symbol index, and hence SIRA concludes that the station is under a mobile environment.

3.2.3 Unequal Modulation and Coding Scheme

SIRA employs unequal MCS (UEQ-MCS) which allows the use of multiple MCSs for a given frame. UEQ-MCS encodes and modulates the data messages using primary MCS with rate R_p until the OFDM symbol index I_U from which the data symbol suffer from inaccurate CSI. The corresponding secondary MCS with rate R_s is used for the

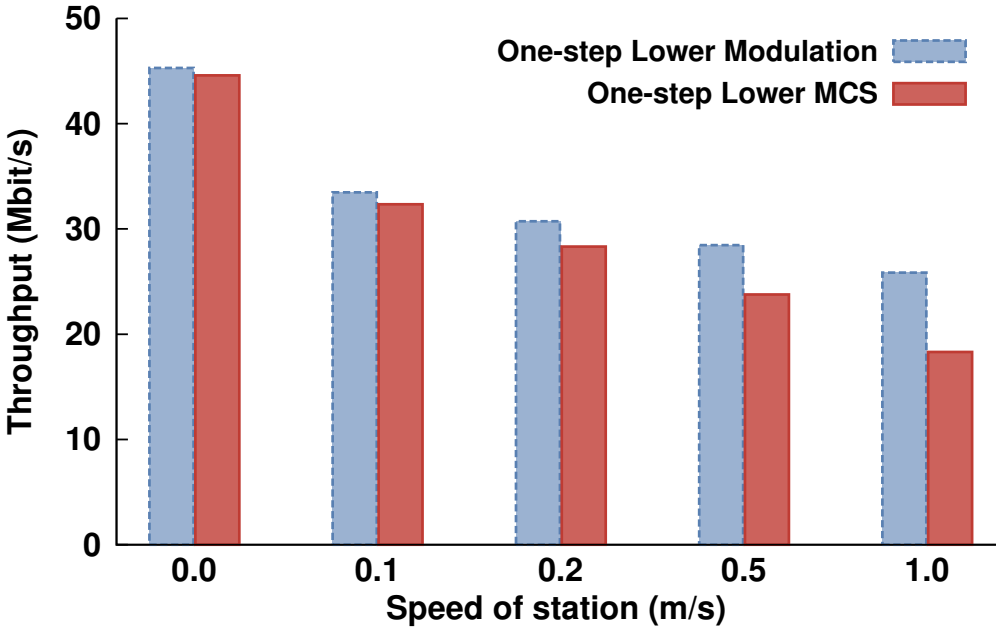

Figure 3.2: Throughput performance.

residual OFDM symbols only when mobility is detected according to Section 3.2.2.

UEQ-MCS imposes two challenges. First, the secondary MCS should be defined. Note that R_p is selected by Inter-RCA which only considers the channel condition. Using the second best choice of the Intr-RCA as the secondary MCS is one of good candidates. In general, the second best choice of Inter-RCA is the one-step lower MCS. However, the use of the MCS does not appropriate because the difference between the required SNR of the best and second best MCS to achieve a specific FER is only around 3 dB as presented in [47] while Intuitively, we can use the second best choice of inter-RCA as the secondary MCS of intra-RCA, but the second best MCS, used for the first retry, is the PHY rate which aims to the second best throughput. It is straightforward that the secondary MCS shall be used for a purpose for the robustness improvement. Therefore, we have defined to be the highest MCS that uses one-step lower modulation

Algorithm 1: SIRA pseudo code.

Data: $\underline{\mathbf{SNR}}$, SNR_{th}, R_p

Result: I_U, State

Initialize, $I_U = 0$, State = Static;

if $\underline{\mathbf{SNR}}$ is monotonically decreasing **then**

  for $i \leftarrow 1$ **to** K **do**

    if $\mathrm{SNR}_i < \mathrm{SNR}_{th}(R_p)$ **then**

      $I_U \leftarrow i \times N_S$;

      State $\leftarrow$ Mobile;

      Feedback I_U

    end

  end

else

  State $\leftarrow$ Static

end

and less than or equal to the coding rate of R_p. Fig. 3.2 depicts the performance for both cases when SIRA uses one-step lower modulation and one-step lower MCS as the secondary MCS. The result of one-step lower MCS shows much lower throughput performance than that of one-step lower modulation. It means that the use of one-step lower MCS can not mitigate the caudal losses. As shown in Table 1.1, we define 8 pairs of primary and secondary MCSs for UEQ-MCS.

The other challenge of UEQ-MCS is how to determine I_U. As illustrated in Algorithm 1, if the $\underline{\mathbf{SNR}}$ monotonically decreases, SIRA tries to find the first I_U from the beginning of the frame that satisfies the condition $\mathrm{SNR}_i < \mathrm{SNR}_{th}(R_p)$. We define SNR_{th} as the minimum SNR at which the theoretical coded BER of R_p is less

than roughly 10^{-4} based on the most popular error rate model [50].[1] The receiver then feedbacks I_U to the transmitter by using zero-overhead feedback protocol described in the following section. Based on the feedback value of I_U, the transmitter can prepare the next A-MPDU data frame by selecting the appropriate primary-secondary MCS pair. Table 3.1 summarizes the primary-secondary MCS pairs and the corresponding SNR_{th}.

UEQ-MCS is easy to implement in practice. Note that the baseline 802.11 WLAN already uses two different MCSs for a single frame. That is, data OFDM symbols are transmitted with the best MCS chosen by Inter-RCA while the signal fields of the preamble, i.e., L-SIG and HT-SIG, are transmitted with BPSK and $1/2$ coding rate. The different code rate can be obtained by the punctured convolutional coding which is the default error-correcting code in IEEE 802.11 [1]. Basically, all bits of the original message are encoded/decoded with lowest coding rate, i.e., 1/2, regardless of the target coding rate. Higher coding rate is obtained by the puncturing/depuncturing of the specific pattern of the code rate from the output of encoder/decoder. In short, UEQ-MCS can reuse the legacy 802.11 encoder/decoder, then omits/adds some of encoded/decoded bits by using the puncturing pattern of R_p and R_s depends on the bits' location. Therefore, SIRA uses R_p for the data OFDM symbols whose indices are smaller than I_U, while the rest are encoded/modulated with R_s.

3.2.4 Zero-overhead Feedback

The requirement of the feedback information I_U from receiver to transmitter in SIRA imposes undesirable overhead. To avoid the undesirable overhead, we introduce zero-overhead feedback protocol, which is the same technique used in the high throughput

[1] At this threshold, frame error rate is about 50% if the frame length is 1000 bytes, which means that SIRA is relatively conservative [11, 47].

Table 3.1: Primary-secondary MCS pairs and SNR thresholds.

R_p		R_s		SNR_{th} (dB)
MCS 0	BPSK, $1/2$	MCS 0	BPSK, $1/2$	-
MCS 1	QPSK, $1/2$	MCS 0	BPSK, $1/2$	3
MCS 2	QPSK, $3/4$	MCS 0	BPSK, $1/2$	6
MCS 3	16QAM, $1/2$	MCS 1	QPSK, $1/2$	10
MCS 4	16QAM, $3/4$	MCS 2	QPSK, $3/4$	13
MCS 5	64QAM, $2/3$	MCS 3	16QAM, $1/2$	16
MCS 6	64QAM, $3/4$	MCS 4	16QAM, $3/4$	18
MCS 7	64QAM, $5/6$	MCS 4	16QAM, $3/4$	20

signal field (HT-SIG). HT-SIG provides not only the explicit information (e.g., MCS, length and so on) by using bit stream but also the implicit information whether the frame is HT format by using 90° rotated constellation relative to BPSK. Similarly, SIRA piggybacks I_U in BlockAck (Block Acknowledgment). Let $P_{i,j}$ denotes the j^{th} pilot symbol on OFDM symbol i. The pilot symbols can be substituted for 90° rotated symbols, $\tilde{P}_{i,j}$, for piggybacking as follows:

$$\begin{aligned} \tilde{P}_{i,j} &= \varphi_k \times P_{i,j}, \\ \text{s.t. } \varphi_k &= \begin{cases} e^{j\frac{\pi}{2}}, & \text{if } b_k = 1, \\ e^{j0}, & \text{if } b_k = 0, \end{cases} \\ i &= \lfloor k/N_p \rfloor, \quad j = k \bmod N_p, \end{aligned} \tag{3.4}$$

where $\mathbf{b} = [b_0, b_1, \cdots]$ is the binary representation of I_U. b_0 is used for the signature of whether the BlockAck carries the piggyback information. The receiver can extract φ_k by comparing the known pilot sequence, $P_{i,j}$ with the received pilot symbol of the

previous symbol, $P^r_{i-1,j}$, before pilot-based phase offset tracking. It is obvious that the feedback does not aggravate the performance of the phase offset tracking.

3.2.5 SIRA Structure

An example of SIRA operation is described in Fig. 3.3. The transmitter first sends the A-MPDU with the primary MCS 7 which is chosen by Inter-RCA over the mobile channel. Based on the mobility detection algorithm of SIRA, the receiver detects mobility by using the measured SNR distribution from pilot subcarriers. SIRA then finds the first group of symbols M which meets the condition $\mathrm{SNR}_M < \mathrm{SNR}_{th}(\mathrm{MCS}\ 7)$. The receiver then informs $I_U = M \times N_S$ from which the data OFDM symbol suffer from the user mobility to the transmitter via zero-overhead feedback. Finally, the next A-MPDU is modulated and coded unequally using the primary-secondary MCS pair based on the feedback information, I_U, and the receiver then executes the mobility detection algorithm.

3.3 Simulation

We now show the effectiveness of our approach based on the simulation results. In order to demonstrate the performance gain of the proposed scheme more extensively, we have conducted trace-driven link level simulations.

3.3.1 Trace-driven Link Level Simulation

All features of IEEE 802.11n PHY/MAC are embedded in our trace-driven link level simulator by using GNU Radio and IT++ libraries [51, 52]. We collect the fine-grained channel traces using IWL5300 NIC and the 802.11n CSI tool on laptop [39] which reports the measured CSI for every successfully received packet [36, 39]. We collect 14

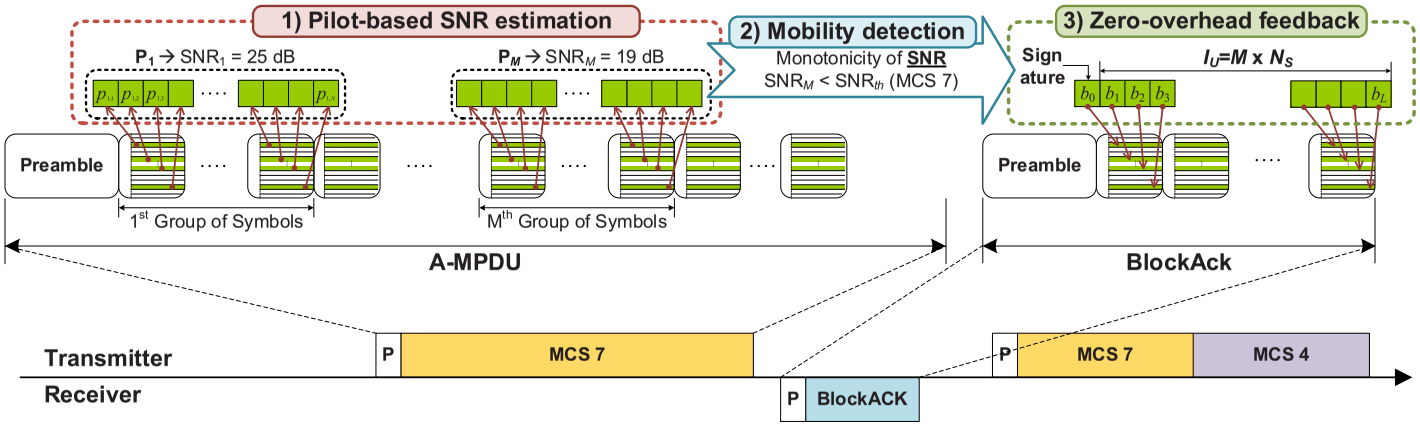

Figure 3.3: SIRA framework.

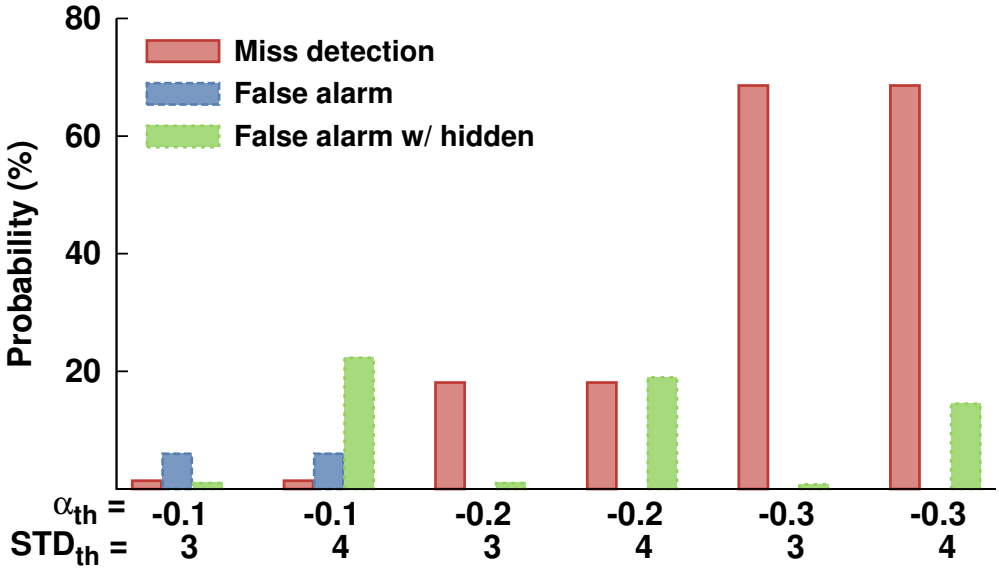

Figure 3.4: Mobility detection accuracy of SIRA.

traces with various speeds of the receiver at different locations (red points in Fig. 2.2). Each CSI contains the complex channel frequency responses, which represent amplitude and phase differences between transmitter and receiver, of 30 OFDM subcarriers.[2] The channel model of the simulator is built by linearly interpolating the measured CSIs over time and frequency domains. We also have implemented SGRA, one of the best inter-RCAs for comparison purpose.

3.3.2 Mobility Detection Accuracy

Before verifying the benefit of SIRA, we investigate impact of α_{th} and STD_{th}, which directly affects the performance of SIRA. Fig. 3.4 shows the detection accuracy with various α_{th} and STD_{th} values in terms of miss detection and false alarm probability.

[2]The device driver we used just reports the channel responses of a group of 30 subcarriers instead of all the 56 subcarriers.

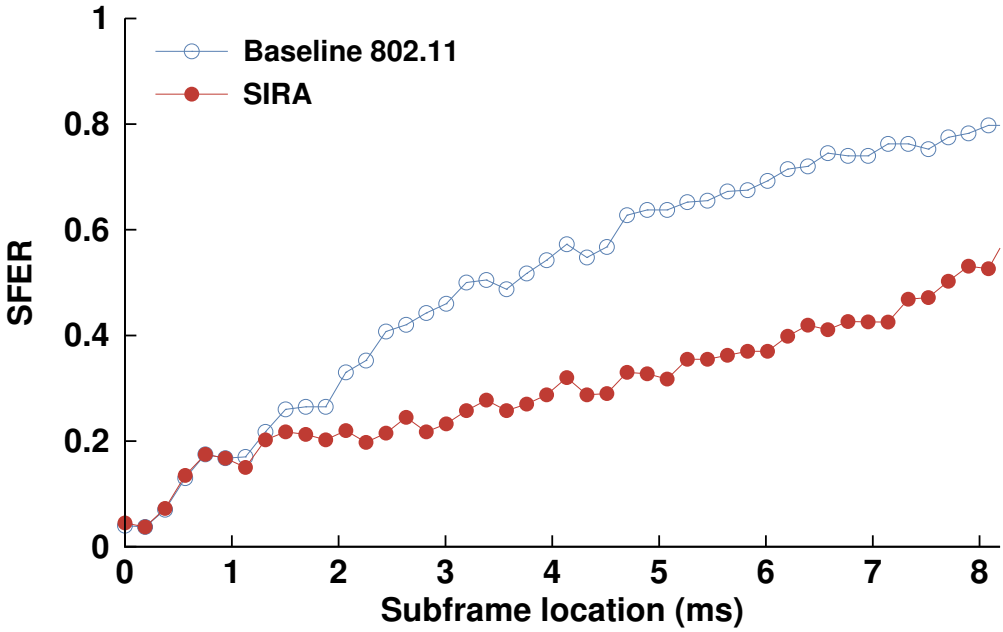

Figure 3.5: Subframe error ratio.

For larger values of α_{th}, miss detection probability increases as increases while false alarm probability decreases. $\mathrm{STD}_{th} = 3$ is the best choice with respect to false alarm probability. Based on this observation, we set α_{th} as -0.1 and STD_{th} as 3 throughout this chapter. Therefore, SIRA achieves over 98% detection accuracy. With respect to the false-alarm probability, SIRA yields below 6% error.

We then evaluate the accuracy of I_U prediction. I_U prediction error is only around 200 symbols which is much smaller than the maximum number of symbols, i.e., 2500.

3.3.3 Performance Comparison

Fig. 3.5 shows the average SFER performance under mobile traces where the fixed MCS 7 achieves the best performance, when disabling A-MPDU, due to the short range between transmitter and receiver during the collection of the traces. The baseline

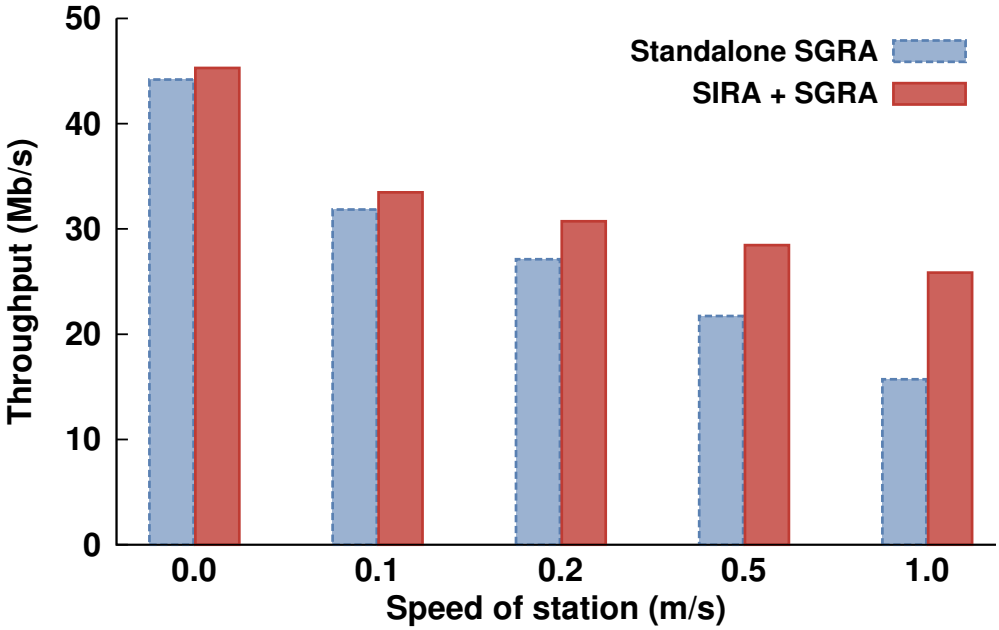

Figure 3.6: Throughput performance.

802.11 suffers from the caudal losses, even if the channel condition is good in terms of RSS. This is similar to the tendency shown in Fig. 2.5(b). However, SIRA significantly mitigates the SFER explosion, roughly by 20% on average.

Fig. 3.6 depicts the throughput performance of standalone SGRA and SIRA interplaying with SGRA in various traces including static. If standalone SGRA is used, the throughput seriously decreases along with the increase of the degree of user mobility, as explained in Section 2.3.3. However, the joint use of intra/inter-RCAs, i.e., SIRA+SGRA, remarkably alleviates the throughput degradation, and also shows higher throughput performance than standalone SGRA for all traces. Especially, when a station moves at an approximate constant speed of 1 m/s, SIRA achieves the maximum 56% throughput gain. Furthermore, SIRA shows slightly better throughput in static trace, not only because the wireless channel changes even if stations hold their posi-

tion, but also because SIRA requires no extra overhead.

3.4 Summary

In this chapter, the issue of unreliable transmission in A-MPDU of IEEE 802.11 is addressed, especially for the rapid dispersive fading channels. To resolve the issue, we have developed SIRA, a method for selecting the appropriate PHY rates on intra-frame basis by using PHY information without any protocol overhead. Our results show that the proposed scheme is effective and yields significant performance gain for all traces including static. To our best knowledge, in Wi-Fi networks, this is the first rate control algorithm to address the issue of quickly adapting time-variant wireless channel during one-frame duration.

Chapter 4

ChASER: Channel-Aware Symbol Error Reduction

4.1 Introduction

As we describe in the previous chapter, due to considerable increases in user mobility and frame length through aggregation, the wireless channel remains no longer time-invariant during the (aggregated) frame transmission time. However, the existing IEEE 802.11 standards still define the channel estimation to be performed only once at the preamble for coherent OFDM receivers, and the same channel information to be used throughout the entire (aggregated) frame processing. Our experimental results in Chapter 2 reveal that this baseline channel estimation approach seriously deteriorates the Wi-Fi performance, especially for pedestrian mobile users and the recently adopted frame aggregation scheme.

In this chapter, we propose Channel-Aware Symbol Error Reduction (ChASER), a new practical channel estimation and tracking scheme for Wi-Fi receivers. ChASER utilizes the re-encoding and re-modulation of the received data symbol to keep up with the wireless channel dynamics at the granularity of OFDM symbols. Our extensive, trace-driven link-level simulation shows significant performance gains over a

wide range of channel conditions based on the real wireless channel traces collected by the off-the-shelf Wi-Fi device. In addition, the feasibility of its low-complexity and standard compliance is demonstrated by Microsoft's Software Radio (Sora) prototype implementation and experimentation. To our knowledge, ChASER is the first IEEE 802.11n-compatible channel tracking algorithm since other approaches addressing the time-varying channel conditions over a single (aggregated) frame duration require costly modifications of the IEEE 802.11n standard.

4.2 Revisit of Channel Estimation Algorithms

Numerous channel estimation algorithms have been proposed to enhance the accuracy of the estimation in a rapid dispersive fading channel environment. The work done in [15, 16] can be used to estimate the wireless channel based on the linear interpolation of partial channel information, i.e., pilot signal. However, the technique is inappropriate for 802.11n where the pilot subcarriers are not spaced closely to estimate the channel fluctuation of data subcarriers in frequency domain.

It is worth noting that the authors in [17] have proposed midamble-based channel estimation techniques for high mobility vehicular channel (e.g., 802.11p vehicle-to-vehicle communication specification [18]), and found to improve the performance but suffer from two major disadvantages: (1) protocol overhead incurred by addition of the midamble; and (2) deviation from the 802.11n standard. In particular, the latter makes it extremely costly and impractical for large-scale adoption by commercial 802.11n vendors.

Other notable techniques include spectral temporal averaging (STA) and constructed data pilot (CDP) estimation methods proposed in [19, 20], both of which also use the estimated transmit data symbols which can be obtained based on the information from

the receiver's demapper to track the channel variation. However, according to the results provided in [19, 20], the error rate performance appears too high to be acceptable in practical communication environment, because the information is obtained in the absence of error correcting.

The authors in [21] have proposed the iterative channel estimation with postamble, the concept of which is similar to that of the turbo channel estimation [22]. Unfortunately, the requirement of the iterative operation brings high computational complexity which is undesirable for Wi-Fi. Moreover, the postamble causes incompatibility with the 802.11n standard.

In contrast, the channel estimation technique proposed by ChASER is able to "chase" the channel dynamics within the A-MPDU duration up to its maximum length for pedestrian mobility, 802.11n standard-compliant, and of low computational complexity with no additional overhead.

4.3 ChASER Design

In this section, we describe the ChASER scheme designed to minimize caudal losses by tracking the channel accurately during the course of demodulation/decoding while satisfying the latency requirement, i.e., completing the frame reception process within the SIFS (16 μs) interval.

ChASER is composed of three main blocks: channel estimator using unknown data symbols, adaptive filter, and CRC-assisted channel corrector.

4.3.1 Channel Estimation using Unknown Data Symbols

As shown in Fig. 4.1, the received signal (Y) is processed by demapper and decoder sequentially, whose output are $\hat{D}$ and D, respectively. In order to exploit the error

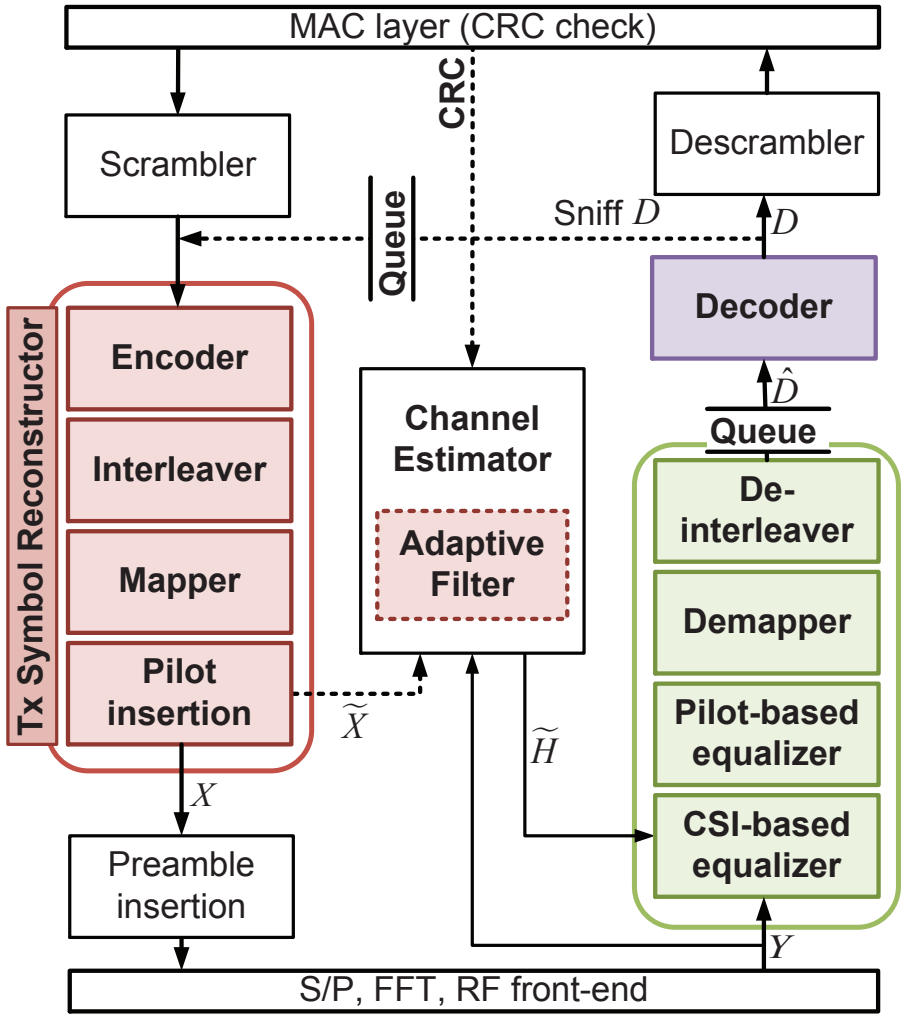

Figure 4.1: Block diagram of ChASER. The dashed block and lines are the additional processing needed for ChASER.

correcting gain of the channel coding, we reconstruct the original OFDM signal based on the D rather than $\hat{D}$, based on which STA and CDP conduct the reconstruction without error correcting gain [19, 20]. ChASER re-encodes and re-modulates D as done by the DSP block of the transmitter, which is composed of encoder, interleaver, and mapper. Note that the known sequence is inserted for pilot subcarrier. We refer to the block as *symbol reconstructor*. Afterwards, utilizing the same methodology as the preamble-aided channel estimation scheme as described in Section 2.2.1, we can estimate CSI by replacing the denominator of LS estimator (i.e., Eq. (2.1)) from known sequence (X_{LTF}) with the reconstructed OFDM symbol ($\widetilde{X}$) as follows:

$$\widetilde{H}_i = \frac{Y_i}{\widetilde{X}_i}, \tag{4.1}$$

where $\widetilde{H}_i$ and Y_i represent the estimated CSI and the received symbol of the i^{th} OFDM symbol, respectively.

Note that by using the transmit processing blocks of 802.11n as shown in Fig. 4.1, no additional processing blocks are needed in ChASER design. Moreover, since error correcting capability of the channel decoder is exploited, ChASER estimates the CSI with high accuracy.

4.3.2 Adaptive Filter

Unfortunately, even if the original transmit symbols are reconstructed with the help of the channel coding, the estimation errors might still exist, which will in turn result in error propagation and performance degradation.

To mitigate the error propagation, we develop an adaptive filter using exponential weighted moving average (EWMA), with step size equal to μ:

$$\widetilde{H}_i = (1-\mu)\widetilde{H}_{i-1} + \mu\frac{Y_i}{\widetilde{X}_i}. \tag{4.2}$$

The choice of μ has a trade-off between the estimation error and the convergence speed.

Proposed filter can smoothen out the sharp edge of $\widetilde{H}_i$ comes from estimation error, and hence we can alleviate error propagation and the resultant performance degradation. Furthermore, one of the merit of the proposed filter is that it only requires memory storage for the CSI estimated at the preceding OFDM symbol, $\widetilde{H}_{i-1}$, and has low computational complexity.

4.3.3 Adaptive Filter for MIMO

In the case of MIMO, the adaptive filter presented in Section 4.3.2 should be modified, because the amount of the known information ($\widetilde{X}_i$) is smaller than that of the desired value ($\widetilde{H}_i$).

To improve the adpative filter for MIMO, we formulate our objective function as follows:

$$\begin{aligned} &\min \left\| H_i - \widetilde{H}_{i-1} \right\|_2, \\ &\text{s.t. } Y_i = H_i \widetilde{X}_i, \end{aligned} \tag{4.3}$$

where H_i and $\widetilde{H}_i$ represent the real channel response and the estimated CSI of the i^{th} OFDM symbol in the form of $N_{\text{rx}} \times N_{\text{tx}}$, respectively. N_{rx} and N_{tx} are the number of receive and transmit antennas, respectively. Y is the received symbol and $\widetilde{X}$ is the recreated symbol at the receiver . It is well known that the objective function is convex [53], and hence we can use Karush-Kuhn-Tucker (KKT) conditions given by

$$\begin{aligned} &Y_i - H_i \widetilde{X}_i = 0, \\ &\tfrac{\partial}{\partial H_i} \mathcal{L}(\widetilde{X}_i, v_i) = 0, \end{aligned} \tag{4.4}$$

where the Lagrangian is given by

$$\mathcal{L}(\widetilde{X}_i, v_i) = \text{Tr}\left\{ (H_i - \widetilde{H}_{i-1})^\dagger (H_i - \widetilde{H}_{i-1}) \right\} + {v_i}^\dagger (Y_i - H_i \widetilde{X}_i). \tag{4.5}$$

From these conditions, H_i can be easily obtained in a closed form as

$$H_i = \widetilde{H}_{i-1} + \frac{e_i \widetilde{X}_i^{\dagger}}{\widetilde{X}_i^{\dagger} \widetilde{X}_i}, \tag{4.6}$$

where the estimation error $e_i = Y_i - \widetilde{H}_{i-1}\widetilde{X}_i$.

The solution is similar to the normalized least-mean squares (NLMS) filter which is used for delayed-tap channel equalization. The filter has the lead of low-complexity, memory load and simplicity of practical implementation [53]. By applying tunable parameter of NLMS, step size (μ), we formulate the adaptive filter for ChASER as follows:

$$\widetilde{H}_i = \widetilde{H}_{i-1} + \mu \frac{e_i \widetilde{X}_i^{\dagger}}{\widetilde{X}_i^{\dagger} \widetilde{X}_i}, \tag{4.7}$$

where $\widetilde{H}_0$ is initialized by the CSI from LTF. The choice of μ has a trade-off between the estimation error and the convergence speed.

The proposed adaptive filter meets our challenges because it only requires small memory storage for the CSI estimated at the preceding OFDM symbol, $\widetilde{H}_{i-1}$, and has low computational complexity, $\mathcal{O}(N_{\mathrm{rx}} \times N_{\mathrm{tx}})$.

4.3.4 CRC-assisted Channel Correction

It is generally accepted that A-MPDU is very efficient in error-prone environments thanks to the selective retransmission capability. To achieve this, A-MPDU attaches CRC at the end of each subframe to detect bit error as shown in Fig. 2.1. Let us consider the case when a subframe is successfully received; no bit error observed. Since all the bits, D, of the subframe are decoded correctly, the reconstructed symbols are exactly the same as the original transmitted symbols. Therefore, we can obtain the error-free CSIs from unknown data OFDM symbols, which are known symbols from now on. In this case, ChASER updates the estimated CSI, $\widetilde{H}_i$, based on the LS estimator, Eq. (4.1), instead of the proposed adaptive filter, Eq. (4.2).

This achieves the same effect that the transmitter opportunistically injects LTF at the end of every subframe, called midamble [17]. However, our approach has no extra protocol overhead, which wastes air time.

4.3.5 Summary of ChASER Operation

Algorithm 2: CSI update of ChASER.

input : X_{LTF}, $\widetilde{X}_i$, Y_i, $\widetilde{X}_{i-1}$, Y_{i-1}, $\widetilde{H}_{i-1}$

output: $\widetilde{H}_i$

for each OFDM symbols *i* **do**

  if is HT-LTF **then**

    /* $i = 0$ */

    $\widetilde{H}_i \leftarrow \frac{Y_i}{X_{\mathrm{LTF}}}$

  else if includes CRC and passes CRC check **then**

    if has data bits of the next subframe **then**

      /* $\widetilde{X}_{i-1}$ is known */

      $\widetilde{H}_{i-1} \leftarrow \frac{Y_{i-1}}{\widetilde{X}_{i-1}}$

      $\widetilde{H}_i \leftarrow (1-\mu)\widetilde{H}_{i-1} + \mu\frac{Y_i}{\widetilde{X}_i}$

    else

      /* $\widetilde{X}_i$ is known */

      $\widetilde{H}_i \leftarrow \frac{Y_i}{\widetilde{X}_i}$

    end

  else

    /* unknown data symbol */

    $\widetilde{H}_i \leftarrow (1-\mu)\widetilde{H}_{i-1} + \mu\frac{Y_i}{\widetilde{X}_i}$

  end

end

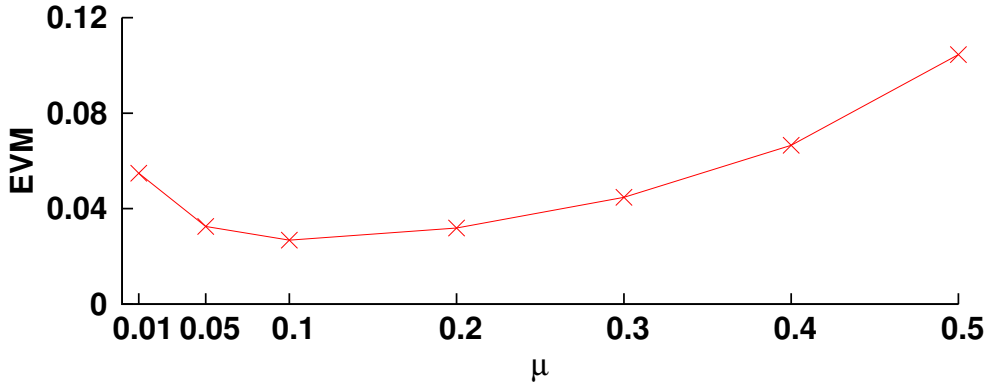

Figure 4.2: EVM performance with various μ values.

Algorithm 2 summarizes the overall CSI update procedure of ChASER depending on whether current symbol is known or not. First, if the current symbol is known, such as HT-LTF or all data bits decode correctly, the LS estimator is used. If not, the adaptive filter is used. However, even though the symbol contains CRC and the corresponding subframe passes CRC check, we cannot be assured that all data bits are decoded correctly if CRC is followed by data bits of the next subframe, which does not pass CRC check yet. In such case, there is potential error in the current OFDM symbol, whereas the preceding OFDM symbol should be known, because all the containing bits pass CRC check. Hence, the CSI of the known preceding symbol, $\widetilde{H}_{i-1}$, is first updated based on the LS estimator, and then the current CSI, $\widetilde{H}_i$, is estimated by using the adaptive filter.

4.3.6 Impact of Step Size μ

Before verifying the benefits of ChASER, we investigate the impact of step size, μ, which directly affects the performance of ChASER. For larger values of step size, the tracking speed is very fast, but the steady state estimation error is large and vice versa.

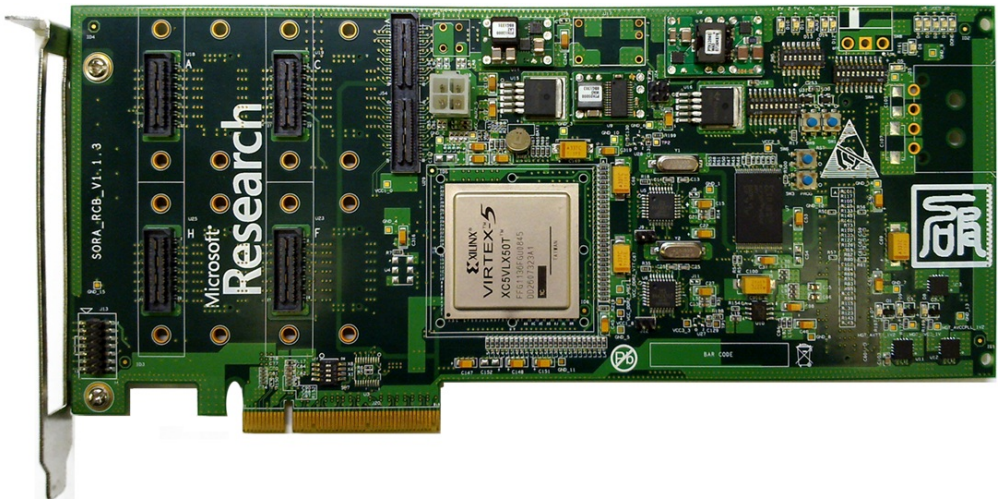

Figure 4.3: Radio control board of Microsoft Software Radio (Sora).

To determine an appropriate μ, we run ChASER with various values on all collected traces of the trace-driven link level simulator. We observed the best EVM performance with $\mu = 0.1$ as shown in Fig. 4.2, and hence we set μ as 0.1 throughout the chapter.

4.4 Testbed Experiments

4.4.1 Prototype Implementation on SDR Platform

To verify the feasibility of the proposed scheme, we have implemented ChASER using the Sora radio control board (RCB) and Sora SDK version 1.6, which supports 802.11a only. We created and inserted several essential features of the IEEE 802.11n standard such as HT-preamble, increased number of subcarriers, and A-MPDU, and embedded them as part of the platform. The operation of ChASER is pipelined with DSP functions of the IEEE 802.11n over multiple cores based on Sora User-Mode Extension (UMX) as specified in Section 4.3 to satisfy the latency constraint. Due to

some limited capabilities of the decoder of Sora SDK, ChASER updates the CSI at every 4 OFDM symbols in our implementation.

4.4.2 Testbed Settings

Our testbed operates at 5.22 GHz band and all the experiments have been done under a clean channel environment; no interference signal was detected throughout the test. We first install the programmable AP equipped with AR9380 NIC, $ath9k$, and $hostap$ [34, 37, 42]. We let Sora operate as the receiver of the AP, whose downlink buffer is always filled with A-MPDUs, each of which consists of several 1000-byte MPDUs. Since Sora testbed is too heavy to move swiftly, we moves the AP at an approximately, pedestrian speed, e.g., 0 m/s, 0.3 m/s, 0.6 m/s, and 1 m/s on average, and sets the transmission rate as MCS 3 (16QAM and 1/2 code rate).[1] Basically, $T_{\max}$ is set to 10 ms throughout this chapter. The following results are averaged over 5 runs, where each run lasts for about 100 seconds.

4.4.3 Performance Comparison

Fig. 4.4 plots the SFER variation with the increase of subframe index. From the results, we can argue that ChASER can effectively reduce the SFER by conducting more accurate channel compensation compared to the baseline 802.11n, which is quite vulnerable to the unexpected side effect of user mobility. In particular, the slopes of curves corresponding to the ChASER with various extents of mobility are all relatively flat, reflecting the ChASER's superior nature of caudal loss elimination.

[1] Since Sora is inherently lack of fine AGC operation, we tuned the receiver gain offline to an appropriate value. Thus, the AP should move over relatively short distances (e.g., 1 m) so that the tuned value can be valid for a while. Moreover, because the capabilities of RF front-end of Sora is far from being decent, it is difficult to use a higher order MCS where ChASER may achieve significant performance gain over the baseline 802.11n.

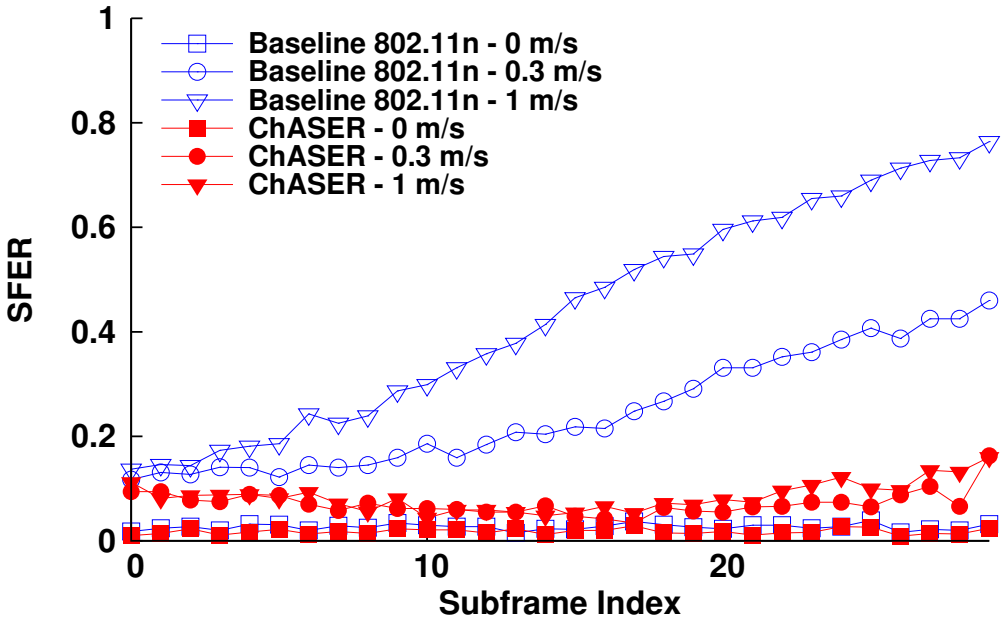

Figure 4.4: Subframe error ratio.

Fig. 4.5 shows the throughput performance, where ChASER presents the maximum 58% throughput gain over the baseline 802.11ac. Furthermore, we have found that the channel status still varies with time even in static trace (0 m/s), where the ChASER's resilience towards caudal losses are still in effect, whereby the slight throughput gain is observed as shown in Fig. 4.5.

Figs. 4.6(a) and 4.6(b) show the received data symbol positions derotated by CSI from LTF or ChASER when the sender moves at an average speed of 1 m/s. In the case of the baseline 802.11n, the derotated symbols are widely disseminated on I-Q plane while the symbols demodulated by ChASER are located in the vicinity of 16QAM signal constellations.

As we explain in Section 2.2.1, the dispersion mainly depends on the accuracy of the CSI used for compensating the distorted symbols. Therefore, we conclude that

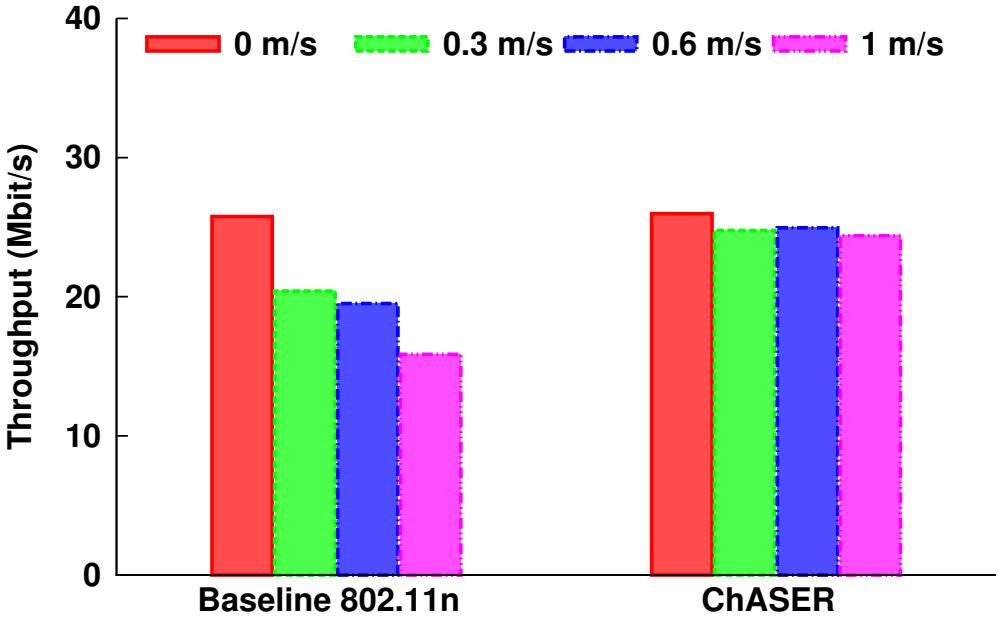

Figure 4.5: Throughput.

ChASER estimates CSI with high accuracy and hence repress the distortion caused by user mobility.

4.5 Simulation

In order to demonstrate the performance gain of the proposed scheme more extensively, we have conducted trace-driven link level simulations.

4.5.1 Simulation Methodology

All features of IEEE 802.11n PHY/MAC are embedded in our trace-driven link level simulator by using GNU Radio and IT++ libraries [51, 52]. We collect the fine-grained channel traces using IWL5300 NIC and the 802.11n CSI tool on laptop [39] which re-

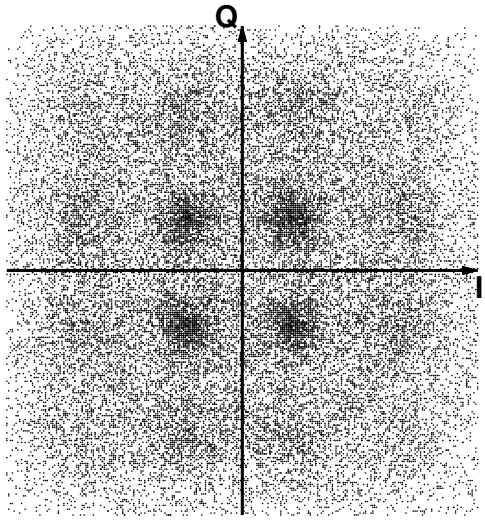

(a) Baseline 802.11n.

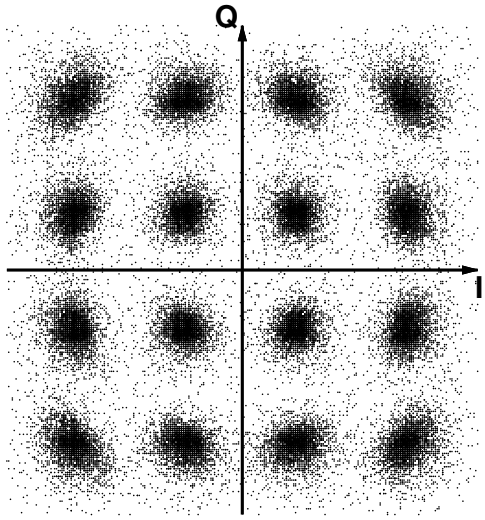

(b) ChASER.

Figure 4.6: Data symbol dispersion at the latter part of A-MPDU. All symbols are corrected by CSI and pilots.

ports the measured CSI for every successfully received packet [36, 39]. We collect 14 traces with various speeds of the receiver at different locations (red points in Fig. 2.2). Each CSI contains the complex channel frequency responses, which represent amplitude and phase differences between transmitter and receiver, of 30 OFDM subcarriers.[2] The channel model of the simulator is built by linearly interpolating the measured CSIs over time and frequency domains.

Moreover, *midamble* and *STA* compared as the existing schemes have been also implemented and embedded into the simulator. In midamble, the training OFDM symbols modulated with BPSK are inserted periodically with the interval of γ OFDM symbols. Note that midamble can achieve better estimation accuracy if the training symbols are inserted more frequently. That is, there is a trade-off between the estimation accuracy and the protocol overhead generated by the training symbols in midamble. We select two training symbol intervals, i.e., 10 and 200 OFDM symbols, as two representatives of a more accurate one and a more efficient one, respectively.

4.5.2 Estimation Accuracy

Fig. 4.7 shows the channel estimation accuracy of various schemes in terms of EVM using the channel trace collected at **C1** in Fig. 2.2, a relatively good channel environment compared to other spots. Fig. 4.7(a) and Fig. 4.7(b) represent the results when the transmission rates are fixed as MCS 7 and MCS 1 in a log-scale, respectively.

As expected, the EVM of baseline 802.11n continuously increases along with the increase of the OFDM symbol index, thus resulting in caudal losses ultimately. In the case of Midamble$_{200}$,[3] the EVM value moves upward and downward periodically,

[2]The device driver we used just reports the channel responses of a group of 30 subcarriers instead of all the 56 subcarriers.

[3]Midamble$_X$ is the midamble whose interval γ is equal to X.

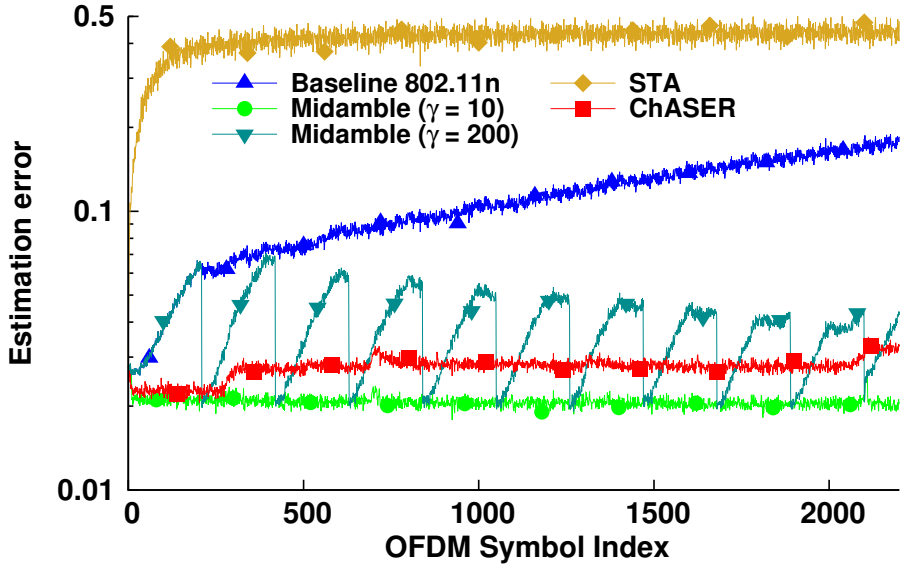

(a) Estimation accuracy with fixed MCS 7.

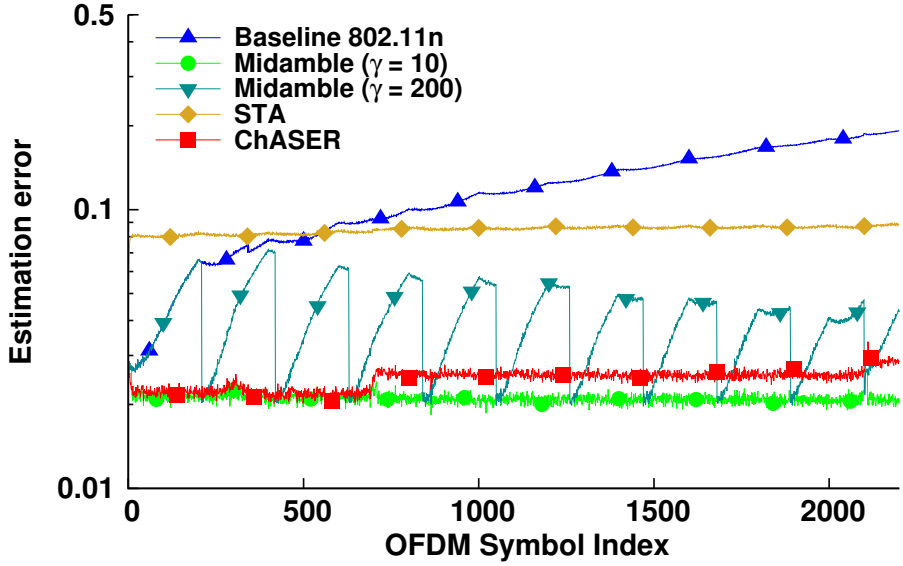

(b) Estimation accuracy with fixed MCS 1.

Figure 4.7: Channel estimation accuracy in mobile traces.

reflecting the estimation error increase as time elapses and the periodic channel updates done by training symbols, respectively.

ChASER achieves similar performance to Midamble$_{10}$ which shows the best estimation performance as shown in Fig. 4.7, while the latter incurs much more protocol overheads compared to the former. In the case of STA, because it uses the output of the demapper rather than that of the channel decoder, channel coding gain is not exploited and the performance is highly vulnerable to the demodulation error. As a result, STA can achieve better performance in the case of MCS 1 (Fig. 4.7(b)) than in the case of MCS 7 (Fig. 4.7(a)).

Table 4.1: EVM performance in various SNR channel traces.

	Low SNR			High SNR		
Modulation	QPSK	16QAM	64QAM	QPSK	16QAM	64QAM
Midamble$_{10}$	0.0367	0.0371	0.0370	0.0210	0.0207	0.0206
Midamble$_{200}$	0.0612	0.0617	0.0614	0.0380	0.0379	0.0378
STA	0.1098	0.4881	0.5194	0.0848	0.2265	0.3721
ChASER	0.0398	0.0459	0.0499	0.0248	0.0250	0.0292

Table 4.1 presents the average EVM values when applying various SNR channel traces. Midamble$_{10}$ shows the lowest EVM by introducing tremendous training overhead, while ChASER shows similar EVM values (at most 1.3% difference) without additional training symbols.

4.5.3 Impact of the A-MPDU Duration

We then investigate how the A-MPDU length will influence the throughput when we apply various channel estimation schemes described earlier. We use MCS 7 and vary

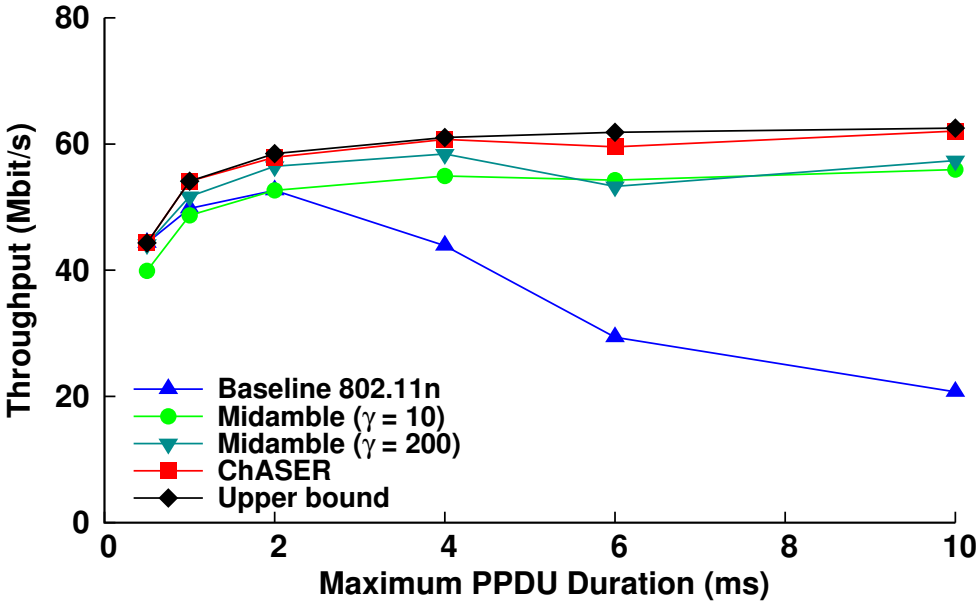

Figure 4.8: Impact of $T_{\max}$ with fixed MCS 7.

the duration $T_{\max}$ of a single A-MPDU transmission. Fig. 4.8 shows the throughput performance.[4]

When $T_{\max}$ is less than 2 ms, all the schemes including the baseline 802.11n yield almost the same throughput performance approaching the upper bound,[5] because the wireless channel is quasi-stationary within the transmission time. When $T_{\max}$ exceeds 2 ms, the performance gaps between the upper bound and the existing schemes become larger while ChASER still achieves a performance close to the upper bound. Particularly, ChASER improves throughput up to 99.5% compared to the baseline 802.11n in this result. It is worth noting that Midamble$_{10}$, which shows the best estimation accuracy in Fig. 4.7, has less throughput gain than the proposed scheme due mainly to

[4]In this simulation, we did not consider STA because it shows undesirable throughput performance (almost zero with MCS 7)

[5]The upper bound is achieved when there is no transmission error.

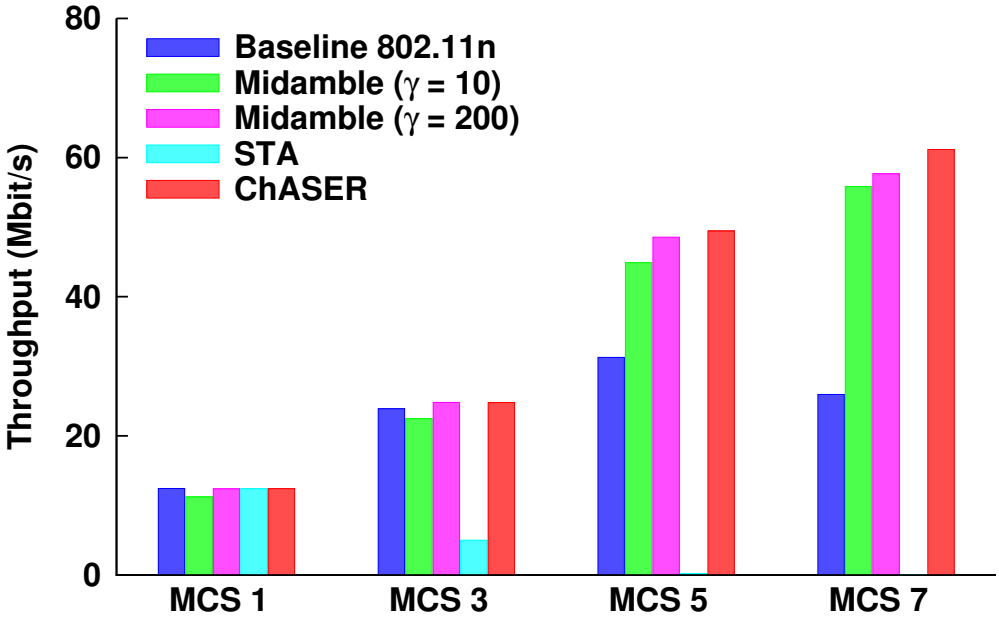

Figure 4.9: Throughput performance comparison in mobile trace.

the protocol overhead incurred by midamble.

4.5.4 Throughput Performance

We now evaluate the throughput performance gain of our proposed algorithm in various communication environments.

One-to-One Scenario with Fixed MCS

Fig. 4.9 shows the throughput results when various MCSs, i.e., MCS 1, MCS 3, MCS 5, and MCS 7, are adopted in mobile trace. ChASER shows the best performance regardless of the adopted MCS although Midamble has slightly better estimation accuracy as presented in Table 4.1, reflecting the tradeoff between throughput degradation due to protocol overhead and throughput enhancement due to estimation accuracy.

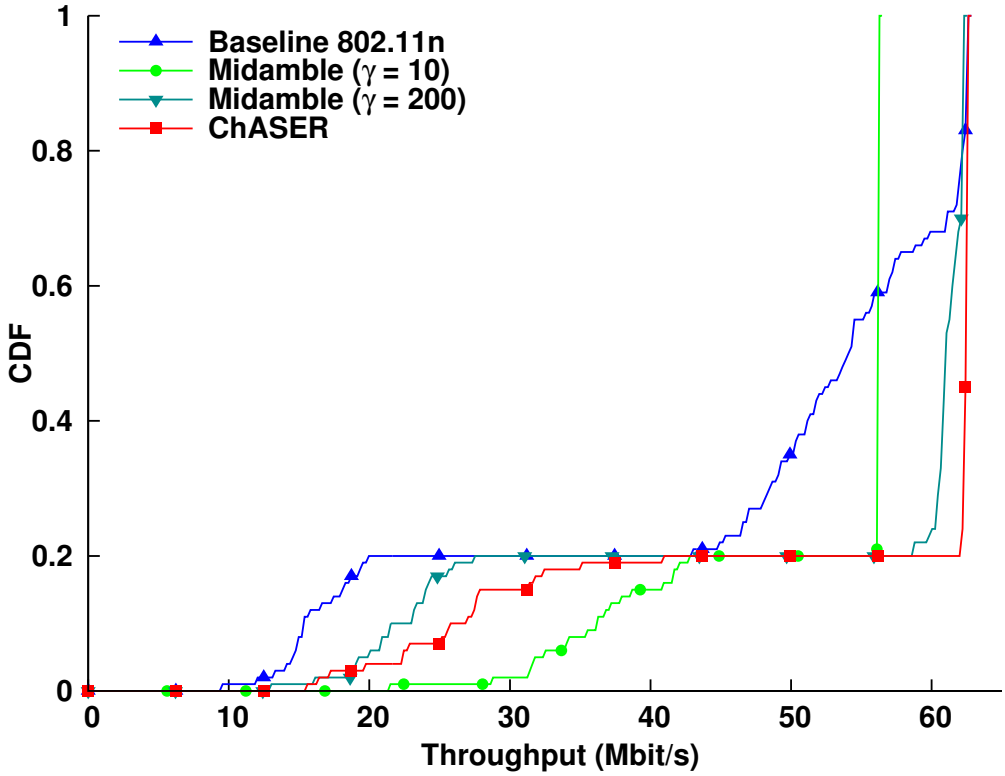

Figure 4.10: Throughput distribution in static traces.

In the case of MCS 1, all schemes including baseline 802.11n present similar performance because MCS 1, whose modulation scheme is QPSK, is robust enough to overcome the impact of user mobility. Moreover, Midamble$_{10}$'s bulky protocol overhead degrades the throughput compared to other schemes.

Based on the simulation result, STA shows the worst performance due to its low estimation accuracy. STA may be useful only when the frame length is very short.

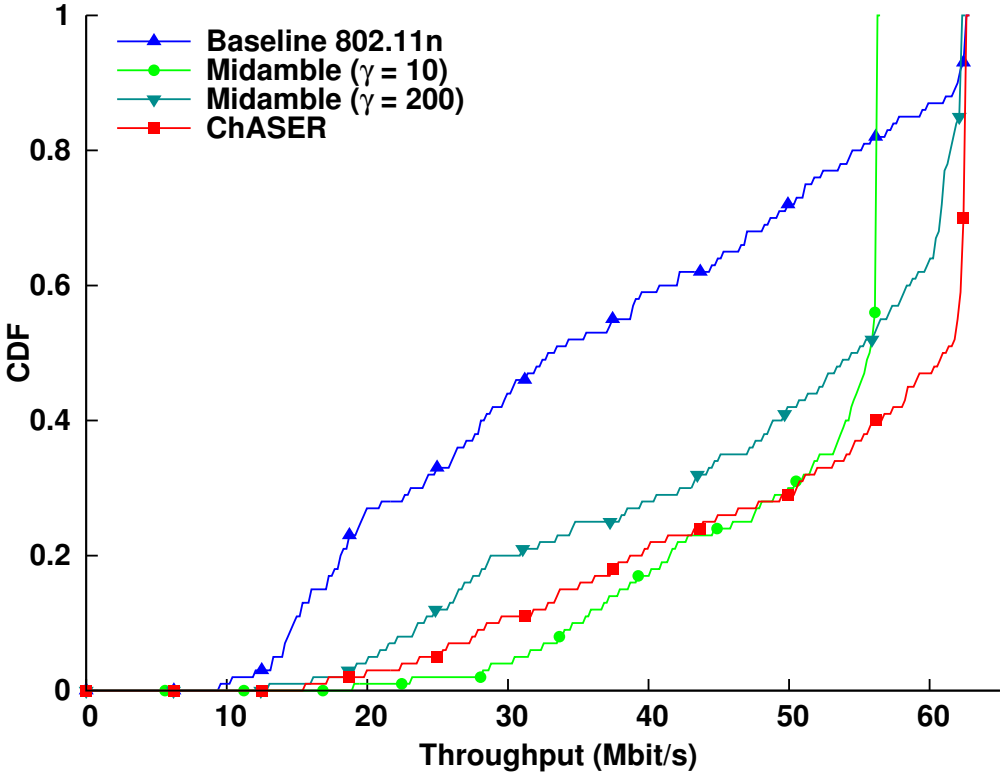

Figure 4.11: Throughput distribution in mobile traces.

One-to-One Scenario with Rate Control Algorithm

In fact, ChASER is an independent block which can be combined with a rate control algorithm so that both frame-level and symbol-level resilience to channel error are enhanced together. We have embedded RRAA, one of the best rate control algorithms, into the simulator on top of various channel tracking algorithms and extensively evaluated the throughput over all the collected traces.

Figs. 4.10 and 4.11 plot the CDF of the throughput with various channel tracking algorithms. Interestingly, The baseline still shows the worst performance for all the cases including static traces even if RRAA chooses the appropriate PHY rate. As stated in Section 6.4.3, the wireless channel is not quasi-stationary with in the A-MPDU duration. Therefore the appropriate channel tracking algorithm, such as ChASER, shows better performance frequently.

We observe that the lines corresponding to ChASER are always right most for relatively high throughput region, e.g., from 50 Mb/s to 60 Mb/s, which is likely to be the region most applications are of interest. In other words, a user can be served with better throughput with higher probability when ChASER is used.

Multiple Node Scenario

At last, in order to evaluate throughput performance in a more general environment, we conduct network-level simulation, letting six nodes be located at six CSI collection points with various levels of mobility and associate with the AP as shown in Fig. 2.2. We make them share the wireless medium upon carrier sense multiple access with collision avoidance (CSMA/CA) and be able to sense each other's signal so that there is no hidden terminal problem during the simulation.

Fig. 4.12 presents the simulation results when six nodes always have uplink A-MPDU to transmit. We divide the six nodes into two groups indicated here as high SNR

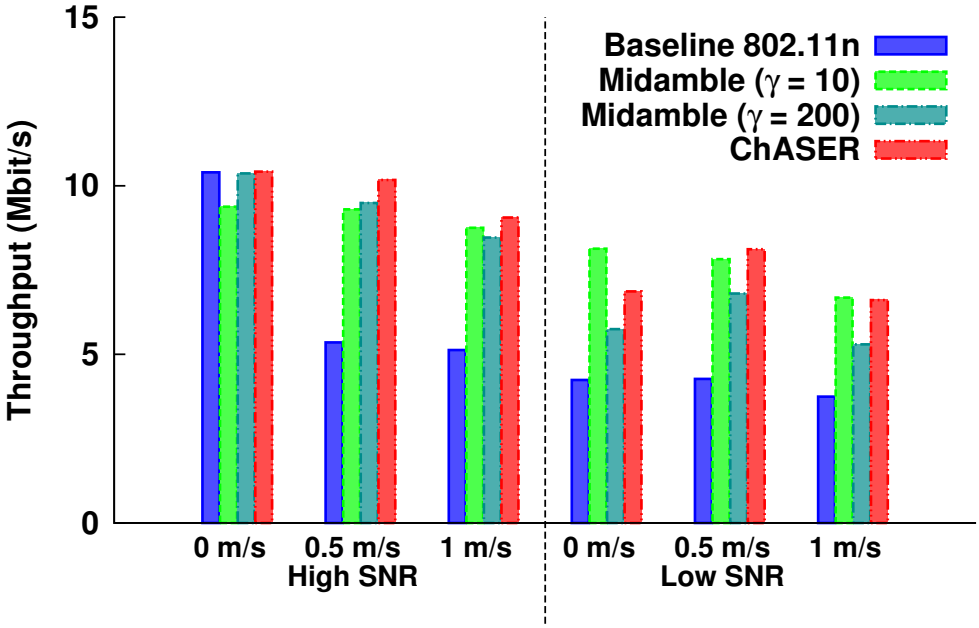

Figure 4.12: Multi-node environments.

and low SNR based on their average SNR values and intentionally control the mobility level of each node so that the three nodes of each group have different mobility levels. We observe that ChASER and Midamble$_{10}$ outperform all the other schemes in all the cases and the former is better than the latter except the case of the static node with low SNR. The reason we find out is that the step size of ChASER, μ, is not selected appropriately in this case, which is one of the issues that we need to address in the future work. In short, ChASER achieves 79.8% and 23.5% higher throughput compared to baseline 802.11n for mobile and static nodes, respectively.

4.6 Summary

This chapter presents ChASER, a low-complexity, standard-compliant channel estimation and tracking design that achieves remarkably high performance even in the presence of pedestrian user mobility and frame aggregation. The primary contribution of ChASER is to reconstruct transmit symbols at the receiver with extremely low estimation errors by exploiting the output of decoder and the existing transmit DSP blocks with low-complexity adaptive filter. The reconstructed data symbols are then used to estimate and track the CSI at the granularity of data symbols, leading to significantly improved robustness against the time-varying channel dynamics over the duration of the aggregated frame. We demonstrate its benefits and feasibility via software-radio prototype implementation and trace-driven link level simulator which reflect the wireless channel characteristics of the real world. We envision the ChASER's channel tracking scheme to be applicable to any communication system that employs coherent modulation, not just Wi-Fi devices considered in this chapter.

Chapter 5

Power Consumption of Wi-Fi: Modeling and Testbed Validation

5.1 Introduction

This chapter presents a quantitative model for the power consumption of Wi-Fi in idle, receive (RX), and transmit (TX) state to characterize the relationship between IEEE 802.11ac features described in Section 1.2 and the power consumption. Our model takes into account all 802.11ac features presented in Section 1.2. To verify our model, we then show the measured power consumption of an off-the-shelf IEEE 802.11ac-enabled NIC by considering the various IEEE 802.11ac very high throughput (VHT) features.

5.2 Revisit of IEEE 802.11ac Features

5.2.1 Wider Bandwidth Channel

The widening of channel bandwidth, called channel bonding, is first introduced in IEEE 802.11n. As shown in Fig. 1.4, IEEE 802.11ac additionally mandates the operation of 40 MHz and 80 MHz bandwidth which are yielded by bonding two and four adjacent 20 MHz channels, respectively. Besides, 160 MHz bandwidth and combining two non-adjacent 80 MHz channels, namely 80+80 MHz, have been optionally defined. When enabling channel bonding, the PHY data rate increases proportionally to the operating bandwidth.[1]

For backward compatibility, IEEE 802.11ac has defined a transmission format of the PHY that replicates 20 MHz legacy PLCP protocol data unit (PPDU) transmission over multiple adjacent 20 MHz channels, referred to as non-VHT duplicate PPDU. Moreover, the preamble of data frame in the bonded channel (e.g., 80 MHz or 160 MHz) takes the form of the replicated 20 MHz preamble structure. By means of this, the station which operates on 20 MHz channel bandwidth can detect and receive the preamble of the data in the bonded channel and the crucial control frames in the form of the duplicate PPDU, such as request-to-send (RTS), clear-to-send (CTS), and acknowledgement (ACK), from the 802.11ac AP.[2]

5.2.2 MIMO and Higher Order Modulation

IEEE 802.11ac supports MIMO utilizing up to eight antennas. Using MIMO technique, we can achieve much higher PHY rate, but requires more accurate channel estimation and compensation to eliminate the spatial interference.

[1] The increasing rate of PHY data rate is slightly larger than that of bandwidth, because the guard band between the bonded channels is removed, and is used for data transmission.

[2] Due to the low data rate of the non-VHT duplicate PPDU, it is not used for data frames.

Modulation and coding scheme (MCS) index represents the pair of modulation type and coding rate.[3] IEEE 802.11ac newly defines 256-QAM, on top of 64-QAM used by 802.11a/n, thus enabling encoding four times as dense as 64-QAM.

It is generally known that higher order MCS index provides faster PHY data rate while lower order MCS index is used for the more reliable communication.

5.2.3 Relation between 802.11ac Features and Power

The 802.11ac VHT features described above provide ever-increasing PHY rate. However, they have drawbacks.

When channel bonding is used, the sampling rate of analog-to-digital converter (ADC) and digital-to-analog converter (DAC) should be increased to handle wider bandwidth signal correctly based on the Nyquist's theorem [6]. Accordingly, the power consumption of ADC/DAC increases proportionally to the bandwidth. Since DAC power is much smaller than ADC power, the power consumption of receiver is more sensitive to the bandwidth [54].

The use of multiple antennas consumes more energy and its growth rate is a linear function of the bandwidth, because the RF-chain of each antenna operates and senses the whole bandwidth separately.

In the case of 256-QAM, it is straightforward that the complexity of its modulation/demodulation process is similar to that of lower modulation types, but the resultant high PHY rate (in bits per second) requires high computing power (in joules per second), especially for a decoder, such as Viterbi [55]. Similarly, when 256-QAM is used, the receiver consumes more energy than the corresponding transmitter. We explain the details in the following section.

[3] Unlike IEEE 802.11ac VHT-MCS index, IEEE 802.11n high throughput MCS (HT-MCS) index is used to denote the combination of the number of streams, modulation, and coding rate.

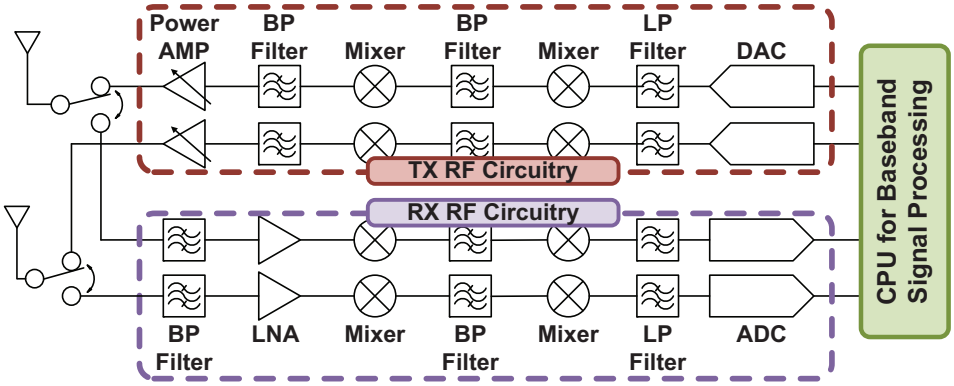

Figure 5.1: Block diagram of RF-chain.

5.3 Modeling 802.11ac Power Consumption

This section presents a quantitative model for the power consumption of Wi-Fi in idle, receive (RX), and transmit (TX) state to validate our explanation in Section 5.2.3.

5.3.1 Power Model of IEEE 802.11ac Receiver

For the power model of an 802.11ac receiver, we acquire and modify a well-designed 802.11n power model in [26]. The power consumption of a receiver (P_{rx}) is given by $P_{\mathrm{rx}} = N_{\mathrm{rx}} P_{\mathrm{rc}} + P_{\mathrm{rb}}$, where N_{rx} is the number of RX antennas, and P_{rc} and P_{rb} are the power consumptions of RF circuitry and baseband processing as shown in Fig. 5.1, respectively.

P_{rc} is categorized into two parts: 1) the constant power consumers, such as low-noise amplifier (P_{LNA}), filter (P_{filter}), mixer (P_{mixer}), and synthesizer (P_{syn}), and 2) the power consumption of ADC (P_{ADC}) which is proportional to bandwidth (B MHz) as follows [55]:

$$P_{\mathrm{ADC}} \approx \frac{3V_{\mathrm{dd}}^2 L_{\mathrm{min}} (2B + f_{\mathrm{cor}})}{10^{-0.1525 n_1 + 4.838}}, \tag{5.1}$$

where where V_{dd}, L_{min}, and n_1 are the power supply, the minimum channel length

for the given complementary metal–oxide–semiconductor (CMOS), and ADC power model coefficient, respectively. f_{cor} is the corner frequency (MHz). So, P_{rc} can be simplified as

$$\begin{aligned} P_{\mathrm{rc}} &= P_{\mathrm{syn}} + P_{\mathrm{filter}} + P_{\mathrm{mixer}} + P_{\mathrm{LNA}} + P_{\mathrm{ADC}} \\ &= \gamma_1 B + \gamma_2, \end{aligned} \tag{5.2}$$

where γ_1 and γ_2 are the receiver circuitry coefficients.

On the other hand, P_{rb}, the baseband processing power of the receiver, includes the power consumption of FFT (P_{FFT}), demodulator (P_{demod}), Viterbi decoder (P_{dec}), and so on as follows:

$$P_{\mathrm{rb}} = P_{\mathrm{FFT}} + P_{\mathrm{demod}} + P_{\mathrm{dec}} + P_{\mathrm{misc}}, \tag{5.3}$$

where P_{misc} is the power consumption of the rest of the processing blocks which are correlated with B [56]. Let N_{ss} be the number of spatial streams. P_{FFT}, P_{demod}, and P_{dec} are functions of $N_{\mathrm{rx}} B \log_2 B$, $N_{\mathrm{ss}} B$, and PHY rate (r Mb/s), respectively. The details are omitted due to space limit. From Eqs. (5.2) and (5.3), P_{rx} can be modeled as

$$\begin{aligned} P_{\mathrm{rx}} = B(&\alpha_1 N_{\mathrm{rx}} + \alpha_2 N_{\mathrm{rx}} \log_2 B + f_{\mathrm{rx}}(N_{\mathrm{ss}})) \\ &+ \alpha_3 N_{\mathrm{rx}} + \alpha_4 r + P_f, \end{aligned} \tag{5.4}$$

where α_1, α_2, α_3, α_4, and f_{rx} are RX model coefficients and P_f is the base power consumption of the NIC (mW).

The power consumption of idle state, P_{idle}, is roughly the multiplication of P_{rc} and N_{rx} owing to almost no baseband signal processing, and hence it is formulated as

$$P_{\mathrm{idle}} = i_1 N_{\mathrm{rx}} B + i_2 N_{\mathrm{rx}} + P_f, \tag{5.5}$$

where i_1 and i_2 are the idle model coefficients.

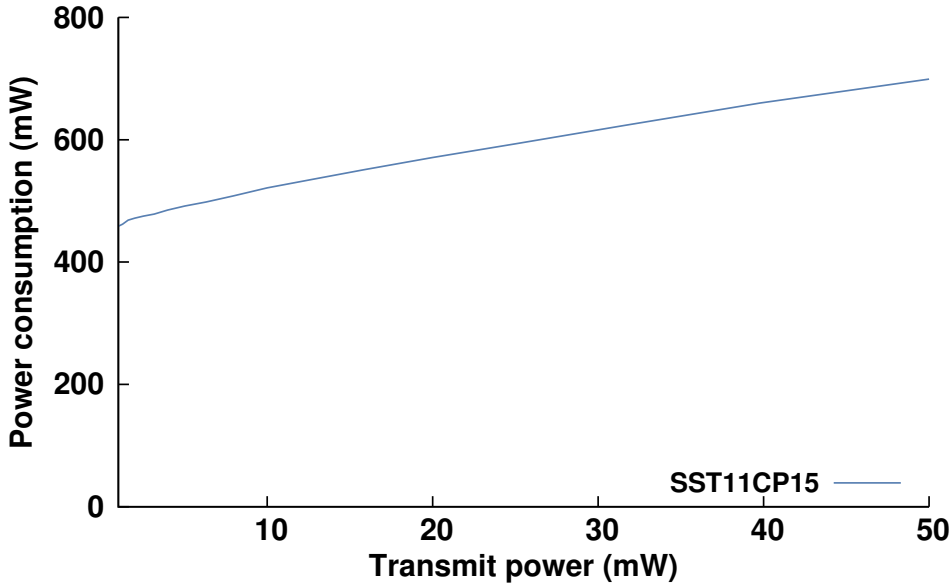

Figure 5.2: Power consumption of SST11CP15 Wi-Fi power amplifier.

5.3.2 Power Model of IEEE 802.11ac Transmitter

Now, we design a novel and accurate power model of an IEEE 802.11ac transmitter. The circuitry and processing paths of the transmitter is reversely similar to those of the receiver except the power amplifier as shown in Fig. 5.1. Therefore, the TX power is composed of the power consumption of radio circuitry (P_{tc}) and the baseband processing (P_{tb}), given as $P_{\mathrm{tx}} = N_{\mathrm{tx}}P_{\mathrm{tc}} + P_{\mathrm{tb}}$, where N_{tx} is the number of TX antennas.

First of all, P_{tc} can then be formulated by

$$P_{\mathrm{tc}} = P_{\mathrm{amp}} + P_{\mathrm{mix}} + P_{\mathrm{syn}} + P_{\mathrm{filt}} + P_{\mathrm{DAC}}. \tag{5.6}$$

The total transmit power (P_t mW) is evenly divided into TX antennas. Let $\hat{P}_t = P_t/N_{\mathrm{tx}}$ be the transmit power of each antenna, and hence the power consumption of each power amplifier (PA) is given as $P_{\mathrm{amp}} = \frac{\hat{P}_t}{\eta(\hat{P}_t)}$, where η is PA efficiency [57].

Since η is a linear-like function of transmit power [4] and $\lim_{\hat{P}_t \to 0} \eta(\hat{P}_t) = 0$ [58], we have

$$P_{\text{amp}} \approx \nu_1 \hat{P}_t + \nu_2 = \nu_1 \frac{P_t}{N_{\text{tx}}} + \nu_2, \tag{5.7}$$

where ν_1 is PA power coefficients, and ν_2 is PA power when $P_t = 0$, caused by the quiescent current of gate voltage. Thus, total PA power is equal to $\nu_1 P_t + \nu_2 N_{\text{tx}}$. Fig. 5.2 shows the power consumption of Wi-Fi's PA (SST11CP15) as P_t [58]. For the PA, ν_1 and ν_2 are about 4.9 and 465, respectively. Briefly, the total PA power highly depends on N_{tx}, not its output power, P_t. Moreover, the power consumption of DAC is highly related to B as follows [55]:

$$P_{\text{DAC}} = \left(\frac{1}{2} V_{\text{dd}} I_0 \left(2^{n_2} - 1\right) + n_2 C_p \left(2B + f_{\text{cor}}\right) V_{\text{dd}}^2 \right), \tag{5.8}$$

where I_0 and C_p are the unit current source and the capacitance, respectively. n_2 is DAC model parameter. Since the others consumes the constant power, Eq. (5.6) can be simplified as

$$\begin{aligned} P_{\text{tc}} &= \nu_1 \frac{P_t}{N_{\text{tx}}} + \nu_2 + P_{\text{mixer}} + P_{\text{syn}} + P_{\text{filter}} + P_{\text{DAC}} \\ &= \kappa_1 \frac{P_t}{N_{\text{tx}}} + \kappa_2 B + \kappa_3, \end{aligned} \tag{5.9}$$

where κ_1, κ_2, κ_3 are the circuitry power coefficients.

The transmit baseband processing block is composed of IFFT, modulator, and encoder, thus its power consumption can be expressed as

$$P_{\text{tb}} = P_{\text{IFFT}} + P_{\text{mod}} + P_{\text{enc}} + P_{\text{misc}}, \tag{5.10}$$

where P_{IFFT}, P_{mode}, and P_{mod} are the power consumption of IFFT, modulator, and encoder. Likewise, P_{IFFT} and P_{mod} are the linear function of $N_{\text{ss}} B \log_2 B$ and $N_{\text{ss}} B$, respectively.

[4] η is known to be exponentially related to transmit power in dBm, thus is linear-like function with respect to transmit power in mW, P_t.

From Eqs. (5.9) and (5.10), the TX power consumption can be modeled as

$$\begin{aligned} P_{\mathrm{tx}} = B(\beta_1 N_{\mathrm{tx}} + \beta_2 N_{\mathrm{ss}} \log_2 B + f_{\mathrm{tx}}(N_{\mathrm{ss}})) \\ + \beta_3 N_{\mathrm{tx}} + \beta_4 r + \beta_5 P_t + P_f, \end{aligned} \tag{5.11}$$

where β_1, β_2, β_3, β_4, β_5, and f_{tx} are the TX power model coefficients.

5.4 Power Consumption Measurement

To validate our model, we show the measured power consumption of a commercial 802.11ac NIC. We investigate how much energy is consumed in IEEE 802.11ac NIC according to its state. The 802.11ac features in Section 5.2 are considered, and the combination of the features is denoted by N_{ant}XB, where N_{ant} and B are the number of active transmit/receive antennas and the bandwidth, respectively. For example, 3X80 stands for the setting using 3 active antennas and 80 MHz bandwidth. The state can be classified into three categories: 1) Idle state, 2) receive state, and 3) transmit state.

5.4.1 Experimental Setting

We have conducted extensive experiments using Qualcomm Atheros 9880 chipset (QCA9880), which is the state-of-the-art NIC available since 2013 [59]. The QCA9880 is installed in a desktop node via a PEX1-MINI-E adapter which converts from mini-PCI express to PCI express [60]. The node is used as a station while running 3.18.0 Linux kernel and open source device driver, $ath10k$ [35, 61]. We use ASUS RT-AC66U as an AP, which is equipped with Broadcom BCM4360 chipset and runs custom firmware, ASUSwrt-Merlin 3.0.0.4 [62, 63]. Both the AP and the NIC support up to 3x3 MIMO, 80 MHz channel bandwidth, and 256-QAM. We place the station approximately 0.5 m away from the AP, where the distance is relatively short.

As for the power consumption measurement of the 802.11ac NIC, we use a similar method presented in [23]. We put a 40 mΩ resistor in front of the power pin of the adapter which supplies 3.3 V to the NIC. By using data acquisition tool, i.e., NI USB-6210 [64],[5] we measure and record the voltage drop across the resistor to obtain the current, and thus can compute the power consumption of the NIC. In the case of the transmit/receive power consumption, we send 600 long data frames (i.e., A-MPDU), and average multiple samples over the actual frame transmission/reception duration except idle duration. Otherwise, for the power consumption in idle state, the recorded samples are averaged over a 6 second run in a controlled environment, where no interference is observed.

5.4.2 Idle State Power Consumption

Fig. 5.3(a) shows the measured power consumption in idle state (P_{idle}). We observe that the use of wider bandwidth consumes more energy in idle state where the NIC does not receive and/or transmit frames actively. When 1X80, mandated in 802.11ac, is used, P_{idle} increases by 26% and 21% over that of 1X20 and 1X40 setting, respectively. This result presents the opposite conclusion from the result studied in [23]. The authors argue that 802.11 devices simply add subcarriers for channel bonding while keeping the sampling rates the same, but the sampling rate of ADC and fast Fourier transform (FFT) size should be increased to decode the baseband signal correctly as discussed in Section 5.2.3. It is well known that higher sampling rate and larger FFT size consume more power. In short, using channel bonding trades off energy cost for PHY rate.

Furthermore, the use of more antennas intensifies the increase of P_{idle} induced by the widening of bandwidth. As an evidence, 3X80 consumes 39% more energy than

[5]NI-6210 provides the maximum 250 kHz sampling rate with 16 bit precision. That is, NI-6210 is able to measure the voltage drop every 4 μs.

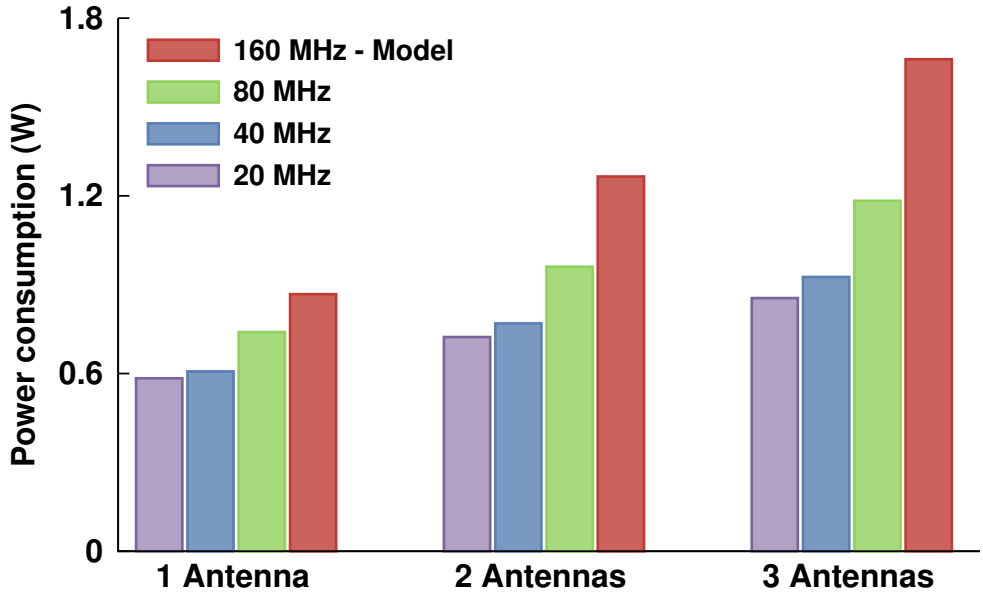

(a) Idle state.

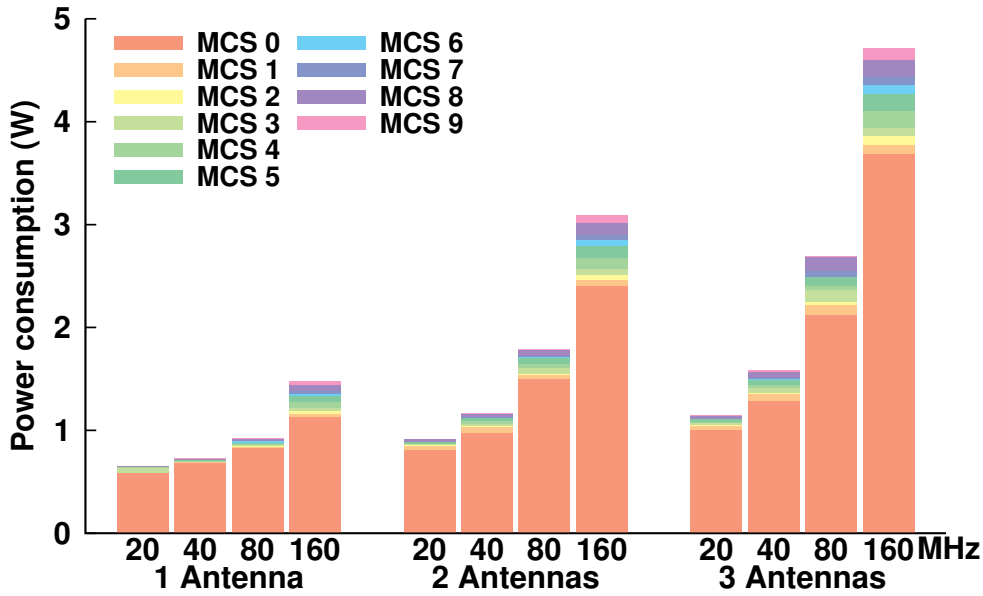

(b) Receive state.

Figure 5.3: Measured idle/RX power consumption of QCA9880, where 160 MHz results are from a measurement-driven model.

3X20. It is due to the fact that each RF-chain listens to the whole bandwidth, and senses the channel with high sampling rate.

5.4.3 Receive State Power Consumption

As shown in Fig. 5.3(b), the measured RX power (P_{rx}) shows a similar trend as P_{idle}. Especially, in the case of 1X20, P_{rx} is approximately equal to or slightly larger than P_{idle}. This is because that the receive RF circuitry, which is the major energy consumer, shall operate at all times even if there is no frame to transmit and/or receive.

On the other hand, the growth rate of P_{rx}, in accordance with the increase of N_{ant} and B, is much higher than that of P_{idle}. It is caused by the fact that the energy cost of 802.11ac receiver is increasingly dominated by baseband processing blocks, such as FFT, minimum mean square error (MMSE) detector, and Viterbi decoder, which are not used at idle state.

In addition, we observe that the NIC consumes more power during frame reception with higher order MCS index, because the power consumption of Viterbi decoder, one of power hungry processing blocks, highly depends on PHY rate [55]. Therefore, the RX power increases with the use of higher order MCS, and the amount of the increase becomes higher when the NIC operates with wider bandwidth. For example, when 3X20/40/80 are used, MCS 9 consumes 144, 300, 569 mW more than MCS 0, respectively.

5.4.4 Transmit State Power Consumption

Fig. 5.4(a) shows the TX power consumption (P_{tx}) with various fixed MCSs when P_t is 0 dBm. Unlike P_{idle} and P_{rx}, the P_{tx} depends slightly on B and MCS, but greatly depends on N_{ant}. This is due to the fact that total PA power, which is the majority of P_{tx}, is greatly influenced by N_{ant} as described in Section 5.3.2. The transmit components

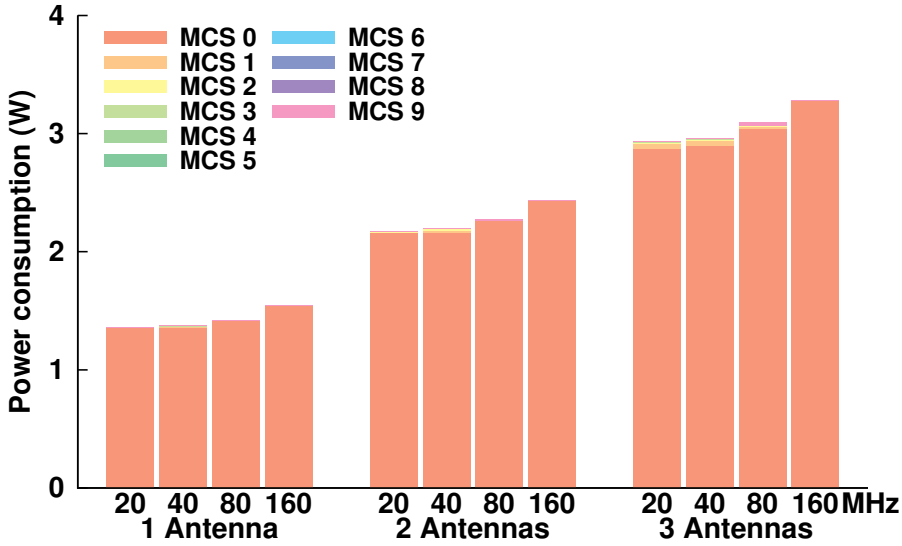

(a) Fixed $P_t = 0$ dBm and various MCSs.

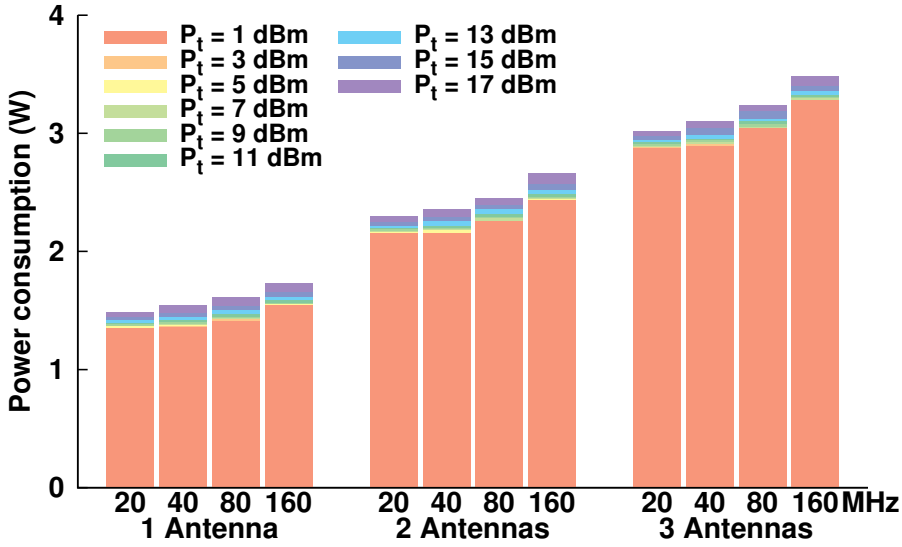

(b) Fixed MCS 0 and various P_t.

Figure 5.4: Measured TX power consumption of QCA9880, where 160 MHz results are from a measurement-driven model.

Table 5.1: Idle and RX power consumption model for QCA9880.

α_1	α_2	α_3	α_4	$f_{\mathrm{rx}}(N_{ss})$			i_1	i_2	P_f
				SS	DS	TS			
0.035	0.48	82.4	0.47	0.156	4.4	8.6	1.978	79.9	472.1

Table 5.2: TX power consumption model for QCA9880.

β_1	β_2	β_3	β_4	β_5	$f_{\mathrm{tx}}(N_{\mathrm{tx}})$		
					SS	DS	TS
0.022	0.038	802.201	0.01	4.352	1.623	1.68	1.71

related to B and MCS, such as DAC, modulator, and encoder, use considerably small or negligible power compared with the corresponding receive blocks of a receiver [55]. Especially, the DAC power is about one forth of the ADC power [54]. Interestingly, due to these aspects, RX power is comparable to TX power when wider bandwidth is used. As an evidence, for 2X80 and 3X80, RX power has come close to TX power.

In Fig. 5.4(b), we additionally depict TX power consumption with various transmit power (P_t) from 1 dBm to 17 dBm. P_{tx} increases as P_t increases but the amount of the growth is independent of N_{tx} and B as explained in Section 5.3.2. Furthermore, the growth from the varying P_t is marginal, e.g., 6.3% of the entire power consumption for 3X80.

5.4.5 Power Model Verification

We now verify our power model through measurement results presented above. As presented in Tables 5.1 and 5.2, we calculate the coefficients of idle, RX, and TX power consumption models for QCA9880 using nonlinear regression analysis of IBM

SPSS [65]. The average estimation error of the proposed power model is below 2.3% for all PHY parameter combinations, and it leads to better accuracy (as high as 2.4 percent point) compared with the model presented in [26].

As discussed in Section 5.2.3, idle and RX power model is highly related to the bandwidth due to the fact that the relevant coefficients (i.e., i_1, α_1, α_2, and f_{rx}) are large enough, but TX power model is not. Moreover, PHY rate coefficient of TX power model (β_4) is negligible while the corresponding coefficient of RX (α_4) is nonnegligible.

Based on the measurement-driven model, we estimate the power consumption when 160 MHz is used as shown in Figs. 5.3 and 5.4.[6] 3X160 consumes 1.9x and 4.1x more energy than 3X20 in idle and RX state, respectively. Furthermore, 3X160 setting consumes even more energy in RX state than in TX state based on our power model. This result is against the common sense that TX is the most energy-hungry state.

5.4.6 Summary

In a nutshell, our major findings are:

- The wider bandwidth is, the more energy is consumed.
- Particularly, idle and RX state powers highly depend on bandwidth, and is comparable to TX state power.

Thus, considering wider bandwidth originated by channel bonding becomes increasingly important to save idle and RX state energy cost for the 802.11ac Wi-Fi which mandates the channel bonding up to 80 MHz. Since most existing researches

[6]Throughout Chapters 5 and 6, the 160 MHz results are obtained by our power model in Section 5.3, because 160 MHz-supporting NIC is not available today.

available in practice attempt to adapt only PHY rate and the number of antennas to save energy as summarized in Section 1.3.5, we propose a novel sophisticate and practical bandwidth control technique to improve Wi-Fi energy efficiency.

Chapter 6

WiZizz: Energy Efficient Bandwidth Management

6.1 Introduction

Recently, a largely growing number of portable devices, such as smartphones, tablets, and laptops, are being equipped with WiFi, the hallmark of the IEEE 802.11 wireless LAN (WLAN), in order to meet the ever-increasing traffic demands at low cost. Encouraged by such success, the emerging 802.11 specification, IEEE 802.11ac, mainly focuses on improving physical layer (PHY) rate via enabling multiple antennas, called multiple-input multiple-output (MIMO), and bandwidth widening, known as channel bonding [2]. Nowadays, however, as the battery-powered portable device users place increasingly complex demands on the functionality of their devices, battery life time satisfaction is becoming increasingly important.

It is not easy to run after two hares, i.e., high data rate and energy efficiency, due mainly to the inherent high power consumption of MIMO and channel bonding. Furthermore, channel bonding is considered the dominant factor of WiFi's power consumption especially for the portable devices, because those devices in practice have a small number (i.e., one or two) of antennas due to the small form factor, while

four times wider operating bandwidth, i.e., 80 MHz [2], is mandated. Additionally, the power consumption is amplified by the inefficient design of WiFi, whose radio frequency (RF) chains operate steadily to receive every incoming frame.

Our extensive experiment presented in Chapter 5 have revealed that the power consumption of IEEE 802.11ac network interface card (NIC) is dominated by the receiver's channel sensing and listening operation (so-called *idle* state) and the reception of frames destined to others. Furthermore, we confirm that WiFi's power consumption increases proportionally to the active channel bandwidth. For example, the use of wider bandwidth consumes as high as 1.4x and 2.3x more energy to sense the channel at idle state and to receive the avoidable frames addressed to others, respectively. Theoretically, if WiFi has the prior knowledge of the idle duration and the destination of the frames, it can sleep or filter out the frames at PHY.[1] In reality, the unpredictable behavior of carrier sense multiple access (CSMA) makes the problem difficult to overcome.

Fortunately, thanks to the duplicated format defined in IEEE 802.11ac, control and management frames can be decoded even when the active bandwidth (e.g., 20 MHz) is much narrower than the operating bandwidth (e.g., 160 MHz) [2]. By exploiting the duplicated format based signaling, we propose a bandwidth control technique, called WiZizz, which handles the channel bandwidth on demand to minimize the needlessly spent energy.

6.2 WiFi Need to Zizz

WiFi is known to be a primary energy consumer in battery-powered portable devices. The root cause is that WiFi preposterously oversamples wireless signal to successfully

[1] 802.11ac has no aversion to filtering avoidable frames at PHY. For example, group ID is used for such frame drop at the risk of disabling virtual carrier sensing.

detect a frame which may or may not exist in near future.

In [30], Zhang *et al.* show that stations spend most of the time in idle state rather than TX/RX and sleep state. For more than 92% of stations, 90% of energy is spent in idle while the fractions of energy spent in TX/RX and sleep are below 20% and 36%, respectively. This confirms that the energy of WiFi is remarkably consumed in idle state even if the PSM is activated.

Moreover, due to the inherent nature of IEEE 802.11, WiFi has to decode and receive the frames destined to other WiFi devices unnecessarily. Our evaluation shows that such needless frame receptions are too costly in a large dense network. The energy cost becomes increasingly dominant along with the usage of wider channel bandwidth.

Fortunately, most crucial frames, such as management and control frames, are transmitted in the format of 20 MHz legacy PPDU (i.e., IEEE 802.11a) over the primary channel or in the duplicated format of legacy PPDU over the entire operating bandwidth as explained in Section 5.2.1. Thus, the receiver can detect and decode such frames easily, even if it only listens to 20 MHz primary channel instead of the whole channel. We called such listening mode *zizz mode*. By letting WiFi in zizz (WiZizz) on demand, we can save energy surprisingly without sacrificing network capacity.

6.3 WiZizz Design

We now describe the details of our approach, called WiZizz, which manages the active bandwidth to minimize the power consumption of a station which enables the channel bonding in 802.11ac standard. WiZizz allows the station to operate with only 20 MHz bandwidth of primary channel (i.e., zizz mode) for a significant portion of time while avoiding needless frame reception. To support WiZizz, 1) AP should be able to let a receiver know when its bandwidth must be changed, and 2) the receiver then should

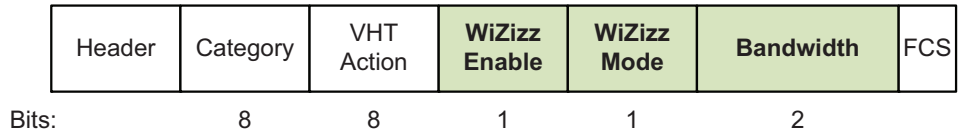

Figure 6.1: WiZizz action frame format.

switch the active bandwidth quickly. It is well known that the receiver is unable to decode the frame transmitted with wider bandwidth than its active bandwidth. However, we can simply solve the issue by exploiting the duplicate format for the purpose of WiZizz signaling.

In addition, as depicted in Fig. 6.1, we have defined a new action frame for WiZizz agreement between the AP and the station. Moreover, the action frame can be used for the intended bandwidth switching as well. WiZizz is classified as dynamic and pseudo-dynamic mode according to the switching delay capability of the station.

6.3.1 Dynamic Mode

We first introduce dynamic mode of WiZizz which controls active bandwidth per frame basis. Fig. 6.2 illustrates an example of the WiZizz operation. If there is no ongoing transmission for a dynamic WiZizz station (i.e., STA1), the station continuously listens to the 20 MHz bandwidth of primary channel. Shortly, it is put to zizz mode.

When the station receives the preceding sequence of a data frame exchange (e.g., RTS/CTS sequence) addressed to it, the station immediately switches from zizz mode to awake mode, where the station enables the full operating bandwidth, within short inter frame space (i.e., SIFS, 16 μs). Note that the AP can decide whether or not to

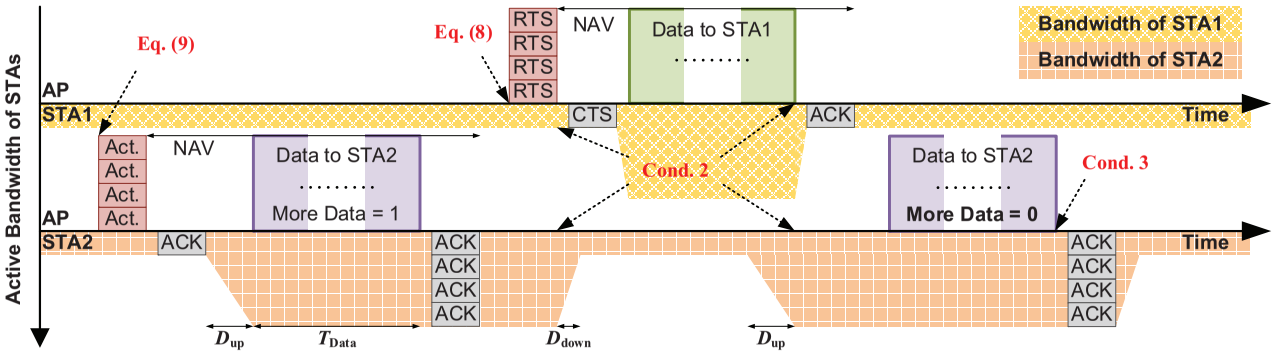

Figure 6.2: WiZizz operation example, and the resultant active channel bandwidth changes. STA1 is capable of using dynamic WiZizz ($D_{\mathrm{up,STA1}}, D_{\mathrm{down,STA1}} <$ SIFS) while STA2 uses pseudo-dynamic WiZizz ($D_{\mathrm{up,STA2}}, D_{\mathrm{down,STA2}} >$ SIFS). The Data frames illustrated in this example are condensed, thus T_{Data} is much longer than the duration of other frames.

send the preceding sequence using the following condition:

$$T_{\mathrm{Data}}(r_{20}) + T_{\mathrm{ACK}} + \mathrm{SIFS} \underset{\text{zizz}}{\overset{\text{awake}}{\gtrless}} T_{\mathrm{RTS}} + T_{\mathrm{CTS}} + T_{\mathrm{Data}}(r_{80}) + T_{\mathrm{ACK}} + 3\mathrm{SIFS}, \tag{6.1}$$

where r_{20} and r_{80} is the PHY rate in 20 MHz and 80 MHz bandwidth, respectively. T is a frame duration. Briefly, if the exchange sequence duration of WiZizz (i.e., RTS/CTS/Data/ACK exchange duration) is longer than the data frame duration with 20 MHz bandwidth, the station remains in zizz mode and the AP send data with 20 MHz PPDU. This is because, when the size of data is small enough, the unacceptable overhead of WiZizz may decrease overall network capacity and the energy efficiency of the receiver. After finishing the data exchange sequence, the receiver switches back to the narrowest bandwidth, and "zizz" again.

However, if the switching delay of a NIC is longer than SIFS, the dynamic WiZizz is inapplicable for the NIC, because it can not receive the following data frame at right time.

6.3.2 Pseudo-dynamic Mode

As presented in Section 6.4.2, QCA9880 chipset is unable to adopt dynamic WiZizz due to the relatively long bandwidth switching delay. To address this challenge in practice, we design pseudo-dynamic mode which controls the active bandwidth in a long-term strategic manner.

Unlike dynamic mode, when a WiZizz station receives the WiZizz action frame whose bandwidth field set to the full operating bandwidth, its active bandwidth becomes wider to prepare the data frame reception, as STA2 does in Fig. 6.2. Note that the action frame is transmitted in the duplicate format of legacy PPDU. The network

allocation vector (NAV) of the action frame is determined by considering the switching delay, D_{up}, which is delivered to the AP at the association stage. The upward-switching follows a similar rule presented in Eq. (6.1), and it is given by

$$T_{\mathrm{Data}}(r_{20}) + T_{\mathrm{ACK}} + \mathrm{SIFS} \underset{\text{zizz}}{\overset{\text{awake}}{\gtrless}} D_{\mathrm{up}} + D_{\mathrm{down}} + T_{\mathrm{Action}} + T_{\mathrm{Data}}(r_{80}) + 2T_{\mathrm{ACK}} + 2\mathrm{SIFS}. \tag{6.2}$$

Shortly, Action/ACK/Data/ACK exchange duration and its switching delay should be shorter than the data frame exchange duration with 20 MHz bandwidth.

On the other hands, the station decides to switch back to zizz mode through any of the following conditions:

Cond. 1: It receives the WiZizz action frame addressed to it, and its bandwidth field set to 20 MHz.

Cond. 2: It receives a frame addressed to another station, and its duration specified in the frame control field is longer than the switching delay ($D_{\mathrm{up}} + D_{\mathrm{down}}$). Afterwards, the station switches back to the full operating bandwidth at the end of the frame as shown in Fig. 6.2.

Cond. 3: It receives a frame, addressed to it, with the more data bit in the frame control field set to 0.[2]

An example of WiZizz operation is described in Fig. 6.2. STA1 (dynamic mode) changes its bandwidth for every frame exchange while STA2 (pseudo-dynamic mode) basically switches its bandwidth when WiZizz action frame is received. Moreover, STA2 starts to zizz when it receives a frame whose duration is long enough to meet **Cond. 2** (i.e., RTS) or whose more data bit is 0 (i.e., meet **Cond. 3**).

[2]If the station in PSM, it can be put to sleep instead of zizz.

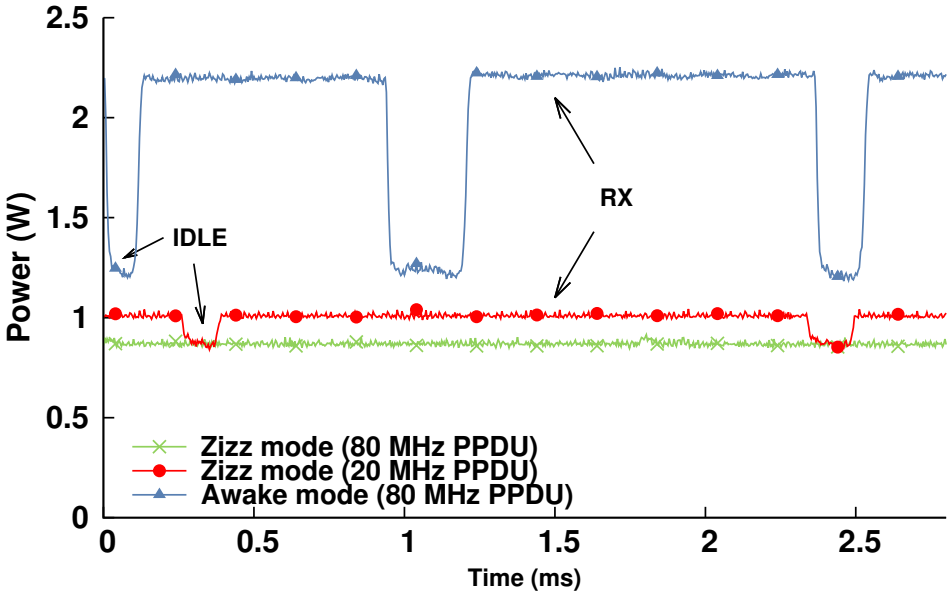

Figure 6.3: WiFi in zizz discards the frame with wider bandwidth.

6.3.3 PHY-level Filtering

A station, which enables WiZizz, is able to achieve an additional energy save effect for the avoidable frame reception. For a frame destined to other stations and transmitted with wider bandwidth, i.e., 40 MHz, 80 MHz, and 160 MHz, than the active bandwidth in zizz mode, i.e., 20 MHz, the station in zizz discards the frame right after decoding the bandwidth information of the preamble. Thanks to the duplicate structure of the preamble, the station can decode the bandwidth information successfully even in zizz mode. This is a kind of PHY-level filtering.

To prove this, we measure and record the QCA9880's power consumptions in both awake and zizz modes, when there are incoming frames addressed to another station with 20 MHz or 80 MHz bandwidth. As shown in Fig. 6.3, a station in zizz consumes constant power when a frame with 80 MHz bandwidth is detected (green line with

cross), which means that the station discards the frame and senses the channel consistently. The station in awake mode, in contrast, consumes more than 2.3x energy for the needless frame reception (blue line with triangle). Additionally, WiZizz station can detect and receive a frame with 20 MHz PPDU as described above (red line with circle), and the reception further requires only marginal energy.

6.4 Testbed Experiments

6.4.1 Prototype Implementation and Testbed Setting

To verify the feasibility of the proposed approach, we have implemented WiZizz using QCA9880 and $ath10k$ [61]. Due to the long switching delay of QCA9880 as shown in Section 6.4.2, pseudo-dynamic WiZizz is implemented in both the AP and station nodes.[3]

The QCA9880 is installed in a desktop node via a PEX1-MINI-E adapter which converts from mini-PCI express to PCI express [60]. The node is used as a station while running 3.18.0 Linux kernel and open source device driver, $ath10k$ [35, 61]. We also use the node as a programmable AP using $hostap$ [34]. Additionally, we have placed the stations 1 m away from the AP, and use the fixed MCS 0 and 3X80 setting for all experiments.

As for the power consumption measurement of the 802.11ac NIC, we use a similar method presented in [23]. We put a 40 mΩ resistor in front of the power pin of the adapter which supplies 3.3 V to the NIC. By using data acquisition tool, i.e., NI USB-6210 [64],[4] we measure and record the voltage drop across the resistor to obtain

[3]Due to the limited modifiability of $ath10k$, we only consider **Cond. 1** in this chapter. So, the AP transmits the action frame at the end of every frame exchange sequence to let the station zizz.

[4]NI-6210 provides the 250 kHz sampling rate with 16 bit precision.

the current, and thus can compute the power consumption of the NIC. The power consumption results are measured in a controlled environment, where no interference is observed. Throughout the chapter, all results are measured at the station side.

6.4.2 Bandwidth Switching Delay

We first examine how long the commercial 802.11ac NIC, QCA9880, takes to switch bandwidth. To estimate the delay, we have measured and recorded the power consumption of QCA9880 over time by varying its operating bandwidth and the number of active antennas, as shown in Fig. 6.4. We measure 15 runs for each setting.

We observe that the upward-switching delay is much longer than the downward-switching delay for all the cases. The delay does not depend on the number of antennas, but on the operating channel bandwidth. For example, switching between 20 MHz and 40 MHz takes less time than that between 20 MHz and 80 MHz, while the delays of both the cases with single antenna and three antennas are almost the same. In average, D_{up} and D_{down} between 20 and 80 MHz is 73.6 and 48.5 μs, but those between 20 and 40 MHz takes 40.5 and 22.7 μs, respectively.

Switching between 20 MHz and 80 MHz is done in two stages as shown in Figs. 6.4(a) to 6.4(d). Presumably, the receiver first converts its bandwidth to an intermediate bandwidth (i.e., 40 MHz), and then the final bandwidth switching is performed. If the bandwidth switching is available without an intermediate bandwidth, the delay may decrease.

6.4.3 Performance Evaluation

We now evaluate the effectiveness and feasibility of WiZizz. Fig. 6.5(a) plots the the power consumption comparison of the receiving station in one-to-one scenario, where the source rate of *Iperf* is varied from 20 kb/s to 20 Mb/s to make different traffic

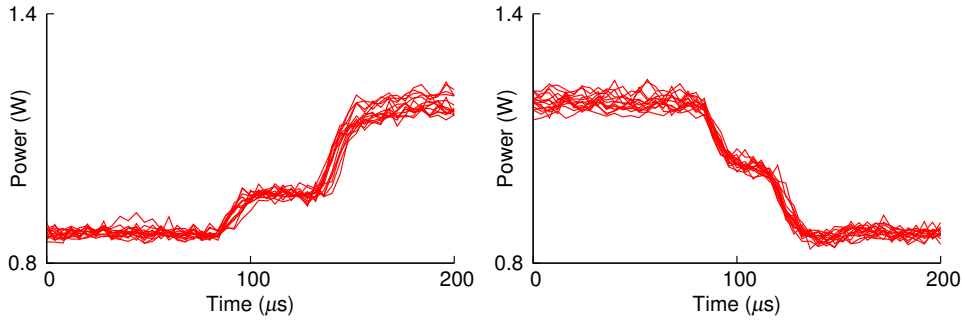

(a) 3X20 ↦ 3X80.

(b) 3X80 ↦ 3X20.

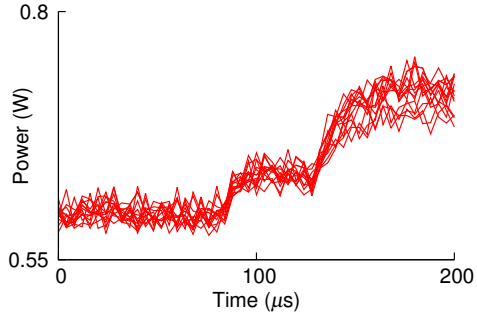

(c) 1X20 ↦ 1X80.

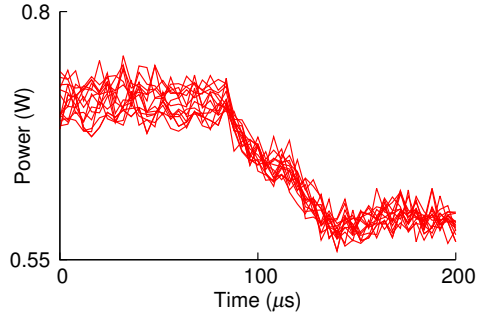

(d) 1X80 ↦ 1X20.

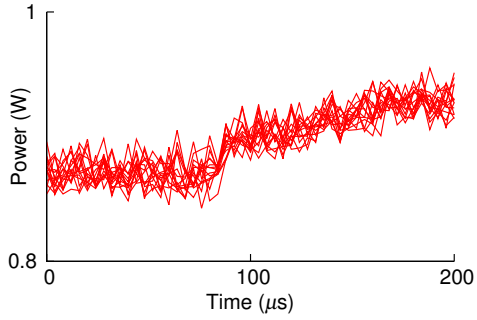

(e) 3X20 ↦ 3X40.

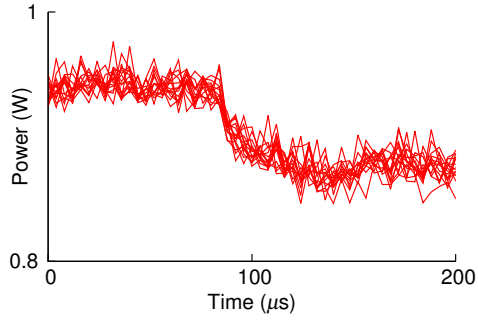

(f) 3X40 ↦ 3X20.

Figure 6.4: Measured bandwidth switching delay of QCA9880. "3X20 ↦ 3X80" stands for the bandwidth switching from 20 MHz to 80 MHz, where three antennas are activated.

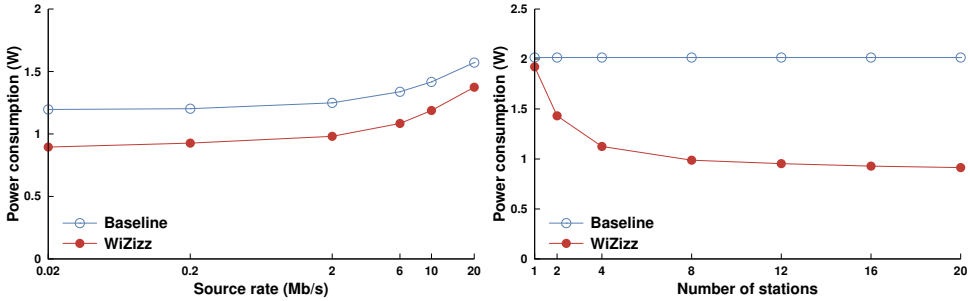

(a) One-to-one scenario.

(b) Multiple node scenario.

Figure 6.5: Measured power consumption.

loads [38]. From the result, we can argue that WiZizz saves energy in idle state because, when the source rate is low (e.g., 20 kb/s), the baseline 802.11ac consumes 34% more power than WiZizz. However, the energy-saving gain decreases as the source rate increases due to the fact that the fraction of time spent in idle is gradually diminished.

We then investigate the impact of the number of stations (N_{sta}) under saturated traffic loads as shown in Fig. 6.5(b). There is a WiZizz station, and the others disable WiZizz. As N_{sta} increases, the power consumption of the WiZizz station (P_{WiZizz}) decreases while that of the baseline 802.11ac station (P_{baseline}) remains the same regardless of N_{sta}. The gain is induced by PHY-level filtering, discussed in Section 6.3.3. Consequently, the maximum 55% energy-saving gain can be achieved by adopting WiZizz.

6.5 Simulation Results

We now evaluate WiZizz's energy efficiency through network-level simulation to provide in-depth performance analysis in more general environments.

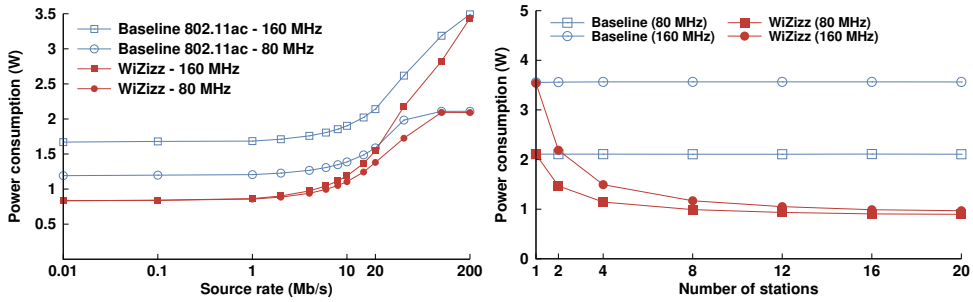

(a) One-to-one scenario.

(b) Multiple node scenario.

Figure 6.6: Performance comparison in ns-3.

6.5.1 Simulation Methodology

We have developed ns-3, where IEEE 802.11ac PHY/MAC layer protocol stacks are additionally implemented [50]. Furthermore, in order to reflect reality well, when a station receives frames transmitted with wider bandwidth than its active bandwidth, the station drops the frame and just senses channel. We use the Rayleigh fading channel model with the assumption of the antenna correlation matrix is the identity matrix. In addition, for the comparison purpose, we have implemented SMPS and the power measurement module based on our proposed model described in Section 5.3.

6.5.2 Constant Traffic Source with Fixed MCS

We first consider the constant traffic source with the fixed MCS 0 with varying traffic loads and N_{sta}. In this simulation, stations with 3 active antennas are evenly spaced on a circle around the AP with the radius of 5 m. There are negligible channel errors.

Figs. 6.6(a) and 6.7(a) shows the power consumption in each idle and RX state with varying traffic loads in one-to-one scenario. As discussed in Section 6.4.3, WiZizz reduces energy cost in idle state. Especially, when 160 MHz bandwidth is used, the max-

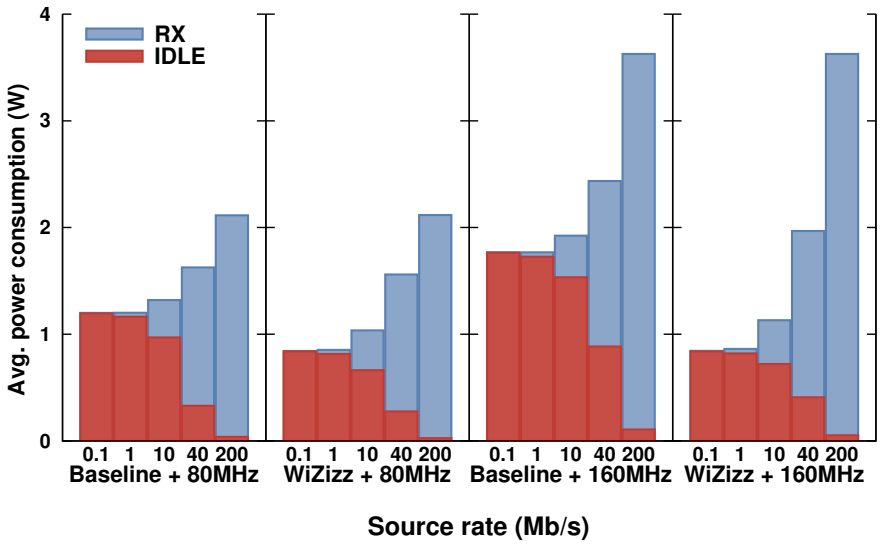

(a) One-to-one scenario.

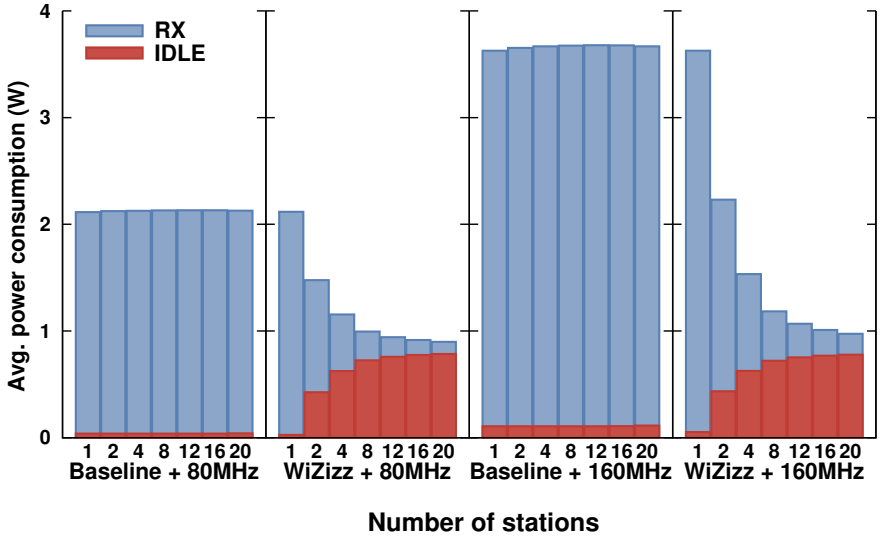

(b) Multiple node scenario.

Figure 6.7: Fraction of power consumption in different states.

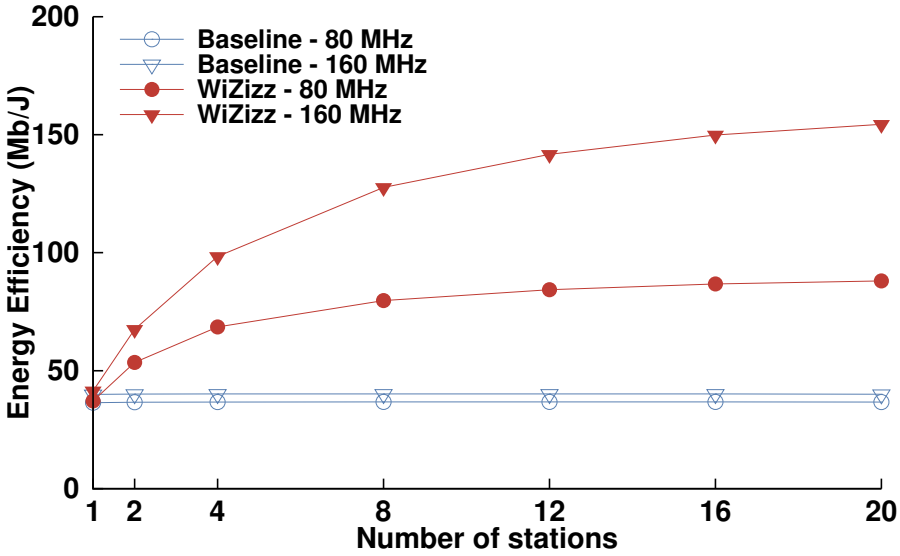

Figure 6.8: Energy efficiency.

imum 53% energy-saving gain can be achieved. As shown in Figs. 6.6(b) and 6.7(b), the baseline 802.11ac station consumes more traumatic energy with the increase in the number of stations, which receive saturated traffic, because the station should decode and receive all the frames including avoidable ones. Thanks to PHY-level filtering, P_{WiZizz} in RX gradually decreases due to the fact that the fraction of RX time decreases while time and energy cost fraction in idle state increases. As a result, WiZizz remarkably reduces the total power consumption (as high as 73%) compared with the baseline.

Fig. 6.8 plots the energy efficiency of the baseline 802.11ac and WiZizz. The baseline 802.11ac shows almost same energy efficiency irrespective of the operating bandwidth and N_{sta}. However, when WiZizz is used, the efficiency increases with the increase of the bandwidth and N_{sta}, because our approach not only saves the energy cost significantly but also its overhead can be neglected thanks to our judicious decision

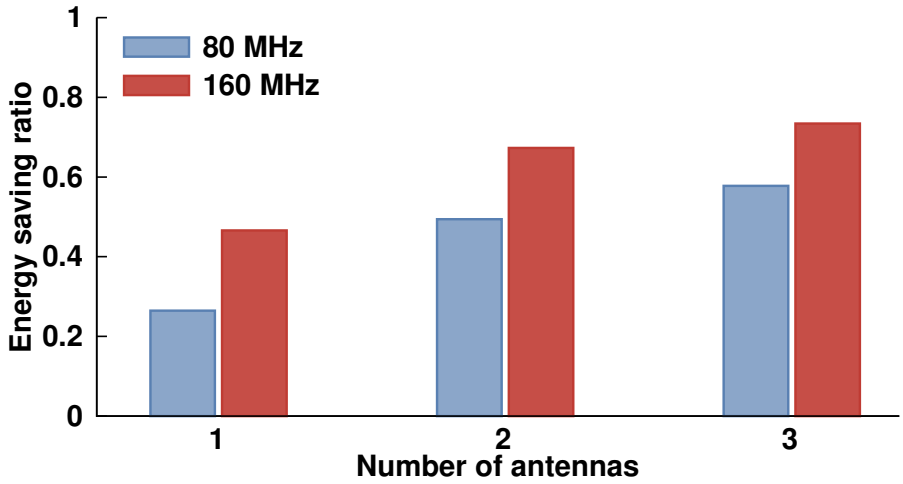

Figure 6.9: Energy saving ratio.

using Eqs. (6.1) and (6.2) and efficient MAC of 802.11ac. Note that frame aggregation features of 802.11ac amortizes the overhead over multiple aggregated frames. In particular, the maximum 3.9x energy efficiency can be achieved when the station operates on 160 MHz bandwidth while contending with 20 stations.

Fig. 6.9 shows the impact of N_{ant}, where N_{sta} is 20. The energy-saving ratio of WiZizz over the baseline (i.e., $\frac{P_{\text{baseline}} - P_{\text{WiZizz}}}{P_{\text{baseline}}}$) increases as N_{ant} and bandwidth increase. Shortly, when more N_{ant} and/or wider bandwidth are used, WiZizz can save more energy.

6.5.3 Comprehensive Traffic Patterns

In order to evaluate the effectiveness of WiZizz in a more general environments, we have implemented various types of traffic, such as voice over IP (VoIP), web browsing, and file transfer protocol (FTP) in ns-3 [66–68]. In this simulation, stations are randomly scattered on a disk around the AP with radius of 50 m, and use ideal rate adaptation which selects the optimal MCS maximizing throughput. We consider both

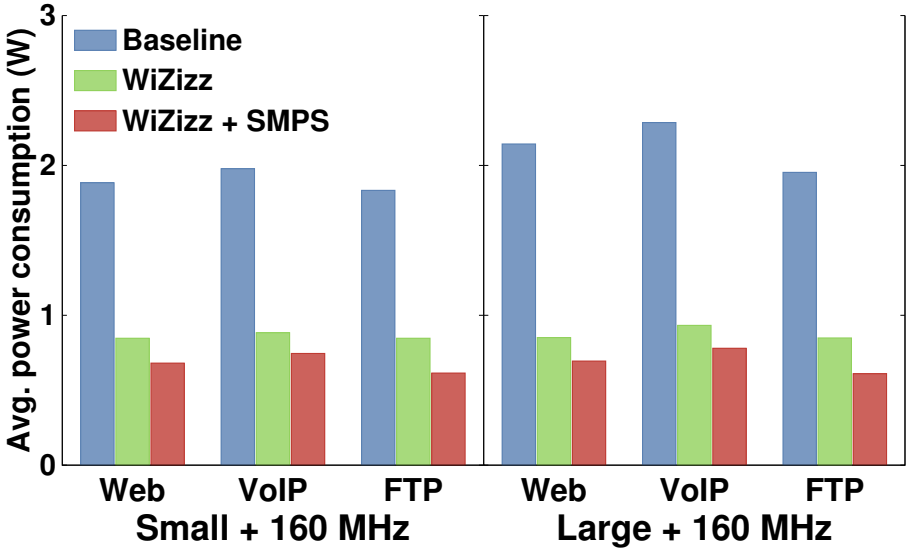

Figure 6.10: Performance comparison with different traffic.

small and large scale networks, where N_{sta} is 20 and 50, respectively.

Regardless of the traffic pattern and network size, WiZizz consistently outperforms the baseline 802.11ac as shown in Fig. 6.10. Specifically, WiZizz reduce about 55% and 60% power consumption compared with the baseline 802.11ac in small and large network, respectively. This is due to the fact that P_{baseline} increases as network size increases while WiZizz stations consume the same power regardless of network size thanks to the PHY-level filtering.

6.5.4 Collaboration with SMPS

Last, we additionally evaluate the performance of WiZizz inter-playing with dynamic SMPS (WiZizz+SMPS), which minimizes idle power from MIMO features. The collaboration allows a station to operate with only one antenna and the narrowest bandwidth for a significant portion of time. As shown in Fig. 6.10, WiZizz+SMPS shows

the least power consumption over all comparative schemes for all tested environments. To conclude, our approach works independently of other power saving schemes, such as SMPS and PSM, and hence the joint use of them is helpful to further minimize WiFi energy cost.

6.6 Summary

In this chapter, motivated by our accurate modeling and extensive measurements of the commercial 802.11ac hardware, we have proposed WiZizz, a practical, standard-congenial bandwidth management that achieves remarkable energy saving. The primary contribution of WiZizz is to minimize the avoidable power consumption in idle and RX state by utilizing the duplicate frame format defined in 802.11ac standard. We demonstrate its benefits and feasibility via open source device driver prototype implementation and network simulation. We envision WiZizz to be a strong and practical battery saver for future WiFi systems.

Chapter 7

Conclusion and Future Work

7.1 Research Contributions

In this dissertation, we propose a couple of compelling algorithms, intra-frame rate adaptation and enhanced channel estimation and tracking, to improve the performance and robustness of the emerging Wi-Fi, i.e., IEEE 802.11n and IEEE 802.11ac based WLAN, for the pedestrian mobile users. Furthermore, we present a new power save mode and protocol to minimize the traumatic energy cost of IEEE 802.11n/802.11ac-enabled devices.

More into detail, the research contribution of each chapter in the dissertation are summarized as follows.

In Chapter 2, To study thoroughly the impact of the pedestrian user mobility, we have conducted experiments using off-the-shelf IEEE 802.11n device to analysis wireless channel dynamics. Based on our measurement results, the wireless channel is abruptly fluctuated when A-MPDU is used, especially for mobile users. We then investigate the impact of user mobility on the performance of A-MPDU in terms of throughput and robustness. The results reveal that the subframe error of A-MPDU dra-

matically increases along with the increase in the gap between the preamble and the corresponding subframe. Moreover, in order to better understand the root causes of the unreliability of A-MPDU in fast time-varying environments, we analyze how badly the OFDM symbols are distorted by the use of the baseline 802.11 channel estimation and compensation techniques which exploit the CSI from the preamble. The dispersion of the received OFDM symbol at the latter part of A-MPDU is much larger than that at the front part of A-MPDU due to inherent limitation of Wi-Fi. Therefore, we conclude that the performance degradation are induced by inaccurate CSI which is only estimated at the beginning of A-MPDU frame and used throughout the entire frame.

In Chapter 3, the issue of unreliable transmission in A-MPDU of IEEE 802.11 is addressed, especially for pedestrian mobile users. To resolve the issue, we have developed SIRA, a method for selecting the appropriate PHY rates on intra-frame basis by using PHY information without any protocol overhead. Our results show that the proposed scheme is effective and yields significant performance gain over the conventional rate control algorithms. To our best knowledge, in Wi-Fi networks, this is the first sophisticate rate control algorithm to address the issue of quickly adapting time-variant wireless channel during one-frame duration.

Chapter 4 presents ChASER, a low-complexity, standard-compliant channel estimation and tracking design that achieves remarkably high performance even in the presence of pedestrian user mobility and frame aggregation. The primary contribution of ChASER is to reconstruct transmit symbols at the receiver with extremely low estimation errors by exploiting the output of decoder and the existing transmit DSP blocks with low-complexity adaptive filter. The reconstructed data symbols are then used to estimate and track the CSI at the granularity of data symbols, leading to significantly improved robustness against the time-varying channel dynamics over the duration of the aggregated frame. We demonstrate its benefits and feasibility via software-radio

prototype implementation and trace-driven link level simulator which well reflect the wireless channel characteristics of the real world. We envision the ChASER's channel tracking scheme to be applicable to any communication system that employs coherent modulation, not just Wi-Fi devices considered in this chapter.

In Chapter 5, we present synthetic analysis on the power consumption of the commercial state-of-the-art IEEE 802.11ac hardware. From this, we reveal that it consumes the energy unnecessarily due to its inherent limitation. That is, Wi-Fi overhears the wireless channel continuously in order to detect unpredictable transmission and receive superfluous frames destined to others. We then confirm that the use of channel bonding is considered the dominant factor of Wi-Fi's power consumption, and it uses most of energy in idle and receive state than transmit and sleep state . Therefore, considering wider channel bandwidth originated by channel bonding becomes increasingly important to save idle and receive state energy for the 802.11ac-enabled Wi-Fi which mandates the channel bonding up to 80 MHz. In addition, we model the power consumption characteristics of the 802.11ac NIC. It is shown that the proposed model accurately captures the power consumption characteristics with high fidelity, at most 2% estimation error for all the possible parameter combinations.

In Chapter 6, motivated by our accurate modeling and extensive measurements of the commercial 802.11ac hardware, we have proposed WiZizz, a practical, standard-congenial bandwidth management that achieves remarkable energy saving. The primary contribution of WiZizz is to minimize the avoidable power consumption in idle and RX state by utilizing the duplicate frame format defined in 802.11ac standard. We demonstrate its benefits and feasibility via open source device driver, $ath10k$ prototype implementation and network simulation, $ns-3$. We then shows the performance gain of our technique over the baseline 802.11ac is found to achieve significant energy saving. Finally, We envision WiZizz to be a strong and practical battery saver for

future Wi-Fi systems.

7.2 Further Research Plans

We conclude the dissertation with a brief discussion of ongoing research on further improving and expanding our contributions.

First, we plan to extend SIRA and ChASER by considering MIMO features of the emerging Wi-Fi devices. The impact of user mobility and CSI estimation accuracy is more pronounced for MIMO, because MIMO techniques require a more accurate channel estimation and compensation procedure to eliminate the spatial interference. Accordingly, we envision that the expected performance gain by this extension may lead to even more significant performance improvement.

Second, though SIRA in Chapter 3 is designed for the intra frame rate adaptation, a fine-grained multi-level rate adaptation could further improve the proposed algorithm depending on the amount of piggy backed feedback information available in a BlockAck frame. We plan to work on the enhancement of mobility detection in terms of accuracy and development of a fine-grained MCS decision, e.g., by utilizing extra information such as SNR distribution across the received A-MPDU.

Third, in Chapter 4, we investigate the impact of step size μ of the proposed adaptive filter, and determine an appropriate μ. However, the larger μ is, the faster ChASER operates but at the increasing risk of higher estimation errors for static scenarios. To optimize ChASER for both performance and speed, it is desired to adapt the value of μ according to the observed mobility pattern. We plan to address this issue in our future work.

Finally, our proposed protocol, WiZizz, further improves the energy efficiency of the station, i.e., battery-powered mobile Wi-Fi device. Nowadays, it is gradually

known that the IEEE 802.11ac-enabled dual-band AP tremendously consumes energy, and it is one of the major power consumer of home appliances. For example, the AP requires roughly a third energy cost compared to the refrigerator that is well-known to be the most energy hungry application. Motivated by this, we have a plan to design energy saving protocol by considering the AP's life pattern.

Bibliography

[1] IEEE 802.11, *Part 11: Wireless LAN Medium Access Control (MAC) and Physical Layer (PHY) specifications*, IEEE Std., Mar. 2012.

[2] IEEE 802.11ac, *Part 11: Wireless LAN Medium Access Control (MAC) and Physical Layer (PHY) specifications: Enhancements for Very High Throughput for Operation in Bands below 6 GHz*, IEEE Std., Dec. 2013.

[3] O. Lee, J. Kim, and S. Choi, "SIRA: SNR-aware Intra-frame Rate Adaptation," *accepted to IEEE Commnu. Lett.*, 2015.

[4] O. Lee, W. Sun, J. Kim, H. Lee, J. Lee, and S. Choi, "ChASER: Channel-Aware Symbol Error Reduction," *accepted to IEEE INFOCOM*, 2015.

[5] O. Lee, J. Kim, and S. Choi, "WiZizz: Energy Efficient Bandwidth Management," *submitted to IEEE SECON*, 2015.

[6] J. G. Proakis, *Digital Communications*. McGraw-Hill, 1995.

[7] M. Gast, *802.11 ac: A Survival Guide*. "O'Reilly Media, Inc.", 2013.

[8] J. Kim, S. Kim, S. Choi, and D. Qiao, "CARA: Collision-Aware Rate Adaptation for IEEE 802.11 WLANs," in *Proc. IEEE INFOCOM*, 2006.

[9] S. H. Y. Wong, H. Yang, S. Lu, and V. Bharghavan, "Robust Rate Adaptation for 802.11 Wireless Networks," in *Proc. ACM MobiCom'06*, Sep. 2006.

[10] M. Vutukuru, H. Balakrishnan, and K. Jamieson, "Cross-layer Wireless Bit Rate Adaptation," in *Proc. ACM SIGCOMM*, New York, New York, USA, 2009.

[11] S. Sen and N. Santhapuri, "AccuRate: Constellation based Rate Estimation in Wireless Networks," in *Proc. USENIX NSDI*, 2010.

[12] X. He, F. Y. Li, and J. Lin, "Link Adaptation with Combined Optimal Frame Size and Rate Selection in Error-Prone 802.11n Networks," in *Proc. IEEE ISWCS*, Oct. 2008.

[13] K. Feng, P. Lin, and W. Liu, "Frame-Aggregated Link Adaptation Protocol for Next Generation Wireless Local Area Networks," *EURASIP Journal on Wireless Communications and Networking*, pp. 1–13, 2010.

[14] S. Byeon, K. Yoon, O. Lee, S. Choi, W. Cho, and S. Oh, "MoFA: Mobility-aware Frame Aggregation in Wi-Fi," in *Proc. ACM CoNEXT*, Dec. 2014.

[15] A. Stamoulis, "Intercarrier interference in MIMO OFDM," *IEEE Trans. Signal Processing*, vol. 50, no. 10, pp. 2451–2464, 2002.

[16] C. Y. Shin and E. J. Powers, "Double Selective Channel Estimation for OFDM Systems," in *Proc. IEEE Asilomar*, Nov. 2005.

[17] S. I. Kim, H. S. Oh, and H. K. Choi, "Mid-amble Aided OFDM Performance Analysis in High Mobility Vehicular Channel," in *Proc. IEEE Intelligent Vehicles Symposium*, Jun. 2008.

[18] IEEE 802.11p, *Part 11: Wireless LAN Medium Access Control (MAC) and Physical Layer (PHY) specifications: Wireless Access in Vehicular Environments*, IEEE Std., Jul. 2010.

[19] A. Bourdoux, H. Cappelle, and A. Dejonghe, "Channel Tracking for Fast Time-Varying Channels in IEEE 802.11p Systems," *Proc. IEEE GlOBECOM*, Dec. 2011.

[20] Z. Zhao, X. Cheng, M. Wen, B. Jiao, and C.-X. Wang, "Channel Estimation Schemes for IEEE 802.11p Standard," *IEEE Intell. Transport. Syst.*, vol. 5, no. 4, pp. 38–49, Oct. 2013.

[21] T. Zemen and L. Bernadó, "Iterative Time-Variant Channel Estimation for 802.11p Using Generalized Discrete Prolate Spheroidal Sequences," *IEEE Trans. Veh. Technol.*, vol. 61, no. 3, pp. 1222–1233, 2012.

[22] M. Zhao, Z. Shi, and M. C. Reed, "Iterative Turbo Channel Estimation for OFDM System over Rapid Dispersive Fading Channel," in *Proc. IEEE ICC 2007*, Jun. 2007.

[23] D. Halperin, B. Greenstein, A. Sheth, and D. Wetherall, "Demystifying 802.11n Power Consumption," in *Proc. USENIX HotPower*, Oct. 2010.

[24] Y. Zeng, P. H. Pathak, and P. Mohapatra, "A First Look at 802.11 ac in Action: Energy Efficiency and Interference Characterization," in *Proc. IFIP Networking*, 2014.

[25] I. Pefkianakis, C.-Y. Li, C. Peng, S.-B. Lee, and S. Lu, "CMES: Collaborative Energy Save for MIMO 802.11 Wireless Networks," in *Proc. IEEE ICNP*, 2013.

[26] C.-Y. Li, C. Peng, S. Lu, and X. Wang, "Energy-based Rate Adaptation for 802.11n," in *Proc. ACM Mobicom*, Aug. 2012.

[27] R. Chandra, R. Mahajan, T. Moscibroda, R. Raghavendra, and P. Bahl, "A Case for Adapting Channel Width in Wireless Networks," *ACM SIGCOMM Computer Communication Review (CCR)*, vol. 38, no. 4, pp. 135–146, 2008.

[28] F. Lu, G. M. Voelker, and A. C. Snoeren, "SloMo: Downclocking WiFi Communication," in *Proc. USENIX NSDI*, 2013.

[29] F. Lu, P. Ling, G. M. Voelker, and A. C. Snoeren, "Enfold: Downclocking OFDM in WiFi," in *Proc. ACM Mobicom*, 2014.

[30] X. Zhang and K. Shin, "E-mili: Energy-minimizing Idle Listening in Wireless Networks," *IEEE Trans. Mobile Comput.*, vol. 11, no. 9, pp. 1441–1454, 2012.

[31] E. Perahia and R. Stacey, *Next Generation Wireless LANs: Throughput, Robustness, and Reliability in 802.11n*. Cambridge University Press, 2008.

[32] IEEE P802.11 Wireless LANs*, TGn Channel Models*, IEEE 802.11-03/940r4, May 2004.

[33] T. Paul and T. Ogunfunmi, "Wireless LAN Comes of Age: Understanding the IEEE 802.11n Amendment," *IEEE Circuits Syst. Mag.*, vol. 8, no. 1, pp. 28–54, March 2008.

[34] HostAP: IEEE 802.11 AP, IEEE 802.1X/WPA/WPA2/EAP/RADIUS Authenticator. http://hostap.epitest.fi/hostapd/.

[35] Ubuntu: A community developed, linux-based operating system. http://www.ubuntu.com/.

[36] Intel Wi-Fi Link (IWL) 5300. http://www.intel.com/products/wireless/adapters/5000/.

[37] Ath9k: Atheros Linux Wireless Driver. http://wireless.kernel.org/en/users/Drivers/ath9k/.

[38] Iperf: TCP/UDP Bandwidth Measurement Tool. http://dast.nlanr.net/Projects/Iperf/.

[39] D. Halperin, W. Hu, A. Sheth, and D. Wetherall, "Tool release: Gathering 802.11n Traces with Channel State Information," *ACM SIGCOMM Computer Communication Review*, vol. 41, no. 1, pp. 53–53, 2011.

[40] A. Bhartia, Y. C. Chen, and L. Qiu, "Harnessing Frequency Diversity in Wi-Fi Networks," in *Proc. ACM MobiCom'11*, Sep. 2011.

[41] K. Tan, J. Zhang, J. Fang, H. Liu, Y. Ye, S. Wang, Y. Zhang, H. Wu, W. Wang, and G. M. Voelker, "Sora: High Performance Software Radio Using General Purpose Multi-core Processors," in *Proc. USENIX NSDI*, 2009.

[42] Atheros AR9380. http://www.qca.qualcomm.com/mobile-connectivity/wi-fi/.

[43] A. Georgiadis, "Gain, Phase Imbalance, and Phase Noise Effects on Error Vector Magnitude," *IEEE Trans. Veh. Technol.*, vol. 53, no. 2, pp. 443–449, March 2004.

[44] A. Kamerman and L. Monteban, "WaveLAN ®-II: A High-performance Wireless LAN for the Unlicensed Band," *Bell Labs Technical Journal*, vol. 2, no. 3, pp. 118–133, April 1997.

[45] S. Kim, L. Verma, S. Choi, and D. Qiao, "Collision-Aware Rate Adaptation in Multi-rate WLANs: Design and implementation," *Computer Networks*, vol. 54, no. 17, pp. 3011–3030, Dec. 2010.

[46] G. Holland, N. Vaidya, and P. Bahl, "A Rate-adaptive MAC Protocol for multi-Hop Wireless Networks," in *Proc. ACM Mobicom*, 2001.

[47] J. Zhang, K. Tan, J. Zhao, H. Wu, and Y. Zhang, "A Practical SNR-Guided Rate Adaptation," in *Proc. IEEE INFOCOM*, April 2008.

[48] D. Halperin, W. Hu, A. Sheth, and D. Wetherall, "Predictable 802.11 Packet Delivery from Wireless Channel Measurements," in *Proc. ACM SIGCOMM*, August 2010.

[49] H. A. Mahmoud and H. A. Mahmoud, "Error Vector Magnitude to SNR Conversion for Nondata-aided Receivers," *IEEE Trans. Wireless Commun.*, vol. 8, no. 5, pp. 2694–2704, May 2009.

[50] The Network Simulator 3 – *ns*-3. http://www.nsnam.org/.

[51] GNU Radio. http://gnuradio.org/.

[52] IT++. http://itpp.sourceforge.net/.

[53] A. Goldsmith, *Wireless Communications*. Cambridge university press, 2005.

[54] J. Thomson, B. Baas, E. M. Cooper, J. M. Gilbert, G. Hsieh, P. Husted, A. Lokanathan, J. S. Kuskin, D. McCracken, B. McFarland *et al.*, "An Integrated 802.11a Baseband and MAC Processor," in *Proc. IEEE ISSCC Digest of Technical Papers*, 2002.

[55] S. Cui, A. J. Goldsmith, and A. Bahai, "Energy-constrained Modulation Optimization," *IEEE Trans. Wireless Commun.*, vol. 4, no. 5, pp. 2349–2360, 2005.

[56] W. Gabran and B. Daneshrad, "Hardware and Physical Layer Adaptation for a Power Constrained MIMO OFDM System," in *Proc. IEEE ICC*, 2011.

[57] D. Qiao, S. Choi, A. Jain, and K. G. Shin, "MiSer: An Optimal Low-energy Transmission Strategy for IEEE 802.11a/h," in *Proc. ACM Mobicom*, Sep. 2003.

[58] SST11CP15 Datasheet. http://ww1.microchip.com/downloads/en/DeviceDoc/70005016C.pdf.

[59] Qualcomm Atheros 9880. http://www.qca.qualcomm.com/mobile-connectivity/wi-fi/.

[60] PEX1-MINI-E. http://www.orbitmicro.com/.

[61] Ath10k: Qualcomm Atheros Linux Wireless Driver. http://wireless.kernel.org/en/users/Drivers/ath10k/.

[62] ASUS RT-AC66U. http://www.asus.com/us/Networking/RTAC66U/.

[63] ASUSwrt Merlin Custom Firmware. http://www.lostrealm.ca/tower/node/79.

[64] National Instruments USB-6210. http://www.ni.com/data-acquisition/multifunction/.

[65] IBM SPSS Statistics. http://www-01.ibm.com/software/analytics/spss/products/statistics/.

[66] ITU-T Recommendation G.711, Pulse Code Modulation (PCM) of Voice Frequencies, Nov. 1988.

[67] R. Pries, Z. Magyari, and P. Tran-Gia, "An HTTP Web Traffic Model based on the Top One Million Visited Web Pages," in *Proc. IEEE Next Generation Internet (NGI)*, 2012.

[68] 3GPP, TR 36.814 V9.0.0: Further Advancements for E-UTRA, Physical Layer Aspects, (Release 9), 2010.

초 록

지난 반세기 동안 무선 근거리 통신망(Wireless Local Area Network, WLAN) 기술은 우리의 일상 생활의 필수 불가결 한 부분이되었습니다. 최근들어 스마트폰, 태블릿, 노트북과 같은 휴대용 장치의 사용이 엄청나게 증가하였고, 그에 따른 증가된 트래픽 지원에 대한 요구 또한 급격하게 증가하였다. 이러한 요구를 매우 낮은 비용 만족시키기 위해서 IEEE 802.11 WLAN의 대표 상품인 Wi-Fi가 매력적인 해결책으로 각광받고 있다.

이 엄청난 성공에 힘 입어, Wi-Fi는 두가지 큰 경향으로 발전하고 있다. 우선, 최신 IEEE 802.11 표준인 IEEE 802.11n과 IEEE 802.11ac는 물리 계층(Physical layer, PHY) 속도 향상을 위해 다중 안테나(Multiple-Input Multiple-Output, MIMO) 기술 및 채널 결합(channel bonding) 기술을 적용하였다 [1, 2]. 다음으로, 매체 접근 제어(Medium Access Control, MAC) 계층의 높은 전송 수율(throughput) 및 효율성(efficiency)을 달성하기 위해, IEEE 802.11n과 802.11ac 표준은 두 가지 종류의 프레임 집적 기술(frame aggregation)인 MAC 프로토콜 데이터 단위(MAC protocol data unit, MPDU) 집적 기술(A-MPDU) 및 MAC 서비스 데이터 단위(MAC service data unit) 집적 기술(A-MSDU)을 정의 하였다. 이러한 프레임 집적 기술은 물리 계층과 MAC 계층의 프로토콜 오버 헤드를 집적된 하부프레임(subframe)으로 분산시켜 큰 성능 향상을 꾀할 수 있다.

이러한 노력으로 Wi-Fi는 수백 배 증가한 물리 계층 속도를 제공할 수 있게 되어

서, Wi-Fi 장착 기기 사용자들의 요구사항을 만족시키기에 충분한 기술력을 갖췄다는 데에 의심할 여지가 없다. 하지만 스마트폰, 태블릿, 노트북과 같은 배터리 구동 휴대(*battery-powered portable*) 장치 사용자들의 증가는 이러한 믿음을 두 가지 관점에서 무너뜨렸다. 첫째, 더 높은 물리 계층 전송 속도와 더 긴 프레임 사용은 Wi-Fi의 신호를 채널 에러 취약하게 만든다. 특히 이러한 현상은 휴대 장치 사용자에게 더욱 두드러진다. 둘째, 최신 IEEE 802.11n과 IEEE 802.11ac 기반의 Wi-Fi 기기들은 다중 안테나 및 채널 결합 기술의 사용으로 기존의 IEEE 802.11a/b/g 기반의 기기들에 비해서 더 높은 파워 소모를 겪게 된다. 더 나아가 오늘날 배터리 구동 휴대 기기 사용자들은 다양한 어플리케이션을 지속적인 사용하기 때문에 배터리 지속 시간 및 신뢰성 있는 통신 기술을 더욱 중요하게 여긴다. 본 학위 논문에서는 이러한 문제점을 해결하기 위해서 Wi-Fi의 신뢰성 및 에너지 효율성 향상을 위한 MAC/PHY 기법을 제안한다.

우선 이러한 사용자 환경 변화 및 기술 발전이 Wi-Fi 성능에 미치는 영향을 확인하기 위해서, 우리는 최신 상용 IEEE 802.11n 및 IEEE 802.11ac 기반의 Wi-Fi 장착 기기들을 이용하여 다양한 실험을 진행하였다. 또한, Microsoft사의 소프트웨어 정의 라디오(software-defined radio)인 Sora를 이용해서 더 구체적인 실험 결과를 도출하였다. 우리의 실험 결과는 A-MPDU를 사용함에 따라 Wi-Fi의 성능이 급격하게 감소하는 것을 확인하였고, 이러한 현상은 보행자 속도로 움직이는 사용자에게 더욱 심하게 관찰되었다. 게다가 우리는 채널 결합 기술이 배터리 구동 휴대기기의 주 전력 소모원인 Wi-Fi의 전력 소모를 크게 심화시킨다는 것을 발견할 수 있었으며, 특히 Wi-Fi는 불필요한 대기 및 수신 동작을 위해서 과도하게 전력을 소모하는 것을 확인하였다.

이러한 발견을 기반으로 우리는 빠르게 변하는 무선 환경에 적응적으로 대처하기 위해서 프레임 내부 전송 속도 제어 알고리즘(intra-frame rate control algorithm)인 SNR(Signal-to-Noise Ratio) 인지 내부 전송 속도 적응(*SNR-aware Intra-frame Rate Adaptation*, SIRA) 기법을 제안한다 [3]. 지금까지 널리 사용된 전송 속도 적응

기술은 프레임 간 전송 속도 저어 알고리즘(inter-frame rate control algorithm)이며, 이는 프레임 손실율이나 수신 신호 세기에 따라서 각 프레임 당 하나의 최적 전송 속도를 선택한다. 하지만 이러한 기존의 전송 속도 적응 기법은 이동성 환경에서 A-MPDU를 사용할 경우 Wi-Fi의 성능을 급격하게 떨어뜨리기 때문에, 제안하는 기법인 SIRA는 사용자의 속도에 따라서 프레임 내부에서 전송 속도를 적응적으로 제어할 수 있도록 한다. 제안하는 기법의 성능은 실제 통신 환경을 잘 재현할 수 있는 측정 채널 기반 실환경 링크 레벨 시뮬레이터(trace-driven link level simulator)를 이용하여 검증되었다. SIRA는 모든 측정된 채널에서 기존 기술에 비해서 월등한 성능을 보여준다. 하지만 이러한 성능 향상에도 불구하고 Wi-Fi의 태생적 한계 때문에, 이동성 환경에서 나타나는 성능 열화를 완전히 제거하지 못한다.

따라서 우리는 이러한 문제를 해결하기 위해서 물리 계청 정보를 이용하여 새로운 채널 추정 및 추적 기술인 채널 인지 심볼 에러 절감(*Channel-aware Symbol Error Reduction*, ChASER) 기술을 제안한다 [4]. ChASER는 수신한 데이터 심볼을 재부호화(re-encoding) 및 재변조화(re-modulation)을 활용하여 직교 주파수 분할 다중화(Orthogonal Frequency Division Multiplexing, OFDM) 심볼 단위로 무선 채널 변화를 추적하는 기술이다. 게다가 제안하는 기법은 낮은 복잡도(complexity)를 가지고 간단히 구현이 가능하다. 우리는 Microsoft사의 Sora를 이용하여 시제품을 구현하였을 뿐만 아니라 제안하는 기법의 성능을 평가 하였다. 종래의 채널 변화를 추적하는 기술들은 IEEE 802.11n 표준을 크게 변경해야하지만 ChASER는 그러한 변경이 필요가 없으므로 IEEE 802.11n에 바로 호환 가능한 최초의 채널 추적 기술이다. 그러나 상기의 제안하는 기법들로는 Wi-Fi의 수율 및 전송 신뢰성(robustness)을 크게 증가키지만, 휴대용 기기 사용자의 다른 요구 사항인 전력 효율적인 Wi-Fi 시스템 설계를 만족시키지 못하기 때문에 이에 대한 연구가 여전히 필요하다.

그러므로 우리는 WiZizz(WiFi in Zizz)라고 불리는 새로운 전력 절감 모드 및 동작을 정의한다 [5]. WiZizz는 신중하게 IEEE 802.11ac의 채널 결합 특성을 활용하여 에너지 효율적으로 대역폭(bandwidth)를 조절하는 기술을 제공한다. 우리는

광범위한 실험 및 측정을 통해서 제안하는 기술이 최대 73%까지 성능 향상이 있는 것을 보여준다. 추가적으로 구현 가능성(feasibility)을 확인하기 위해 상용 IEEE 802.11ac 기기에 제안하는 기술을 적용하여 시제품을 제작하였다. 제안하는 기법은 IEEE 802.11ac 표준을 조그만 수정하면 되기 때문에, 우리가 아는 한 WiZizz는 IEEE 802.11ac에 적합한 최초의 에너지 효율적인 대역폭 관리 기술이다.

요컨데 Wi-Fi의 패러다임 변화에 따라 우리는 WiFi의 신뢰성 및 에너지 효율성 향상을 위해 매우 흥미로운 다양한 알고리즘과 동작 기법을 제안한다. 게다가 본 학위 논문에서는 제안하는 기법의 타당성 및 성능 향상을 이론적인 검증에 그치지 않고 실제 무선 채널 환경을 잘 반영한 실환경 링크 레벨 시뮬레이터를 이용하여 보여주었다. 마지막으로 제안하는 기법의 구현 가능성을 확인하기 위해 소프트웨어 정의 라디오 및 상용 Wi-Fi 장치를 이용하여 시제품 구현 및 제작을 완료하였다.

주요어: 무선 통신, 무선 근거리 통신망(Wi-Fi), 신뢰성, 전력 절감, 전력 소모 모델, 시제품 설계.

학번: 2007-21046